Dissertation
Department of Earth Sciences
Freie Universität Berlin

photo: tableland in the southern part of the Puli Basin

The tablelands in the Puli Basin (central Taiwan) — a geochronological and geomorphological approach to Late Quaternary fluvial sedimentary and erosional processes

曾佳漢
Chia-Han Tseng

Freie Universität Berlin

Freie Universität Berlin

The tablelands in the Puli Basin (central Taiwan)— a geochronological and geomorphological approach to Late Quaternary fluvial sedimentary and erosional processes

Die Hauptterrassen im Puli-Becken (Zentral Taiwan)—
Studien zur Geochronologie und Geomorphologie
spätquartärer fluvialer Erosions- und Akkumulationsprozesse

Dissertation

Zur Erlangung des akademischen Grades
Doktor der Naturwissenschaften (Dr. rer. nat.)

am Fachbereich Geowissenschaften
der Freien Universität Berlin

vorgelegt von
Chia-Han Tseng

Berlin, 2014

Erstgutachterin: Prof. Dr. Margot Böse

Zweitgutachter: Prof. Dr. Bernd Wünnemann

Tag der Disputation: 04.Juni.2014

Acknowledgements

First of all, I would like to thank Prof. Dr. Margot Böse for giving me the chance to do the doctorate in Germany, a country which I find interesting and want to understand more, and for her encouragement and supports for the entire work. Many thanks will also be given to the German Academic Exchange Service (DAAD, Deutscher Akademischer Austausch Dienst) for providing the scholarship to let me complete my work in the past four years without worrying about the living.

I would also like to thank Dirk Wenske, Christopher Lüthgens, Robert Hebenstreit, Tony Reimann, Jacob Hardt, and Marc Bauersachs not only for their valuable opinions and discussions about my research, but also for their great help and suggestions on my stay in Berlin, which really made me have a feeling of "just like home" here in Germany. I also want to thank Mrs. Martine Friedmann for her kind help with some budget affairs and for her delicious home-made cakes. I also appreciate deeply Dr. Phillip Hoelzmann for his valuable comments and discussions on the results of grain size analyses. Special thanks are to Mrs. Anne Beck for her proofreading of my research papers.

Furthermore, I would like to thank Prof. Dr. Manfred Frechen at the Leibniz Institute for Applied Geophysics (LIAG) in Hannover to apply the OSL dating equipments to complete my work, and also a lot of thanks to Dr. Sumiko Tsukamoto for teaching me the professional techniques and allowing me to use her washing machine. I would like to say thank you to technicians there for helping me with all the sample preparations before the OSL measurements.

I am also grateful to have help and supports from Prof. Jyr-Ching Hu (胡植慶教授), Dr. Chao-Lung Tang (唐昭榮博士), (Department of Geosciences, National Taiwan University), Prof. Jiun-Chuan Lin (林俊全教授), Shih-Hung Liu (劉時宏), Yuan-Chang Cheng (鄭遠昌) (Department of Geography, National Taiwan University) during my field work in Taiwan, which let us work more efficiently.

At last, I am very thankful to have full support from my family, especially my mother, so that I can concentrate on my study and life here in Germany. I am also glad and grateful to have full encouragement and being with me side from a person, who is my good colleague, friend and love, Szu-Yuan.

Contents

List of figures

List of tables

Summary

The island of Taiwan has been formed by the orogeny resulting from the convergence of the two tectonic plates, the Eurasian Plate and the Philippine Sea Plate. The climate in Taiwan is influenced by the East Asian Monsoon because of its geographic position, offshore to the southeast of the Eurasia Continent. In the tectonic and climatic contexts, Taiwan is characterized by a diverse topography, i.e., mountains, hills, tablelands, basins, and plains.

A group of intramontane basins with areas larger than 1 km^2 exist in central Taiwan, namely the Puli Basin, the Yuchih Basin, the Sun Moon Lake, and the Toushe Basin. This study focuses on the Puli Basin and aims at linking the tableland formation in the Puli Basin to paleoclimate conditions and to shed light on the tectonic framework and its possible influences on the tableland formation. Results from the Puli Basin were still missing, whereas other basin areas have already been studied. Hence, the results from the Puli Basin will be compared to other areas in Taiwan.

This study relies on various methods, such as topography interpretations from aerial photographs and digital terrain model (DTM), sedimentological analyses including element, mineral, and grain size measurements, and burial age estimation by applying optically stimulated luminescence (OSL) and radiocarbon (^{14}C) dating techniques.

The results demonstrate that:

huge amounts of sediment originating outside the Puli Basin were deposited as an alluvial fan during the transition from the Late Pleistocene to the Holocene (14–9 ka) owing to climate changes. The climate changes could prevail in Taiwan, so that slope movements, mass wasting, and alluvial fans formation were active from high mountains to low-altitude areas during the same period. Local and intermittent tectonic activities and resultant river incision created several levels and tablelands and terraces in the Puli Basin. It is thus concluded that past climate changes, topographical and lithological features, and local tectonic activities have controlled the landform development in the Puli Basin.

Zusammenfassung

Die Insel Taiwan wurde durch die Gebirgsbildung aus der Konvergenz der beiden tektonischen Platten, Eurasischer Platte und Philippinischer Platte, gebildet. Das Klima Taiwans wird wegen seiner geographischen Lage im Südosten des Kontinents Eurasien vom ostasiatischen Monsun beeinflusst. Aufgrund der tektonischen und klimatischen Hintergründe wird Taiwan von einer abwechslungsreichen Topographie aus Bergen, Hügeln, Hochebenen, Becken und Ebenen gekennzeichnet.

In Zentral Taiwan gibt es eine Gruppe von intramontanen Becken mit einer Fläche größer als 1 km^2, darunter das Puli-Becken, das Yuchih-Becken, der Sonne-Mond-See und das Toushe-Becken. Diese Arbeit befasst sich mit dem Puli-Becken und zielt darauf ab, die Bildung der Hauptterrassen im Puli-Becken im Lichte der maßgeblichen paläoklimatischen und tektonischen Begebenheiten zu rekonstruieren. Bislang lagen keine detaillierten Arbeiten zu den Flussterrassen im Puli-Becken vor, wohingegen andere Regionen bereits detailliert untersucht wurden. Folglich wird ein Vergleich der Ergebnisse aus dem Puli-Becken mit vergleichbaren Gebieten im lokalen Kontext Taiwans angestrebt.

Dabei kommen verschiedene Verfahren zu Anwendung, wie topographische Interpretationen von Luftbildern und digitalen Geländemodellen (DGM), sedimentologische Analysen einschließlich Element-, Mineral-und Korngrößenmessungen und Altersdatierungen mittels optisch stimulierter Lumineszenz (OSL) und Radiokohlenstoff (^{14}C) Techniken.

Die Ergebnisse zeigen, dass eine Menge Sedimente, die in das Puli-Becken kamen, während des Übergangs vom Spätpleistozän zum Holozän (14–9 ka) durch Klimaänderungen in Form eines Schwemmkegels abgelagert wurden. Aufgrund von klimatischen Änderungen in Taiwan kam es vermehrt zu Hangbewegungen, Massenbewegungen in größeren Höhenlagen und zu Schwemmkegelbildung in niedrigeren Höhenlagen. Lokale und intermittierende tektonische Aktivitäten und daraus resultierende fluviale Einschnitte haben mehreren Ebenen und Terrassen im Puli-Becken geformt. Es wird der Schluss gezogen, dass die vergangenen Klimaveränderungen, sowie die topographischen und lithologischen Eigenschaften und lokale tektonische Aktivitäten die Landschaft des Puli-Beckens geformt haben.

CHAPTER 1
Introduction

1.1 Background and motives

The global climate change is a significant issue in the human society, for it has caused extreme weather worldwide, e.g., droughts, heavy precipitation, heat waves, and the intensity of tropical cyclones, and thus increased risks of life (IPCC, 2007). To mitigate life and economical costs from the natural hazards owing to the extreme weather, policies and preventive behaviors have to be made on the basis of comprehensive understanding of drivers of climate fluctuation. Studying climate in the past is one of the ways to improve knowledge of mechanisms that force the Earth's climate to change. By analyzing the mechanisms and their magnitude further and reconstructing the paleoclimate, climate scenarios in the future may be predictable. The fluctuations of paleoclimate cannot be measured straightforwardly, so proxy data, such as paleontological, geological, and geomorphological records and indicators, are regarded as responses to the past climate changes. By using the proxy data, the reconstruction of the paleoclimate can be made (Bradley, 2000).

One of the subaerial responses to the variations in the paleoclimate is landform development related to fluvial processes which is the most important geomorphic agent (Ritter et al., 2006). The reason is that rivers exist in different climatic zones on the Earth, from tropical to frigid as well as from humid to arid (Charlton, 2010). When climatic conditions change in respective climate zones, flow and sediment load in rivers, which are factors controlling fluvial processes, vary their own amounts and types accordingly. The type of flow depends on the lithology of the drainage basin, degree of weathering, and magnitude of precipitation, and these three elements decide amounts and types of sediment load in rivers (Charlton, 2010). Alternations of the fluvial processes, i.e., erosion, transportation, or aggradation of rivers, then occur to different extents depending on how the factors fluctuate. Subsequently, various landforms under different fluvial processes are formed, e.g., fluvial terraces, alluvial fans, and flood plains. The analyses of the landforms and their sediments created by rivers can therefore help to reconstruct the landform development in a drainage basin and give implications for the paleoclimate within which the sediments were deposited and the landforms were formed.

The island of Taiwan (121°E, 24°N) is located off the southeastern coast of the Eurasian continent and on the western margin of the Pacific Ocean (Figure 2-5). The location accordingly leads to the climatic patterns of the sub-tropical monsoon to the north and tropical monsoon to the south of the Tropic of Cancer (23.5°N), so the summer and winter monsoons are the main systems controlling

the climate. In addition, Taiwan also lies in the paths of frontal surfaces during the spring and fall as well as tropic cyclones (i.e., typhoons) being formed during the summer and fall every year. Therefore, rivers can develop with abundant water supply almost all the year. On the other hand, the high-relief topography in Taiwan is also suitable for rivers' development, for water in different patterns (e.g., rainfall and groundwater) is easily collected in river catchments (cf. Section 2.2). Various-sized drainage basins bounded by surrounding ridges thus distribute widely, within which various landforms are created by the rivers.

The paleoclimate of Taiwan in the late Quaternary has been revealed on the basis of pollen analyses derived from a peat bog (i.e., the Toushe Basin, 650 m a.s.l.) in central Taiwan (Liew et al., 2006). These palynological proxy data display variations in vegetation in response to the fluctuations of humidity and temperature in the past 96000 years in the submontane zone (500–1500 m a.s.l.). Nevertheless, landform development under fluvial processes could not still be correlated with paleoclimate changes without a timeframe for relevant sediments which is limited especially in the mountain areas in Taiwan.

1.2 Selection of the study area and objectives of this study

Tablelands and terraces, a kind of geomorphological record as climatic proxy data, are the research focus of this study. The cease of the deposition of tableland and terrace sediments reflects changes in sedimentary processes probably due to a certain climatic change or tectonic event (Liew, 1988a and 1988b; Liew and Hsieh, 2000). In the past two decades, studies focused more on the tablelands and terraces distributed in the foothill and plain areas in western Taiwan to figure out neotectonic events (e.g., Chen et al., 2003a and 2003b; Tsai and Sung, 2003; Lee et al., 2004; Lai et al., 2006). Recently, terraces in the mountain areas in central Taiwan are studied to understand the correlation between their formation and the paleoenvironmental changes (e.g., Hsieh and Chyi, 2010; Wenske et al., 2012) applying improved techniques of dating methods (e.g., radiocarbon and luminescence dating methods). The burial ages obtained of material or sediments in the terraces and tablelands hence provide valuable references of a geochronological framework for later research.

In central Taiwan, a group of intramontane basins were formed in a tectonic context (cf. Section 2.1). After these basins had been formed, sediments within these basins were deposited by rivers originating in adjacent areas. These sediments are regarded as proxy data recording climatic conditions in the past in the mountain areas. Deposits in the Yuchih Basin, Sun Moon Lake, and Toushe Basin as the members of the basin group (Figure 2-7), for example, have been studied in terms of paleontology and paleoclimatology (e.g., Tsukada, 1967; T.-C. Huang, 1975; Liew, 1977; Kuo and Liew, 2000; Liew et al., 2006; Lai, 2010; Liew et al., 2013) to find out a link between the

sediments and the past climate. According to results of palynological analyses, the deposition of the sediments in these basins initiated in the Middle Pleistocene (Tsukada, 1967; S.-Y. Huang, 1975; Liew, 1982), and the basins started to be formed at 700–500 ka (Wilcox et al., 2011). The Puli Basin, the largest one in the basin group, has also been studied repeatedly since the 1930s in terms of geomorphology, tectonics, and pedogenics (Hayasaka, 1930; Tomita, 1951; Lu, 1959; Huang, 1978; Chou 1981; Biq, 1989; Chu, 1991; Lu and Malavieille, 1994; Huang et al., 2000; Lu et al., 2002; B.-C. Chen, 2003; M.-M. Chen, 2003; Yang et al., 2007b; Ke, 2009; Chen, 2010; Wilcox et al., 2011; Hsu, 2013). Unlike other smaller basins, however, the Puli Basin is characterized by a topographic diversity (cf. Section 2.2), reflecting an integrated result of various processes in different time intervals, such as fluvial, climatic, and tectonic. Nevertheless, a geochronological framework of the sediments in the Puli Basin was not established in the previous studies mentioned above (Yang et al., 2007b), so the time when the sediments in the basin started to be formed was not clear.

Tablelands in the southern part of the Puli Basin are chosen to be studied for their distinctive features. First, the tablelands have the highest surfaces (cf. Section 2.2) among the landform units in the basin, and are covered by weathered and fine-grained sediments. These phenomena indicate that the tablelands are composed possibly of the sediments deposited in the early stage of the basin development. Second, descriptions about the sedimentary processes and sediment source were focused more on the tableland in the northern part of the basin (i.e., DP tableland in Figure 2-3) in the previous studies because only few outcrops of the sediments of the southern ones were found. Accordingly, discussions on the paleoenvironments reflected by the sedimentary sequences within the terraces and tablelands of the basin were not made as well. Third, these tablelands with more than 100 m in thickness show inclination and deformation on their surface top. This phenomenon is not observed within younger terraces and alluvial plains, showing that tectonic activities were not active after the younger landform units had been formed (Yang et al., 2007b). Fourth, the tablelands (i.e., Uni and SC tablelands) are just next to the Yuchih Basin south of the Puli Basin, so their landform development could have a close link to that of the Yuchih Basin.

On the basis of the background mentioned above, three important questions arise:

1. Does the tableland formation in the Puli Basin link to climate changes in the past?
2. Is the tectonic framework a factor that influences the tableland formation?
3. Is the Puli Basin a sole situation in Taiwan?

Subquestions are also propagated: what material constitutes the tablelands, what processes controlled the tableland distribution and landform development? To find out answers to the

questions, several geomorphological approaches are adopted, such as landform survey by interpreting aerial photos as well as digital terrain models (DTM), and field work. Results of previous studies on stratigraphic sequences and the tectonic framework in the Puli Basin are also reviewed and discussed. These approaches help to understand how local erosional and tectonic processes influenced the landform in the study area. In addition, sedimentological terms, e.g., grain size analyses and determination of mineral and element components, are also applied to understand the lithology and sedimentary processes. Time constraints of the tableland sediments are the key role to help answer the main questions, so geochronological approaches, e.g., optically stimulated luminescence (OSL) and radiocarbon (i.e., ^{14}C) dating methods, are used in this work.

The objectives of this study, therefore, are to reconstruct stratigraphic sequence and time framework of the tableland sediments as well as a model of landform development of the Puli Basin in the tectonic framework. Based on the results and by comparing the complete past climate records and terraces in other river catchments in Taiwan, the main questions arising can then be answered.

1.3 Structure of this dissertation

In this dissertation, an introduction to the study area including other intramontane basins to the south, such as the geographical, geomorphological, geological, and tectonic backgrounds, will first be presented in Chapters 1 and 2 and all the methods applied in the doctoral research, including optically stimulated luminescence dating and radiocarbon dating methods, will then be introduced in general in Chapter 3. In Chapter 4, the genetic mechanisms, sedimentary sequences of the geomorphic units, and landform development in the Puli Basin will be described and discussed by reviewing previous studies and by investigating the tablelands. Chapter 5 shows results of the study on an outcrop in the Uni tableland in terms of sedimentology and chronology will be presented, which has been published as a paper in an international peer-reviewed journal. In Chapter 6, complete results of a geochronological framework and geomorphic evolution of the studied tablelands will be shown. Besides, possible processes related to paleoclimate, fluvial, and tectonics exerting on the Puli Basin will also be discussed and proposed on the basis of the observation of the topography and the dating results. In the last part, the main findings of this study will be summarily presented as overall conclusions.

CHAPTER 2
Study area

2.1 Tectonic and geological setting

2.1.1 Plate tectonics and geological terrains in Taiwan

The island of Taiwan emerged from the ocean as a result of an oblique arc-continent collision between the passive margin of the Eurasian Plate and the Luzon arc of the Philippine Sea Plate which has initiated since 5 ma (e.g., Teng, 1990; Lee et al., 2006; Figure 2-1). This ongoing tectonic activity accompanied by erosion has made the island a rugged topography. On the basis of the GPS (global positioning system) measurements (Yu et al., 1997 and 1999), the Luzon arc, including the Green Island and Orchid Island (i.e., Lanyu) has been moving northwestwards with a velocity of 82 mm/a. The oblique arc-continent collision between the two tectonic plates led to the development of the Okinawa Trough as a back-arc rifting basin to the northeast, the Ryukyu Trench to the east, and the Huatung Ridge to the southeast of the Taiwan island (Ching et al., 2011). The bathymetric features accordingly reveal that the Philippine Sea Plate subducts beneath the Eurasian Plate northward along the Ryukyu Trench (Suppe, 1984; Teng, 1996; Hou et al., 2009); in contrast, however, the Philippine Sea Plate overrides the Eurasian Plate along the Manila Trench (Suppe, 1981; Teng, 1990; Lallemand et al., 2001). The movement pattern of the Philippine Sea Plate shows a clockwise rotation (Seno, 1977; Rau et al., 2008), and has led the collision to propagate toward the south (Dadson et al., 2003).

The movement of the tectonic plate leads to a tectonic stress which has caused numerous tectonic faults in Taiwan. Out of these faults, several main ones divide the geological terrains shown in Figure 2-1, e.g., the Longitudinal Valley Fault between the Coastal Range and the Longitudinal Valley, the Lishan Fault between the Central Range and the Hsuehshan Range, the Chaochou Fault between the Central Range and the Coastal Plain, the Chuchih Fault between Hsuehshan Range and the Western Foothills, and the Deformation fronts between the Western Foothills and the Coastal Plain (Lin et al., 2003). The main lithology of each geological terrain is indicated in Figure 2-2, in which the underground structure is revealed as well. The oldest Pre-Tertiary schist is the main lithology of the Central Range, whereas the youngest alluvium exists in the Coastal Plain, Longitudinal Valley, and the Ilan Plain. The Paleogene slate is widespread within the Central Range, Hsuehshan Range, and Western Foothills.

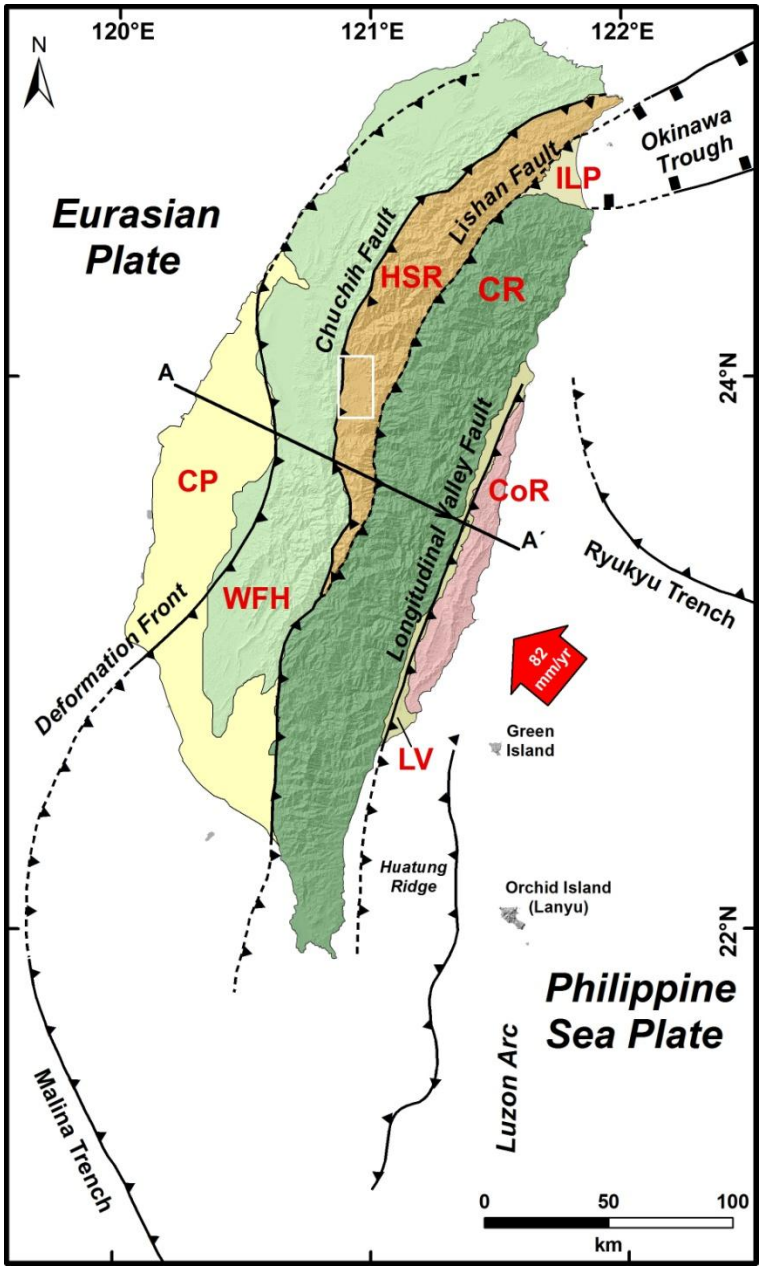

Figure 2-1: Tectonic settings of Taiwan and adjacent region. The Luzon Arc with a rate of 82 mm/a (Yu et al., 1997 and 1999) collides obliquely with the Eurasian Plate and led to the development of the seven geological terrains and diverse bathymetry (Teng, 1990), which are divided by several main tectonic faults. These terrains are: Ilan Plain (IP), Coastal Range (CoR), Longitudinal Valley (LV), Central Range (CR), Hsuehshan Range (HSR), Western Foothills (WFH), and Coastal Plain (CP). The tectonic faults belong to thrusts within the island and their movements bring about uplift of the ground surface, whereas extensional stress leading to the Okinawa Trough, a back-arc rifting basin, is observed offshore to the northeast. The subsidence observed occurs in the Ilan Plain, which is related to the opening of the Okinawa Trough (Ching et al., 2011). The black thick line A-A´ marks the cross-section position of underground structure (cf. Figure 2-2). The white rectangle marks the study area in Figure 2-3.

Earthquakes accordingly occur frequently within Taiwan resulting from the tectonic movements. For example, about 18500 earthquakes per year in average were recorded from 1991 to 2006 by the Central Weather Bureau (CWB) of Taiwan (http://www.cwb.gov.tw). The data also show that there were 49919 earthquakes recorded only during 1999, in which the Chi-Chi earthquake with a magnitude of M_w = 7.6 took place, which was triggered by faulting of the Chelungpu Fault (cf. Chapter 4).

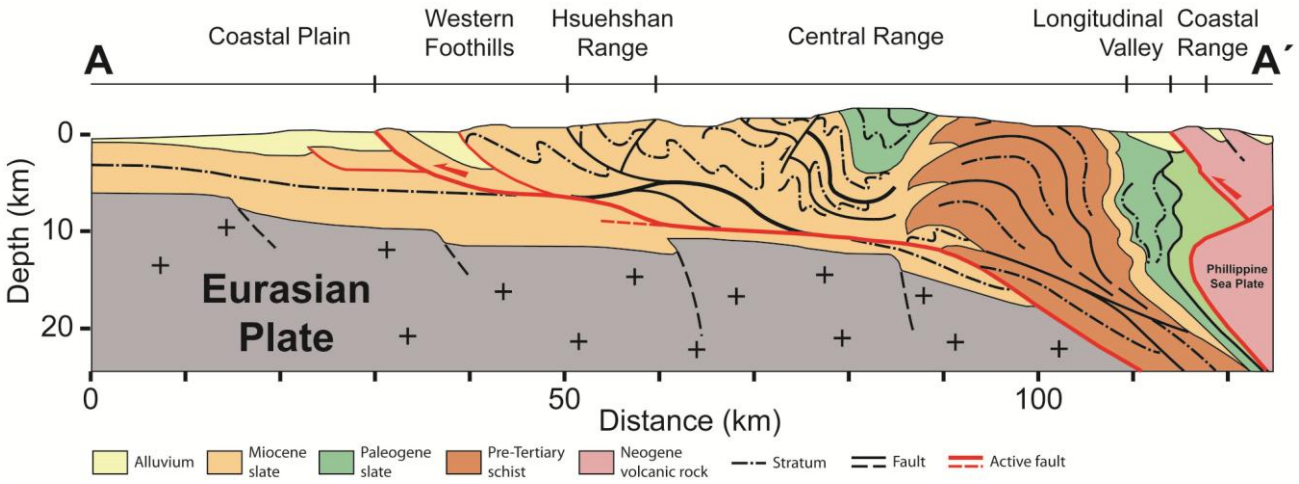

Figure 2-2: Lithology of each geological terrains and underground structure. The position of this cross-section is marked as the black line of A-A´ in Figure 2-1 (modified after Malavieille, 2010). The red solid and thick line marked as an active fault beneath the Hsuehshan Range and Central Range is also termed detachment (i.e., décollement). Movements of the thrusts within the Western Foothills (e.g., the Chelungpu Fault) are proposed to be related to the sliding of the detachment (Chen et al., 2001; cf. Chapter 4).

2.1.2 Uplift and erosion in the Taiwanese orogenic belt

2.1.2.1 Uplift rate

In the tectonic context, the Taiwanese orogenic belt is characterized by active rock uplift (e.g., Willett et al., 2003; Lee et al., 2006). However, owing to the oblique collision between the two tectonic plates, uplift rates differ region by region, and even subsidence of the ground is observed in some areas in Taiwan. For instance, the highest modern uplift rate is estimated 25.8 mm/a in the southern section of the Coastal Range (CoR) by means of leveling measurements and GPS observations (timeframe of the data from 2000 to 2008 by Ching et al., 2011). The same data show that uplift of the mountains is also observed and its modern rates range between 0.2 mm/a and 18.5 mm/a within the interior parts of the Hsuehshan Range and Central Range, and the maximum value is 22.9 mm/a measured in the central northern part of the Central Range (Ching et al., 2011). Subsidence occurs in the coastal plains and coasts of Taiwan, such as present-day rates of 7–20 mm/a in the Ilan Plain (IL), > 15 mm/a in the Coastal Plain (CP) in the southwestern Taiwan, and 5–20.0 mm/a in the northern Coastal Range (Ching et al., 2011). The subsidence of the Ilan Plain is interpreted to reflect the extensional orogenic collapse due to the rapid collision-induced rotation (Ching et al., 2011).

The long-term uplift rates in Taiwan derived from radiometric dating of sediments in fluvial terraces, marine terraces, and boreholes and from mineral cooling rates and fission track are similar to those

of the present-day conditions (e.g., Liu et al., 2001; Hsieh et al., 2004; Liew et al., 2004; Lee et al., 2006; Yang et al., 2007a; Hsieh and Rau, 2009). In the Coastal Range, the Holocene uplift rates are estimated around 10 mm/a (Hsieh et al., 2004; Liew et al., 2004), whereas the subsidence at rates in the Ilan Plain and the southwesternmost coast range from 6–10 mm/a and 6–8 mm/a, respectively (Liew et al., 2004). The uplift rates of the southern Central Range shows inconsistent over the past 6 ma. That is, the uplift rates was slow, i.e., < 1 mm/a, during 6–1 ma and turned much faster, i.e., 4–10 mm/a, from 1 ma to present (Lee et al., 2006). In the eastern Central Range, the uplift rate increased from 7 to 16 mm/a within the past 1.5 ma (Tsao, 1996).

2.1.2.2 Erosion rate

As mentioned above, mountain building in most of the areas in Taiwan is still active by the orogenic processes, so high relief and steepness characterizes the topography. On the other hand, the sub-tropical and tropical climate owing to the geographical position (cf. Section 2-2) causes the ground surface to be influenced by strong weathering. Accordingly, huge amount of regolith is generated and stay temporarily on the hill and mountain slopes, and then this loose material moves downslope by mass wasting processes. High precipitation brought about by typhoons (cf. Section 2-2) and frequent earthquakes in Taiwan reinforce the processes of slope failure and thus increase sediment loads in the rivers in the form of suspended load and bedload (Dadson et al., 2003; Lin et al., 2006). These erosional processes accompanied with tectonic ones control the development of the topography in Taiwan, especially in the mountain areas.

Modern erosion rate is estimated 3.9 mm/a by measuring only the suspended load, and it reaches 5.2 mm/a when including 30% bedload in the rivers in Taiwan, equivalent to 500 Mt/a of sediment yield (data between 1970 and 1999, Dadson et al., 2003). The highest modern erosion rate is observed in the eastern Central Range (6–8 mm/a, Fuller et al., 2006), for this region is subject to higher frequent seismicity and variability in runoff brought by typhoons than others (Dadson et al., 2003). On a million-year scale, the erosion rates are estimated as high as 3–6 mm/a derived from thermochronometric techniques applying to apatite fission track in the eastern Central Range, and 1.5–2-5 mm/a in parts of the Hsuehshan Range and the southern Central Range (Dadson et al., 2003).

River incision rates are in general consistent in the present and the Holocene periods, but still vary in respective regions with different tectonic settings. Decadal river incision rate of 15 mm/a is similar to those on a Holocene scale, 5–12 mm/a, derived from the dating results of organic material deposited on strath terraces (Dadson et al., 2003). By applying the same dating technique, estimated river incision rates of 6 mm/a and 11 mm/a since the late Holocene on river terraces in a

marble gorge in the eastern Taiwan (i.e., the Liwu River) are obtained (Liew, 1988b, cited in Schaller et al., 2005). A cosmogenic nuclide-derived incision rate is estimated 26 ± 3 mm/a since 6.5 ka in the same river catchment. These high river incision rates are interpreted that those rivers flow through areas within which tectonic activities have been or turned to be active (Dadson et al., 2003).

2.2 Geological background in the Puli Basin and the adjacent region

2.2.1 Bedrock

The Puli Basin and Yuchih Basin lie in the southern section of the Hsuehshan Range, within which low-level metamorphic bedrock exposes and is dated from the Eocene to Oligocene (Huang et al., 2000). The Eocene-Oligocene Paileng Formation with a thickness of over 1000 m as the majority of the bedrock in this region, being composed of quartzitic sandstone intercalated with argillite, almost encloses these two basins (Huang et al., 2000). According to the in situ measurements, the Paileng Formation strikes northeast and dips 40–50 degrees toward the east. Only at the northwestern and southeastern edges of the Puli Basin expose the Oligocene Shuichangliu Formation and the Eocene Shihpachunghsi Formation, respectively (Figure 2-3). The Shihpachunghsi Formation and the Tachien Stone extend southward and contact with the eastern edge of the Yuchih Basin. According to the data revealed by seismic reflection (Ke, 2009), the underground bedrock surface in the Puli Basin appears in a disk-like shape (Figure 2-4), which is agreement with the area of sediments in the basin. The seismic reflection data also point out that sediments just overlying the bedrock have the same deformation pattern as the bedrock surface, but the uppermost alluvium (i.e., material of the alluvial plain) remains horizontal without any distortion.

2.2.2 Faults

A reverse fault (i.e., the Tili Fault), exposing in southeastern part of the Puli Basin and through the Yuchih Basin, is the boundary of the Paileng Formation and the Shihpachunghsi Formation. However, the traces of the Tili Fault and another fault in the western part (i.e., Meiyuan Fault) are not observed in unconsolidated sediments but only in the bedrock. This phenomenon indicates that the two faults were not active any more after the alluvium was deposited (Figure 2-3). By integrating other data of seismic reflection and boreholes (Mouthereau et al., 2001), the underground structure beneath the Puli Basin and the further western area is revealed (Figure 2-4). The underground positions and orientations of the faults imply that these faults could connect with a detachment (i.e., décollment) existing as deep as 10 km (Figure 4-5; cf. Chapter 4). Furthermore, this potential detachment system gives a possibility that the Puli Basin and the other basins were formed as piggyback basins. The Taichung Basin in central western Taiwan has been identified to be

a piggyback basin, for the detachment system has developed underground (Kao et al., 2013; cf. Chapter 4).

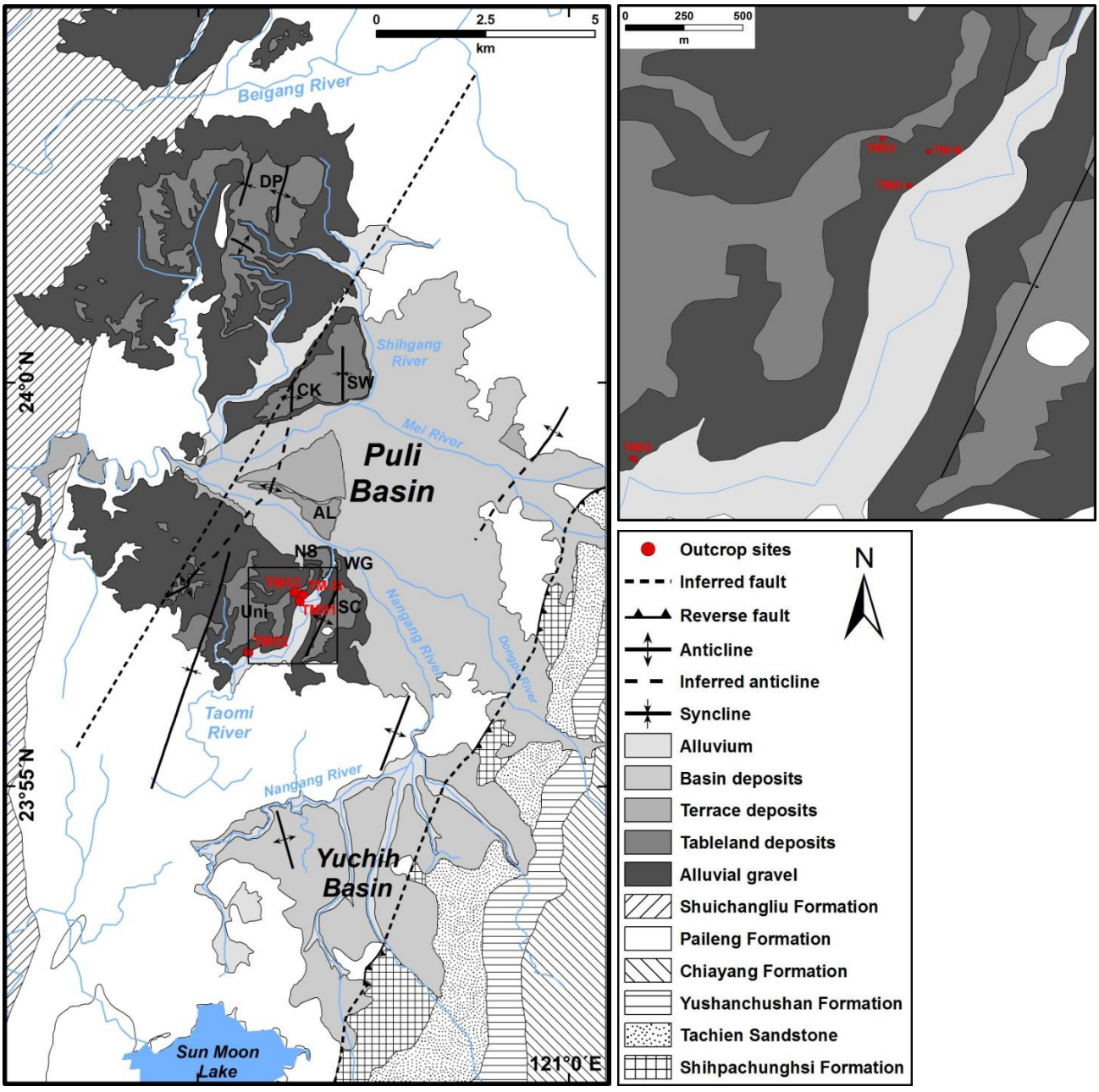

Figure 2-3: Geological settings in the Puli Basin and the adjacent region. Faults and folds are distributed parallel or sub-parallel to each other in NE-SW direction, reflecting a northwestward tectonic stress acting in this region in the past. These geological structures are not observed within the younger landforms, such as the alluvial fan at the valley mouth of the Mei River and alluvium along river channels (after Huang et al., 2000; B.-C. Chen, 2003; M.-M. Chen, 2003; Yang et al., 2007b).

2.2.3 Folds

Folds are distributed parallel or sub-parallel to each other but are only observed within the tablelands in the Puli Basin, whereas the younger landform units are not influenced by the tectonic activities. In the Yuchih Basin, an anticline exists in the western part (B.-C. Chen, 2003). In addition to the folds near the ground surface, the seismic reflection data (Ke, 2009) reveal that three folds also exist within the Paileng Formation underlying the unconsolidated sediments in the Puli Basin (cf. Chapter 4). The three parallel folds, i.e., the Ailan Anticline, Puli Syncline, and the Tanan Anticline (from the west to the east), extent southwards beneath the Yuchih Basin (Huang et al., 2000; Ke, 2009).

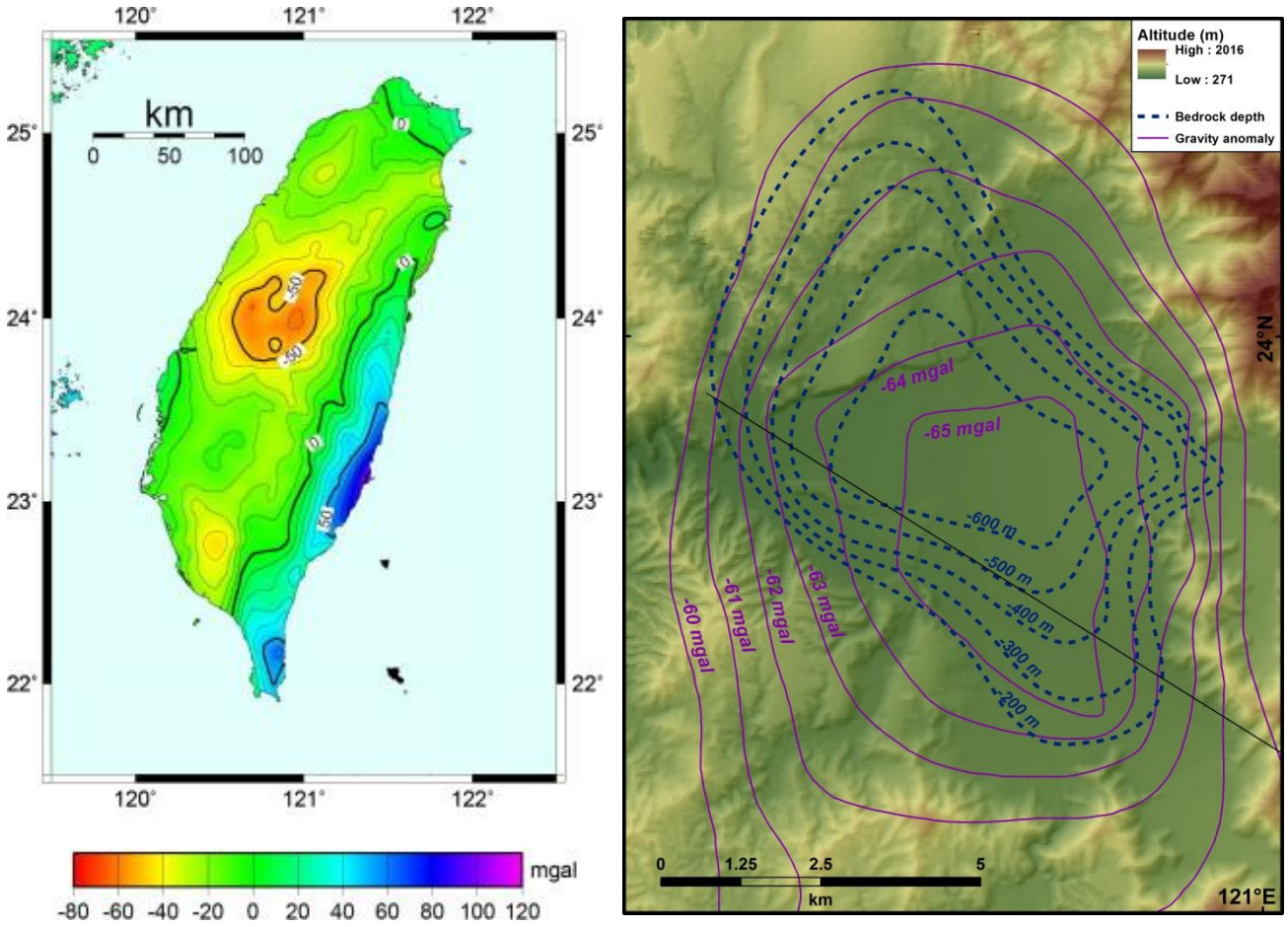

Figure 2-4: Gravity anomaly and depths of the underground bedrock surface in the Puli Basin. The bedrock was curved inward to appear in a disk-like shape, revealed by the seismic reflection (Ke, 2009). This shape is consistent with that of the modern topography in the Puli Basin, inferring that the development of the basin was controlled by past tectonic activities. The location with the lowest value of gravity anomaly is the Puli Basin (left, Yen et al., 1995), indicating that material with low density exist beneath the basin (Lin, 2005).

2.3 Geographical background and geomorphic features

2.3.1 The Taiwan Island

The island of Taiwan is located at the northwestern Pacific Ocean (121°E, 24°N), about 130 km separated from the Eurasian Continent by the Taiwan Strait (Figure 2-5). The East China Sea to the north and the Luzon Strait to the south, divide the Taiwan from Japan and the Philippines, respectively. The Tropic of Cancer (23.5°N) passes through the central southern part of Taiwan, and accordingly two types of modern climatic conditions, humid subtropical and tropical wet and dry, have controlled the climate in the island. At such a geographical position, Taiwan is also influenced by monsoons originating from Siberia in autumns and winters and from the South China Sea in summers. In May and June, high pressures leading to the monsoon create a persistent stationary front (i.e., the Meiyu front), which give weak but continuous rainfall to the island. In addition, typhoons between July and September may bring about strong wind and precipitation as well. Subsequently, the annual average rainfall in Taiwan can be up to 2500 mm (Central Weather Bureau (CWB) of Taiwan, http://www.cwb.gov.tw).

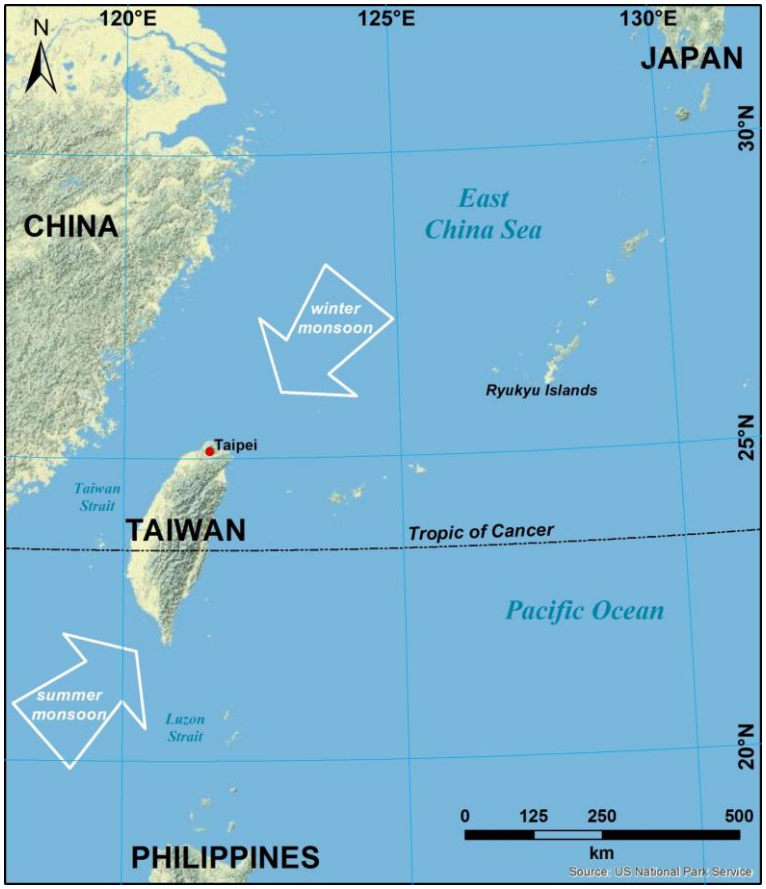

Figure 2-5: Position of Taiwan. Taiwan is located at the northwestern Pacific Ocean, about 130 km from the Eurasian Continent. The geographical position makes Taiwan's climate subject to monsoons, fronts, and typhoons, which bring an average of 2500 mm precipitation every year. Erosional processes resulting from the strong rainfall accordingly have been shaping the topography of Taiwan.

The island is about 400 km long and 150 km wide, with a total area of 36000 km^2. 70% of the area is characterized by rugged mountains and foothills in the central and eastern parts, whereas plains and basins are distributed in the western areas and within mountain ranges. On the basis of topographical features and tectonic settings, seven geological terrains are defined (Figure 2-1; Teng, 1990): Ilan Plain (IP), Coastal Range (CoR), Longitudinal Valley (LV), Central Range (CR), Hsuehshan Range (HSR), Western Foothills (WFH), and Coastal Plain (CP). The highest point (3952 m a.s.l., Yushan or the Jade Mountain) of Taiwan is located in the Central Range, which is also the highest peak in East Asia. Among these geological terrains, the Western Foothills have the most diverse topography. Basins (e.g., the Taipei Basin and Taichung Basin), tablelands (e.g., the Linkou Tableland and Pakua Tableland), alluvial fans, hills, and even volcanoes to the north of the Taipei Basin (i.e., the Tatun volcano group) can be observed (Ho, 1988). Noticeably, a basin group has been formed in the southern section of the Hsuehshan Range in central Taiwan. Within these basins, tablelands (i.e., Puli tablelands), fluvial terraces, alluvial plains, and a lake (i.e., the Sun Moon Lake) are observed as well (Huang et al., 2000).

In Taiwan, the tablelands, i.e., flat elevated lands, are former fluvial terraces, alluvial fans, and sea terraces which were uplifted by tectonic activities and/or then dissected by rivers flowing over (e.g., Teng, 2007). As shown in Figure 2-6, Tomita (1937) distinguished the distributions of tablelands and Lin (1957) afterwards pointed out that sediments comprising the tablelands were deposited as early as in the beginning of the Quaternary. Development of these tablelands are controlled by local tectonic settings (Shih et al., 1996; Delcaillau et al., 1998; Delcaillau, 2001; Chen et al., 2004; Chen et al., 2007; Yang et al., 2007b), such as faulting (e.g., the Linkou Tableland and Pakua Tableland) and crustal uplift (e.g., the Hengchun Tableland and Puli tablelands).

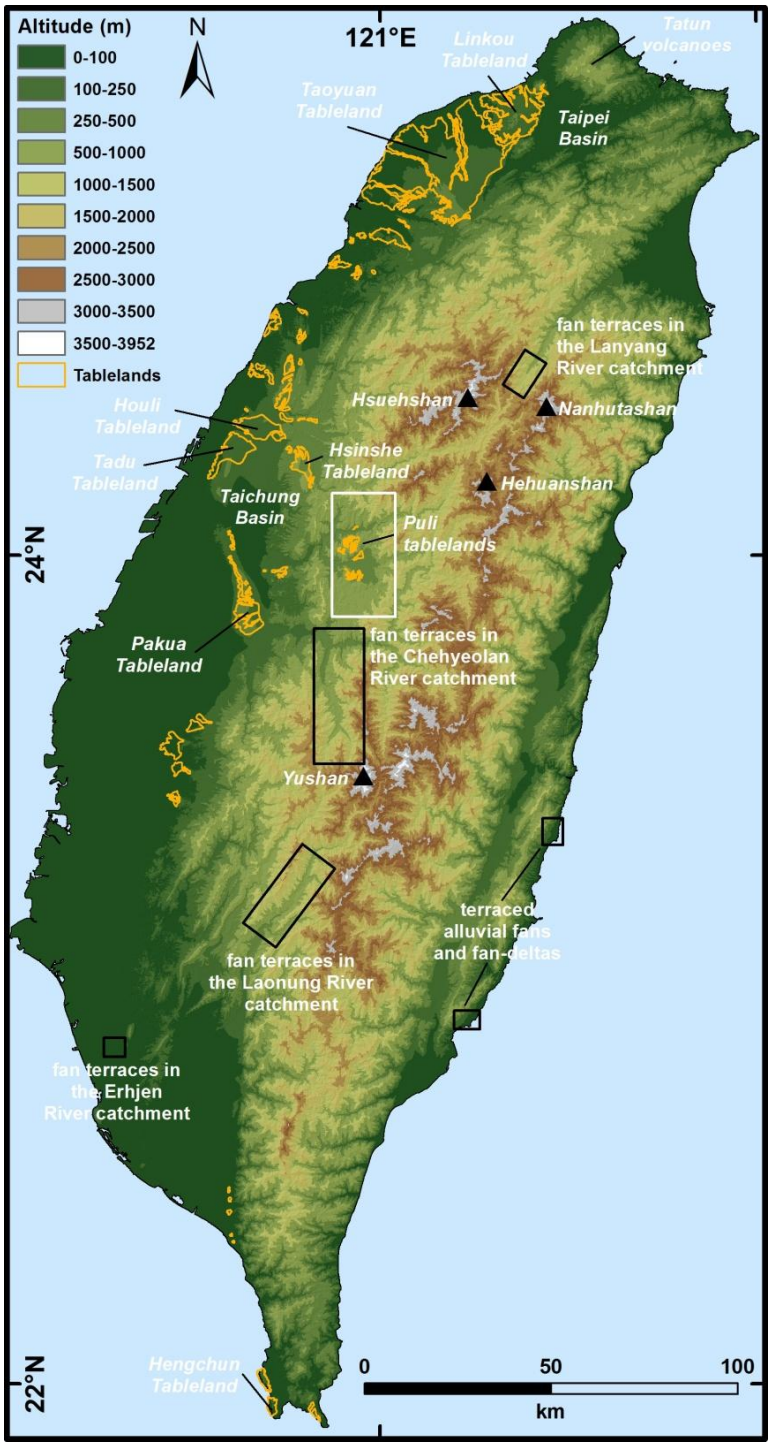

Figure 2-6: Topography of Taiwan. In addition to the complex geological background (cf. Section 2.1), high relief and various geomorphic features characterize the Taiwanese topography. There are more than 100 mountain peaks higher than 3000 m in altitude, e.g., the Yushan (3952 m, black solid triangle), Hsuehshan (3886 m), Nanhutashan (3742 m), and the Hehuanshan (3417 m). 70% of the island is mountain and hill area, and the rest are flat or gently rolling plains in the northern and western parts, on which 90% of the population lives. Some geomorphic units with flat surfaces, such as tablelands and terraces, develop in the Western Foothills, but some of them are also formed in basins (e.g., the Puli Basin) and river valleys (e.g., the Chenyeolan River) in the mountain areas. The white rectangle marks the study area of this work, whereas the black ones indicate regions where fluvial and fan terraces developed along the trunk rivers or at beaches studied by previous research (cf. Chapter 6).

2.3.2 The Puli Basin itself and adjacent region

The Puli Basin and other smaller intramontane basins are located in the center of the Taiwan island (121°E, 24°N; Figures 2-6 and 2-7). The altitudes of the basin surfaces range between 380 m and 830 m a.s.l. (Yang et al., 2007b). The Puli Basin in the northernmost position among these basins has the biggest area (120 km^2) including an alluvial plain and tablelands which have nearly the same size. The following basins in size order are the Yuchih Basin (500–700 m a.s.l.), Sun Moon Lake (750 m a.s.l.), Toushe Basin (650 m a.s.l.), Chungkui Basin (600–620 m a.s.l.). These basins are distributed between the Beigang River to the north and the Jhuoshuei River to the south, aligning up in a NNE-SSW direction parallel to the tectonic setting (Figure 2-1). The Puli Basin together with the Yuchih Basin belongs to the Beigang River system, whereas rivers in the other basins drain into the Jhuoshuei River. Except the Sun Moon Lake, all the basins are drained nowadays. The Yuchih Basin, for example, had not been drained until about 6 ka according to the stratigraphic sequences revealed by borehole analyses (B.-C. Chen, 2003).

The Nangang River originating from the Yuchih Basin and the Mei River coming from the Central Range are the main river systems in the Puli Basin. Together with their tributaries, such as the Taomi River, Dongpu River, and Shihgang River, these two rivers have deposited alluvial deposits in the Puli Basin and Yuchih Basin. Accompanied by tectonic activities, the fluvial processes of these rivers have created various geomorphic features, especially in the Puli Basin. Tablelands, fluvial terraces, alluvial fans, and alluvial plains characterize the topography in the Puli Basin, whereas only terraces and floodplains are observed in the Yuchih Basin (B.-C. Chen, 2003). The natures of the individual geomorphic units are briefly described in the following paragraphs (Figure 2-8).

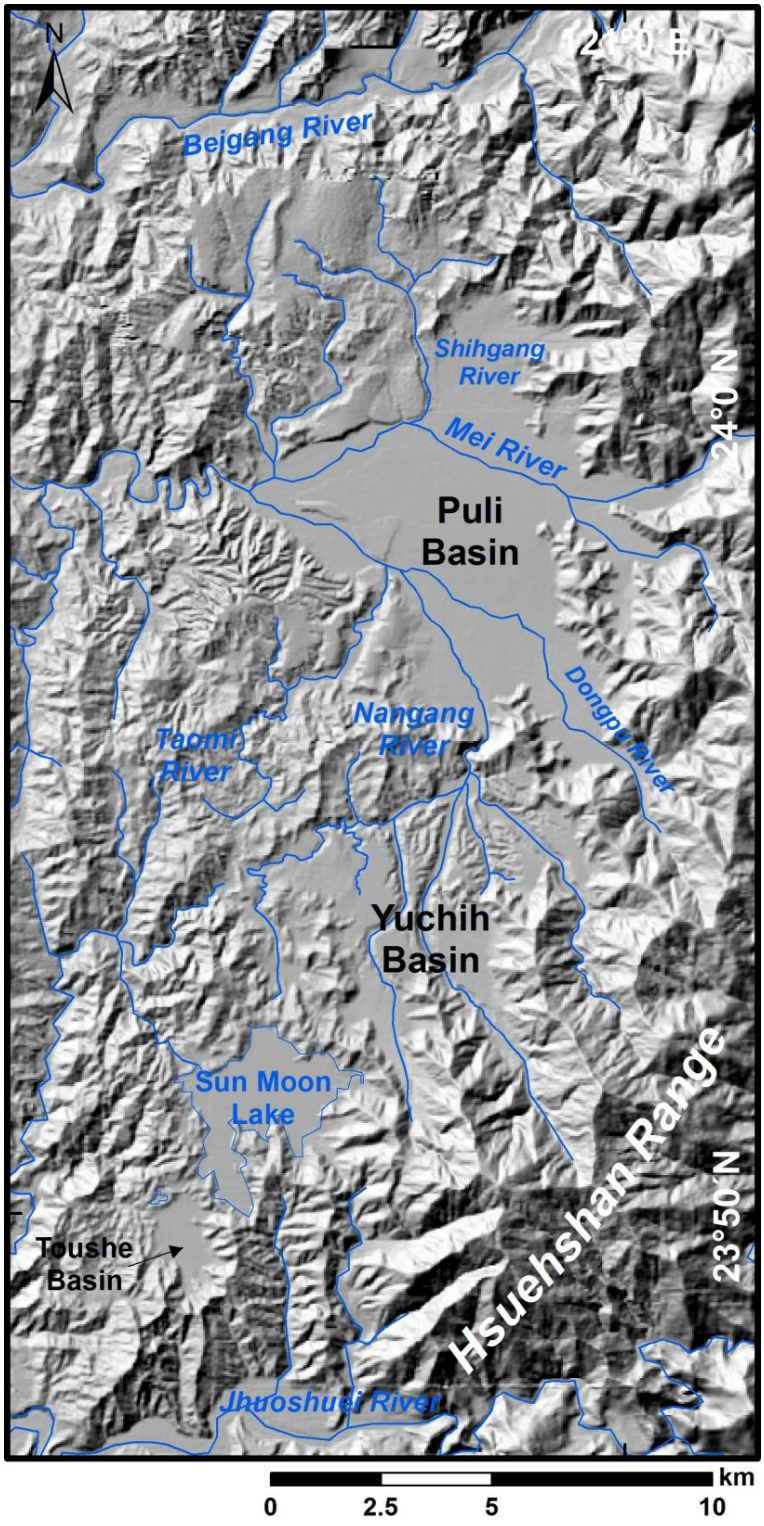

Figure 2-7: Topography of the Puli Basin and adjacent region. Several basins are distributed in the southern section of the Hsuehshan Range, surrounded by the mountains with altitudes over 1000 m a.s.l. on the eastern and western sides, and bounded by the Beigang River and the Jhuoshuei River to the north and south, respectively. The rivers coming from the east and south have deposited sediments which fill the Puli Basin and the Yuchih Basin. Being influenced by both fluvial and tectonic processes, various landforms within the basins have been formed. The resolution of the digital terrain model (right) is 40 m/pixel, generated between 1983 and 1985 by the Ministry of the Interior of Taiwan applying a technique of photogrammetry.

2.3.2.1 Alluvium

The alluvium is observed along river channels, e.g., in the Taomi River and Shihgang River valleys in the Puli Basin, and the Nangang River and other tributaries in the Yuchih Basin. These areas are subject to flood events when heavy precipitation brought about by typhoons during summers and autumns.

2.3.2.2 Alluvial fans

Alluvial fans are observed both in the Puli Basin and Yuchih Basin. They formed at valley mouths of the Mei River (440–500 m a.s.l.) in the eastern part, and of the Nangang River (450–490 m a.s.l.) and Dongpu River (450–570 m a.s.l.) in the southeastern part of the basin (Yang et al., 2007b). In the southern part of the Yuchih Basin, the topography and the sediments at the river mouths also reflect sedimentary environment of alluvial fans.

2.3.2.3 Alluvial plains

The alluvial plains are widespread in the Puli Basin and Yuchih Basin. In the Puli Basin, the lowest point of the alluvial plain is located at the western end of the basin (380 m a.s.l.), where is the confluence of the Nangang River and the Mei River. Dissection of these two rivers is not much into the plain, so the height difference is less than 10 meters.

The alluvial plain is the higher one of the two landform units observed in the Yuchih Basin, and its lowest point is at the northern end of the basin, with a altitude of about 500 m a.s.l. This alluvial plain has been dissected by the rivers and has the height difference of at least 50 m between the plain surfaces and the river beds (B.-C. Chen, 2003).

2.3.2.4 Terraces

The terraces are distributed along the Nangang River and the Mei River in the central and eastern parts of the basin (390–490 m a.s.l.) in the Puli Basin. The height difference between their treads and the modern river beds ranges from 2 to 3 meters (Yang et al., 2007b).

2.3.2.5 Tablelands

The tablelands (420–830 m a.s.l.) in the Puli Basin occupy half of the basin area, and are distributed in the northwestern (e.g., DP tableland) and southeastern (e.g., Uni and SC tablelands) parts of the basin. In the central western part, tablelands with lower altitudes also exist, such as CK, SW, AL, NS, and WG tableland and whose altitudes of the top range between 420 m and 530 m a.s.l. The present tableland surfaces are interpreted as the ancient surfaces of the Puli Basin (Tomita, 1951; M.-M. Chen, 2003). These tablelands had undergone tectonic processes, so that they are deformed and tilted on their surfaces (Yang et al., 2007b).

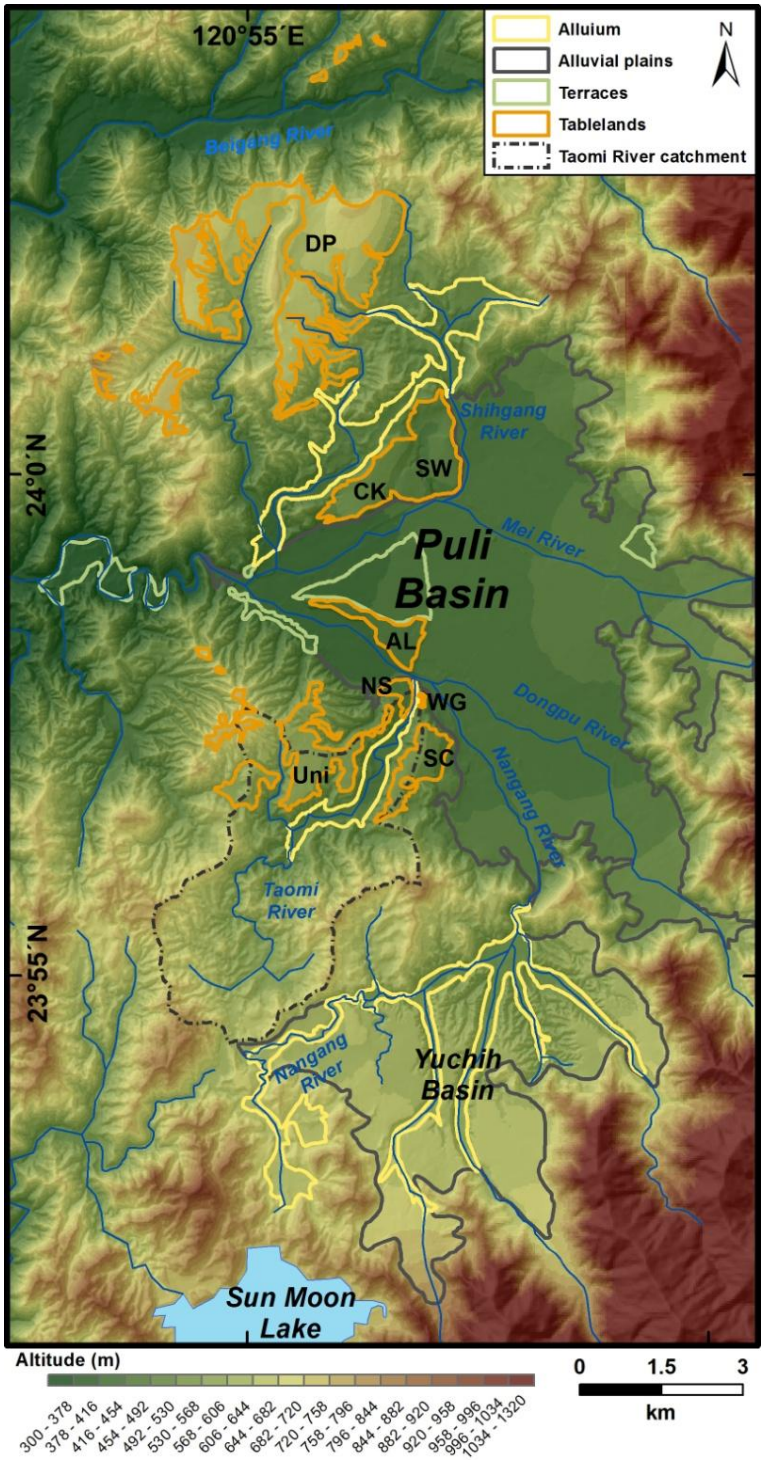

Figure 2-8: Distribution of geomorphic units in the Puli Basin and the Yuchih Basin. Various geomorphic units characterize the topography in the Puli Bain, whereas only two types of landforms are observed in the Yuchih Basin. The Uni and SC tablelands were formed associated with the Taomi River, whose modern catchment area is also marked. The tablelands in the Puli Basin are DP: Dapingding, SW: Shueiwaku, CK: Chihkan, AL: Ailan, NS: Niousiangchu, WG: Wugongku, SC: Shueichiang and Uni: university.

CHAPTER 3
Methods

3.1 Strategy for method utilization in this study

To establish a chronological framework and understand sedimentary processes and topographical features, a number of methods and techniques in need were applied in the field and in laboratories. In this chapter, methods and techniques applied in this study will be introduced and described in general, following a summary of the strategy and procedures.

The strategy and procedure of the methods and techniques are listed as the following contents:

- Necessary information and data of the study area are collected first, such as a geological map, orthophoto base maps and aerial photos.
- A digital terrain model (DTM) with a high resolution (i.e., 2 m/pixel, cf. Section 3.2.1) in the downstream area of the Taomi River is produced (cf. Appendix A3 for the DTM error report), based on which together with the data collected before a field work in the study area is planned.
- Description and record of selected outcrops are made in detailed, including bedding, texture, imbrication direction (for gravel layers), and spatial relationships between respective sediment layers. Samples of studied material are collected for sedimentological analyses (cf. Section 3.2.2) and for dating methods (luminescence dating, cf. Section 3.3 and radiocarbon dating, cf. Section 3.4).
- Grain size analyses and luminescence dating are executed in laboratories at the Leibniz Institute for Applied Geophysics (LIAG) in Hannover, Germany.
- Radiocarbon dating is made in the Poznań Radiocarbon Laboratory, Poland.
- The analyses of minerals and elements are carried out at the Freie Universität Berlin in Berlin, Germany.

3.2 Utilized techniques and field work

3.2.1 Geological map and orthophoto base maps interpretation, digital terrain model

To understand the topography and geological settings in the Puli area before field work, a geological map in a scale of 1:25000 (Huang et al., 2000) was analyzed. The geological map, on which contour lines with 20 m interval are presented, shows positions and distributions of sediments and bedrock as well as traces of faults and folds existing in the region. However, the geological map has been published for over ten years, so the present topographical conditions in the field may have changed

due to human activities or natural hazards (e.g., landslides). Therefore, latest orthophoto base maps (issued by the Aerial Survey office, Forestry Bureau of Taiwan in 2009) were also used for a reference to make a plan of field work. The orthophoto base maps with a scale of 1:5000 are aerial photos which have been orthorectified to correct geometric distortion, to provide the information of roads and paths, vegetation, and outcrops in a bird's eye view.

A self-generated digital terrain model (DTM) with a 2 m horizontal resolution of a small region within the study area was also applied for landform analyses. By calculation in a program module (Leica, 2006, cf. Chapter 5), the relief of the ground can be extracted and digitalized based on stereo-pairs of aerial photos, the same as those for the generation of the orthophotos. With this high resolution DTM, small-scaled landform features can be revealed (cf. Chapter 5).

The outcrops were positioned by means of the Global Positioning System (GPS). The coordinate system adopted is the Universal Transverse Mercator Projection System (UTM). The unit of this system is meter, so it is convenient to estimate distances and sizes of the studied outcrops and geomorphic features. A DTM with a 20 m horizontal resolution generated by the Ministry of Interior of Taiwan was also analyzed, with which locations of the outcrops were cross-checked. In addition, this DTM was applied to analyze possible fluvial avulsion, sizes of river valleys, ranges of geomorphic units, and landform disturbance in the Puli Basin and Yuchih Basin. In Chapter 6 of this paper, parts of the results based on the DTM are shown.

3.2.2 Sedimentological analyses

The sedimentological analyses of the outcrops were executed on site and in laboratories. In the field, each studied outcrop was photographed and sketched. Its basic natures, including thickness, depth, lateral extension, stratigraphic sequences were recorded. For a sediment unit, its bedding was measured with a clinometer, and color (humid condition) of fine-grained fractions (e.g., matrix) was described by comparing with the Munsell Color Chart (Munsell Color, 1992). Sorting and roundness of the coarse-grained fractions (e.g., clast) were classified according to the criteria (Powers, 1953; Anstey and Chase, 1974). Imbrication directions of long axis of clasts (e.g., Figure 7.4 of Charlton, 2010) which point out paleocurrent directions are also recorded.

Samples of studied sediments including clast and matrix parts were taken for further sedimentological analyses in laboratories: grain size distribution (< 2 mm), mineralogical composition and element concentration. The former is intended to understand possible sedimentary environments, and the latter is to find out potential sources of the sediments. Before the grain size analysis, samples smaller than 2 mm in diameter (after dry sieving) were immersed in aqua ammoniae (NH_4OH) and stirred thoroughly for at least 12 hours to separate grain clusters.

Afterwards, the samples were measured with a Beckman and Coulter ISO 13320 (Aqueous Liquid Module 2824) laser diffraction particle size analyzer in the LIAG. Analysis results were then classified into 116 fractions, which were converted into a standardized grain-size classification according to FAO (2006). For the mineral and element determinations, sediment samples were first ground into powder with a mortar and pestle or an automatic grinding machine. The prepared samples were then dried at 150 °C for one day. To determine the mineralogical composition of sediments, a XRD (X-ray diffraction) Rigaku Minflex 600 was applied. For the element analysis, an ICP-OES 2100 DV Perkin Elmer (inductively coupled plasma optical emission spectrometer) was used. The two analyses were done at the Freie Universität Berlin. The results of the sedimentological analyses are stated in Chapter 5 of this dissertation.

3.3 Burial ages of sediments determined by optically stimulated luminescence (OSL) dating

3.3.1 Introduction

Optically stimulated luminescence dating (OSL) has been applied to estimate approximate deposition timing of sediments in geomorphological research. In contrast to radiocarbon dating, the OSL dating methods can determine burial ages directly from various fluvial sediments, including floodplain deposits, alluvial fans, and terraces (Rodnight et al., 2006; Chen et al., 2009). With this dating method, geochronology of the studied sediments deposited by different fluvial processes in the Puli Basin can be established.

Detailed technical specifications of the luminescence dating will not be discussed in this study, for they are far beyond the scope of this study. Aitken (1985), Aitken (1998), Murray and Olley (2002), and Preusser et al. (2008) have published monographs and papers to depict the basics of the techniques. In this section, general introductions to the concepts and principles will be briefly described. In addition, emphases on sampling skills and uncertainties of ages will also be put in the latter sections. The results of OSL dating from this work are presented and discussed in Chapters 5 and 6.

3.3.2 Principles and sampling

Luminescence phenomena are observed commonly in natural minerals, after the minerals are exposed to radiation released by radioactive decay. A proportion of energy transferred by the radiation will excite electrons in the crystal from an energy level to a higher one. The energy absorbed by minerals is stored within the crystal lattice of the minerals, and accumulates as the radioactive decay continues over time. After some time intervals, the energy stored can be released

again by some forms of energy exerted externally. In some minerals, e.g., quartz and feldspars, the energy is released in the form of light, which is called luminescence. There are two common forms of energy exerted externally to generate the luminescence, i.e., heat and light. The luminescence stimulated by heat is termed thermoluminescence (TL), and that stimulated by light is optically stimulated luminescence (OSL). By measuring the luminescence signals, the total amount of radiation (or energy) absorbed by the minerals during burial can be calculated. When this energy is divided by the amount of energy which the minerals receive from surrounding radioactive elements or isotopes each year, then the burial age of the minerals can be determined. This can be expressed by the following relationship:

$$\text{age (a)} = \frac{\text{total energy accumulated during burial (Gy)}}{\text{energy received each year from surroundings (Gy/a)}}$$

The Gy (i.e., Gray) in the above relationship is the SI (Système International) unit of absorbed radiation. This measure is also known as dose. It is defined as unit joules per kilogram (J/kg). The total energy or dose during burial of a sample can be calculated in laboratories, and the dose estimated is termed equivalent dose (D_e). The energy received each year is the dose rate in the environment, which can be derived by measuring the surrounding concentrations of radioactive isotopes, such as uranium (U), thorium (Th), and potassium (K), applying ICP-MS (inductively coupled plasma mass spectrometry) analyses (cf. Chapters 5 and 6). In addition to radioactive isotopes, cosmogenic radiation also contributes to a part of the environment dose rate (Prescott and Hutton, 1988; Olley et al., 1996). Depending on different positions (e.g., latitudes, depths), the amount of cosmic ray which sediments have received varies (Prescott and Hutton, 1994). The age of quartz estimated by the OSL can be up to 500 ka (Murray and Wintle, 2003).

Material for OSL dating must be avoided from exposure to the sun light, for the sun light possesses radiation with high energy which can release all luminescence in minerals. This process that zeros the luminescence signals in minerals is termed bleaching or resetting. Therefore, samples of the studied sediments must be preserved in dark condition all the time before being processed in laboratories. Before sampling, at least 20 cm thick outer material of studied sediments should be removed first, because it has been exposed to the sun light. Afterwards, an opaque plastic or stainless steel tube with one end sealed is horizontally hammered into the sediments until it is almost entirely buried. In this study, 5 x 20 cm stainless steel tube is used for fine-grained material (e.g., TM01-A, TM01-B, TM01-S, TM02-B, TM02-E, and TM02-F). For gravel sediments (e.g., TM02-A and TM03-A), 10 x 20 cm ones are applied for collecting enough fine-grained matrix. Once the tubes

are taken out from the sediment layer, aluminum foil and opaque tapes are used to seal the ends of the tubes. In the end, 1 kilogram sediment surrounding the tubes is collected for the dose rate measurements and water content estimation.

3.3.3 Applied measurement protocol, and equivalent dose (D_e) and dose rate determination

The measurement protocol applied in this study to estimate the D_e of quartz is the single-aliquot regenerative-dose (SAR, Murray and Wintle, 2000; Murray and Wintle, 2003). The SAR procedure is used routinely because it appears to give accurate results for dating quartz if it is applied correctly. An aliquot means a small sub-sample of quartz. In the SAR protocol, each aliquot is repeatedly measured for several cycles to avoid the problems with luminescence properties of individual quartz grains in different aliquots.

Quartz grains mounted on a small (around 1 cm in diameter) stainless steel disk (i.e., an aliquot) are exposed to blue light (470 nm) with different doses in each measurement cycle. Luminescence signals stimulated by the blue light are then counted by a photomultiplier tube (Murray and Wintle, 2003; Preusser et al., 2008). When all the measurement cycles are complete, a dose response curve of each aliquot is then generated. By calculating, a D_e value for the aliquot measured is then determined. A number of D_es from different aliquots present a D_e distribution, which will further be calculated statistically (cf. Chapters 5 and 6) to give a reliable D_e value for the studied sediment.

To determine the dose rate, a separate sample from the direct surroundings of the luminescence sample is collected in the field. This has to be dried first. Afterwards, 700 g of the dried sediment is sealed and stored in an air tight Marinelli-beaker for at least one month to obtain ^{222}Rn equilibrium. Then high-resolution gamma-ray spectroscopy using a High-Purity Germanium N-Type coaxial detector is applied to determine the radionuclide content of a sample.

3.3.4 Applications of OSL to fluvial sediments and its uncertainties

For fluvial sediments, the D_e distribution usually appears scattered and skewed toward higher D_e values when it is expressed in a histogram (Wallinga, 2002). This phenomenon is interpreted that during sediment transport in rivers, mineral grains are not sufficiently exposed to sunlight, so that their luminescence signal is incompletely reset (Olley et al., 1998; Olley et al., 1999; Wallinga, 2002). Incomplete bleaching of mineral grains generates higher D_e values and accordingly overestimates the burial ages of sediments. Therefore, uncertainties of the OSL age of fluvial sediments are usually higher than those (i.e., 5–10%, Murray and Olley, 2002) of well-bleached mineral grains (Forman et al., 1988). To observe well-bleached mineral grains of fluvial sediments, single-grain OSL measurements are suggested (Wallinga, 2002). The reason is that single mineral grains are the

smallest unit during transport in rivers. However, the single-grain OSL measurements using a laser stimulation system require more aliquots (n = 100), and are hence time consuming. Thus, a smaller aliquot size (i.e., tens of grains per aliquot) could be a proper choice, since it yields similar results to those of the single-grain measurements (Duller, 2008).

3.4 Age of organic material estimated by radiocarbon dating

To cross-check the burial ages of the sediments derived from the OSL dating, organic material (i.e., charcoal fragments in this study, TM-C) sampled within the same sediment layer (i.e., TM01-A) was dated by applying the radiocarbon dating. Carbon (C) and its isotopes (i.e., ^{12}C, ^{13}C, and ^{14}C) are part of any organic material. As soon as the organic material is dead, or does not exchange the carbon isotopes with those in the atmosphere (e.g., through respiration or photosynthesis), the decay of the radioactive ^{14}C with the half-life of 5730 years starts. By calculating the amount of ^{14}C inside the organic material, the time when it became dead can be estimated. The present dating limit is up to 62000 years before present (Plastino et al., 2001).

The dating measurements were executed in the Poznań Radiocarbon Laboratory in Poland. The detailed sample preparations and measurement procedures are described in Chapter 5, as well as the dating results. It has to be emphasized that the age of organic material derived from the radiocarbon dating can only represent a maximum deposition timing of the studied sediments. The reason is that the organic material could have not been alive before it was transported to the deposition site. In this study, the burial ages of the studied sediments are well in agreement with that derived from the radiocarbon dating, so the timing of sediment formation is reliable.

CHAPTER 4
Genesis, sedimentary sequence and landform development of the Puli Basin

In this chapter, information of the genesis, sedimentary sequences and landform development of the Puli Basin will first be presented by reviewing earlier studies applying different methods. Second, on the basis of previous research and the investigations in the field, these issues will be discussed and resultant new viewpoints will also be proposed.

4.1 Genesis of the Puli Basin

In the 1930s, Japanese researchers (e.g., Hayasaka, 1930; Tomita, 1951) started to study the Puli Basin and the other intramontane basins. Afterwards, with the advances of various methods (e.g., global positioning systems, gravity surveys and seismic reflection), the genesis of the Puli Basin has been a significant research topic, and some different perspectives have been proposed since the past three decades. According to the results of the earlier studies, the genetic mechanisms of the Puli Basin comprise three main processes: (1) faulting and downwarping (Hayasaka, 1930; Tomita, 1951; Lin, 1957; Ke, 2009); (2) strike-slip faulting (Biq, 1989; Lu and Malavieille, 1994; Lu et al., 1997; Lu et al., 2002); and (3) detachment movements (Wilcox et al., 2011). However, because these mechanisms differ fundamentally regarding the directions of tectonic stress controlling the growth of the basin, they were examined by means of geodetic and geophysical methods (e.g., global positioning system (GPS) applied by Chen et al., 2001 and seismic reflection by Wang et al., 2002).

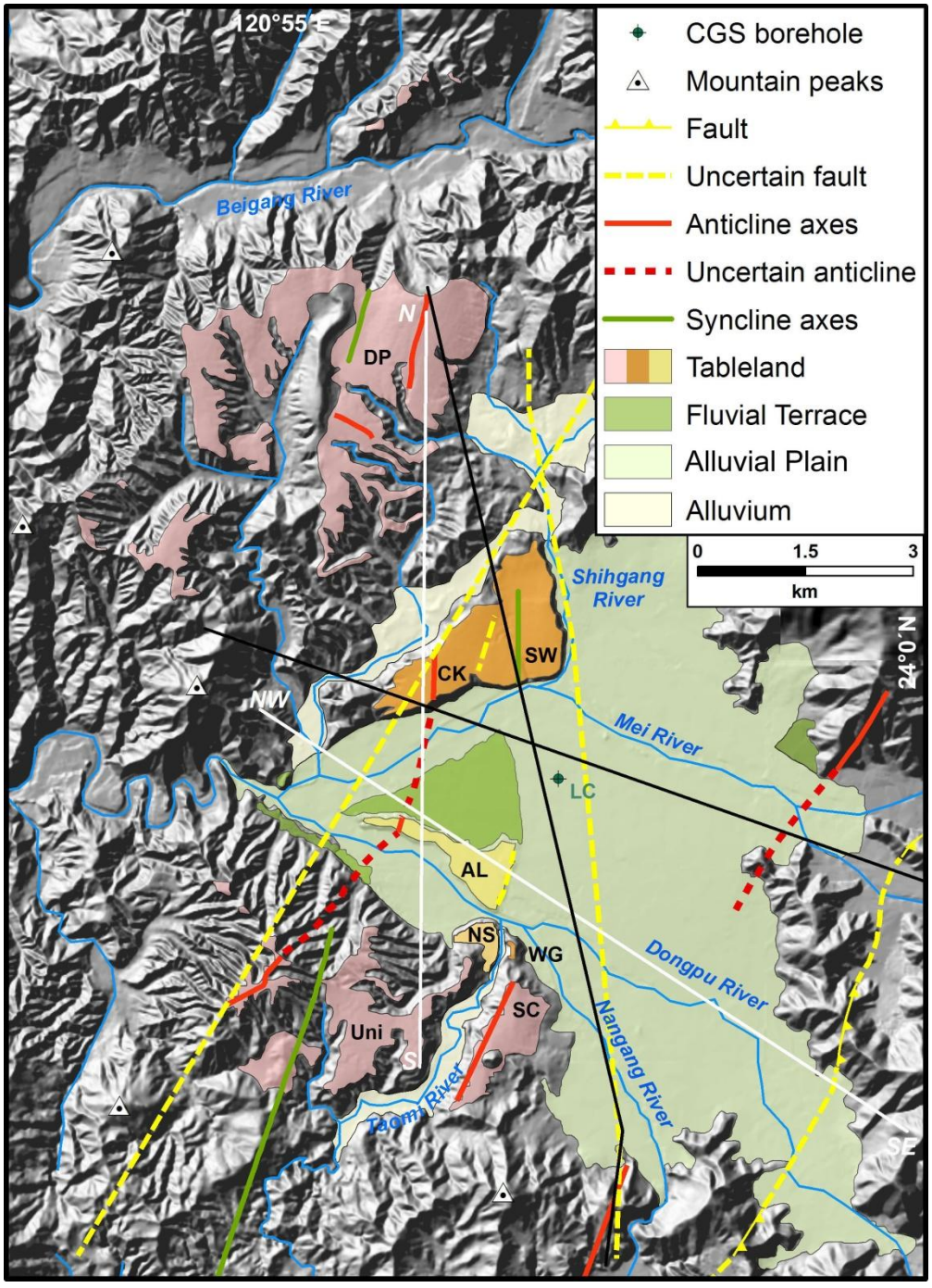

Figure 4-1: Geomorphic units and tectonic setting in the Puli area. The DTM has a resolution of 20 m/pixel, being produced by the Ministry of the Interior of Taiwan. These geomorphic units differentiate mainly from their material and heights, reflecting results of fluvial and tectonic processes in the past (according to data from Huang et al., 2000 and Yang et al., 2007b). The two black lines are the cross-section profiles shown in Figure 4-3. The two white straight lines represent the profile of the geomorphic evolution model shown in Figure 4-14. The local names of the tablelands are: DP: Dapingding, SW: Shueiwaku, CK: Chihkan, AL: Ailan, NS: Niousiangchu, WG: Wugongku, SC: Shueichiang and Uni: university. LC: Lancheng, the name of the borehole made by the CGS (Central Geological Survey of Taiwan).

4.1.1 Faulting and Downwarping

Downwarping is a process in which a stratum or a formation is bent downward to become a depression or syncline, respectively. Hayasaka (1930) first investigated the Puli region and thought that faulting first led to the depression. Afterwards, this depression was then down warped to become the present-day concave landform. Tomita (1951) found that the surfaces of the northwestern (DP and CK) and the southwestern tablelands (i.e., Uni and SC) tilted toward the east, and the hill slope on the eastern margin of the basin faces toward the west (Figure 4-1). Therefore, Tomita inferred that downwarping created a disk-like shape of the Puli Basin and the recent topography. Lin (1957) made detailed descriptions of the geomorphic features in the Puli region. He not only thought that either downwarping or faulting was the genetic mechanism of the Puli Basin, but also proposed the possible period of the Early Pleistocene when the Puli Basin was formed, by comparing and correlating spatial relationships among the sediments. Huang (1978) applied geomorphologic quantitative analyses to study the northwestern tablelands (i.e., DP and CK). He used parameters such as height and relief to obtain characteristics of the tableland topography by means of quantification and statistical analysis. Huang also analyzed inclinations, types, and patterns of the slopes in this area. With these results, he distinguished the DP and CK tablelands into different geomorphic surfaces according to height. He then proposed that downwarping after formation of the DP and CK tablelands had caused an inclination towards the basin center. Yang et al. (2007b) estimated a vertical surface displacement of the Uni tableland by about 180 m and suggested that it resulted from tectonic activities (Figure 4-2).

Figure 4-2: The Uni and SC tablelands. The height difference of about 180 m (Yang et al., 2007b) of the Uni tableland surface is thought to result from downwarping (Tomita, 1951). The SC tableland is even lower than the Uni tableland across the Taomi River, reflecting ground subsidence of the land to the east of the tablelands.

To understand the underground material properties and structures, Chen (1984) first applied geoelectric resistivity method in the Puli Basin. His results show that a normal fault possibly exists under the unconsolidated sediments in the southeastern part of the basin. Yen et al. (1995) measured a lower gravity anomaly in Taichung and the Puli region in central Taiwan. The gravity anomaly value in the center of the Puli Basin is about -66 mgal, whereas it is about -60 mgal on the edge of the basin (Figure 2-4). This phenomenon shows that the underground structures have a concave form.

High-resolution shallow seismic reflection showed distinct underground structures in the Puli Basin (Wang et al., 2002). According to their results, the bedrock is at 400–600 m below the surface, and an anticline is observed in the bedrock. Huang (2008) improved the results, showing that there are two anticlines and one syncline within the bedrock. In addition, he also proposed that sediments just above the bedrock have the same deformation pattern as the bedrock surface, whereas the upper ones (i.e., sediments of the alluvial plain) appear horizontal. Ke's (2009) N-S and E-W seismic reflection profiles further show that the underground bedrock surface has the shape of a disk, and the deepest point is about 720 m below the surface in the center of the basin (Figure 4-3). In addition, his results show that no normal fault as inferred by Chen (1984) exists in the bedrock. Accordingly, he proposed that downwarping caused by the compressional stress was the genetic mechanism forming the Puli Basin.

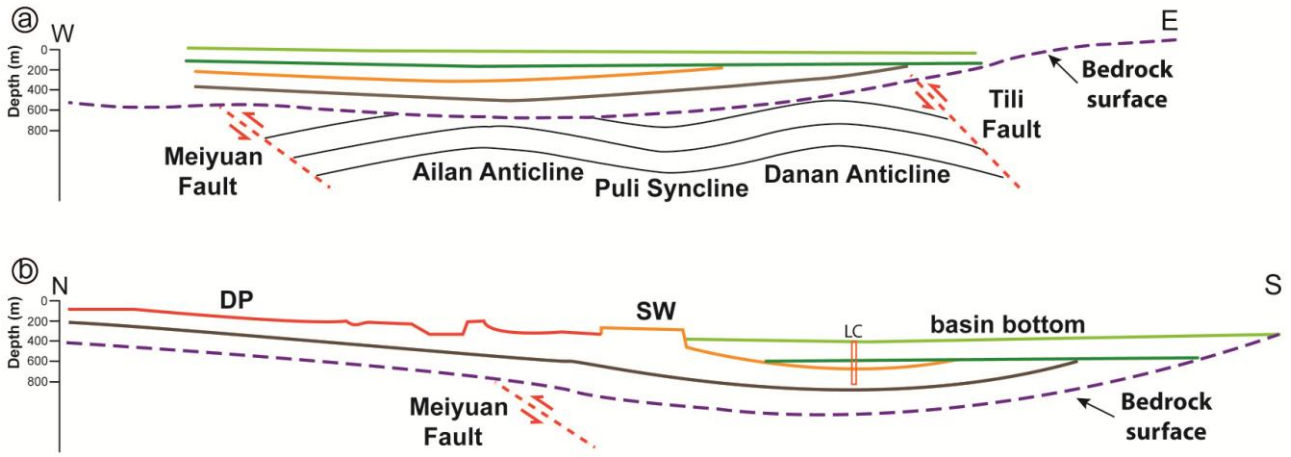

Figure 4-3: E-W and N-S profiles of the underground structures of the Puli Basin. Being derived from seismic reflection, the green lines represent the younger unconsolidated sediments in the basin center, unconformably overlying the gravel layer bounded by the orange/red line and the dashed line. The length and position of the CGS borehole (LC) are also shown (modified after Ke, 2009).

4.1.2 Strike-slip faulting

Shear stress resulting from the oblique collision between the tectonic plates has also been taken into consideration to explain the possible genetic mechanism of the intramontane basins in central Taiwan. Biq (1989) assumed that a large amount of strain accumulated in the Yushan-Hsuehshan Zone, which is a megashear zone through the highest part of Taiwan. This shear stress was released to trigger parallel thrusts with a left-lateral component and then strike-slip faulting occurred. Therefore, grabens were generated when the strata were pulled apart by the N-S extensional stress caused by the movements of parallel thrusts on the eastern and western sides of the Puli Basin (Figure 4-4). Lu et al. (1997) also suggested that thrust was the main strain pattern in the Hsuehshan Range at the beginning of the orogeny. Afterwards, this pattern turned into transtension in the later stage of the plate collision. Accordingly, they also proposed that a graben origin resulting from strike-slip faults was the genetic mechanism of the intramontane basins. Lu and Malavieille (1994) and Lu et al. (2002) argued the same concept that the Puli Basin is a pull-apart basin formed in a strike-slip shear zone.

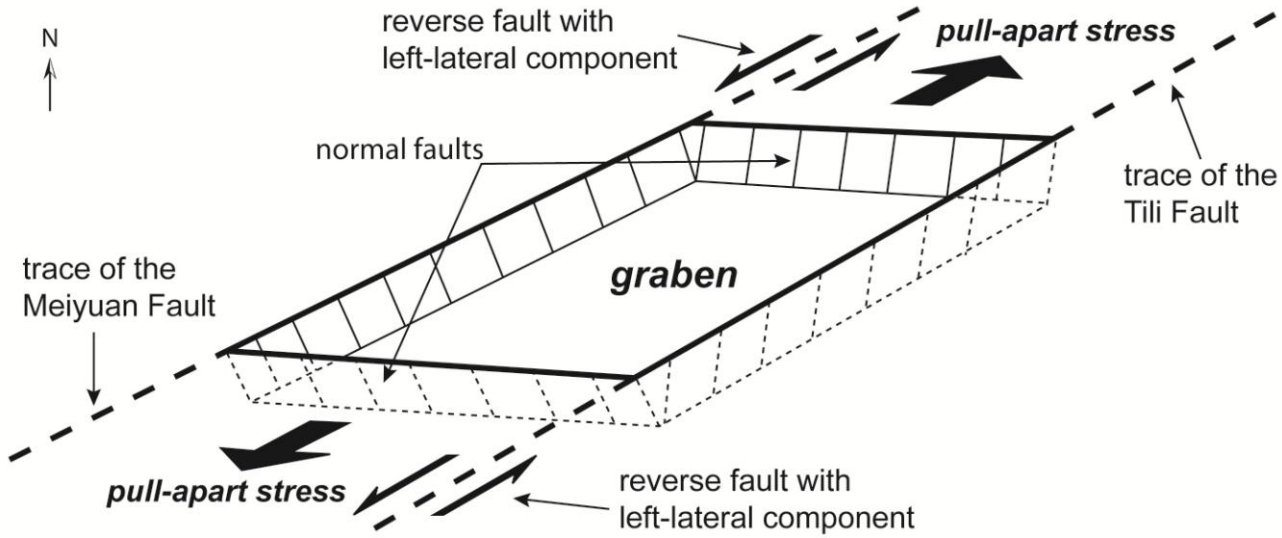

Figure 4-4: Graben structure proposed as the genesis of the Puli Basin. A tectonic graben is formed by activities of strike-slip faults and normal faults. The Tili Fault and Meiyuan Fault were assumed to have left-lateral component of slip due to the change in the tectonic stress patterns. However, normal faults which should also exist to induce sinking of the ground are not detected.

B.-C. Chen (2003) studied the deformation and displacement of the geomorphic units in the Puli Basin and proposed possible tectonic structures and activities. He considered that a north-south left-lateral strike-slip fault along the Shihgang River caused the dislocation of the old channels, and

led to ground subsidence east of the fault as well. He assumed this potential fault extends through the basin to the Yuchih Basin (Figure 4-1). Besides, Chen also defined a ramp on the eastern limb of the CK Anticline as a fault scarp, as well as the eastern scarp of the AL tableland, and suggested that these scarps could result from faulting within the basin. On the basis of these observations, he proposed that stress with E-W compression and N-S extension created the Puli Basin and the other intramontane basins.

4.1.3 Detachment movements

Chu (1991) analyzed the stress direction (NW-SE) of faulting in the early Tertiary bedrock near the Puli Basin. His results show that the hanging wall above thrusts was uplifted in the Western Foothills (WFH), and the back area became a relative depression, the location of the Puli Basin. Such a depression is called a piggyback basin (Ori and Friend, 1984; Kao et al., 2013). Wilcox et al. (2011) proposed the Puli Basin to be a piggyback basin, probably formed between 700 ka and 500 ka according to the slip restoration along the Chelungpu Fault and the Shuangdong Fault and an assumption of about 45 mm/a shortening across the WFH (Figure 4-5). Interpreting the results of GPS measurements of the coseismic uplift in the front of the WFH caused by the 1999 Chi-Chi earthquake (M_w = 7.6) in central Taiwan, Chen et al. (2001) proposed ramp structures beneath the WFH and the CR (Central Range). These ramps, together with the Shuangdong Fault and the Shueilikeng Fault (about 10 and 5 km west of the Puli region, respectively) reconstructed by seismic reflection (Chiu, 1971; Suppe, 1986) possibly connect a detachment (i.e., décollement) about 5 km beneath the Puli Basin surface (Yue et al., 2005). Therefore, detachment movements are considered to be associated with the genetic mechanism of the Puli Basin and the other intramontane basins.

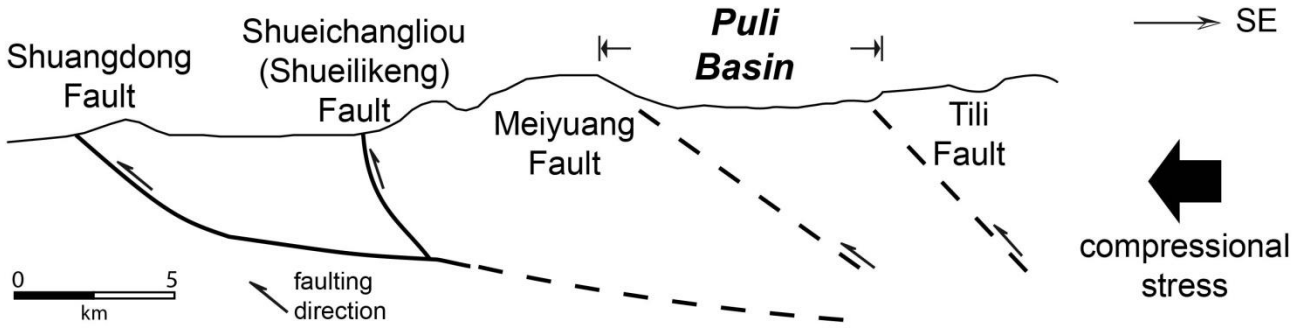

Figure 4-5: Underground positions and orientation of reverse faults beneath the Puli Basin and the further western region. The compressional stress caused by the plate convergence had led to the reverse faulting in this region. This underground structure is inferred to be related to a detachment system (Chen et al., 2001). Wilcox et al. (2011) assume that the Puli Basin was formed as a piggyback basin by such a detachment system, which is also the genetic mechanism for the Taichung Basin.

4.2 Sedimentary sequence and relative timing

The distribution and types of sediments in the basin were described (Hayasaka, 1930; Tomita, 1951; Shih et al., 1996; B.-C. Chen, 2003; M.-M. Chen, 2003; Yang et al., 2007b). Although lacustrine sediments are observed within the sedimentary sequence, the assumption of a lake that filled the basin in the past is not a consensus among these studies. Hence, more evidence is required (e.g., more exposures and compositions of the sediments) to clarify this question. The sediments in the Puli Basin were deposited in three periods which are characterized by sedimentary facies differing from those in the other periods. In this section, the characteristics of these sedimentary facies will be delineated chronologically and then their potential formation time in the sedimentary sequence will be established.

4.2.1 Sedimentary facies

4.2.1.1 Fluvial and lacustrine deposits

Hayasaka (1930) and Tomita (1951) assumed that rivers flowed into the Puli Basin after it was formed, causing a lake to fill the basin owing to a lack of outlets. The oldest sediment, clay material, interbedded with lignites and fine sands in some places, was then deposited. An exposure of the clay material with a thickness up to 100 m was found on the southern bank of the Beigang River by Tomita (1951). He observed that the clay layer with a bedding of about 20° dipping toward the east overlies the bedrock. Shih et al. (1996) obtained similar results to those of Tomita (1951) from the survey of the exposure on the northern edge of the DP tableland and estimated a thickness of 130 m for the clay layer. However, this clay layer was not observed and reported in recent studies (e.g., B.-C. Chen (2003), M.-M. Chen (2003) and Yang et al. (2007b), probably owing to a dense vegetation cover or retaining wall.

Tomita (1951) also pointed out that a stratified gravel layer, with a grain size of 5−8 cm, was deposited above the clay material as the basin was depressed again, inducing stronger stream power. The lake was hence filled with gravel and then was drained. B.-C. Chen (2003) also observed exposures of thin to massive sand layers as intercalations of the gravel and interpreted this sedimentary facies as the depositional conditions of a braided river. Lin (1957) proposed that this fluvial gravel layer could be correlated with the Toukoshan gravel formed in the Middle Pleistocene.

Lu (1959) and Chou (1981) investigated coal and clay deposits in the Puli and Yuchih Basin areas and defined three groups of the sediments based on field observation. The groups are (from bottom to top): lower gravel with interbedded clay, clay with interbedded sand, and upper gravel. In the southern part of the DP tableland, B.-C. Chen (2003) and M.-M. Chen (2003) found an exposure of

lacustrine sediments (about 450 m a.s.l.) around 5 m above the bedrock in a river valley and described them as mud and peat. These sediments are about 4 m thick and are intercalated between the fluvial gravel layers.

4.2.1.2 Alluvial gravel and lacustrine deposits

Hayasaka (1930) and Tomita (1951) observed clast-supported, unstratified and coarser gravel (15–20 cm in diameter) as an alluvial fan sediment unconformably overlying the finer gravel, exposed on the northern edge of the DP tableland by the Beigang River. Ichimura (1937) clarified the gravel composition as white quartz sandstone and black clay slate (a slate consisting of clay minerals and quartz) transported from the adjacent Paileng Formation and Shueichangliu Formation. The Paileng Formation is located around the basin except in the northwestern part of the tableland DP, where the Shueichangliu Formation is situated (Figure 2-3). Shih et al. (1996) observed the same exposure and estimated that the thickness of the gravel layer is about 150 m. On the northern scarp of the DP tableland, M.-M. Chen (2003) described the gravel layer (angular to sub-rounded) with a thickness of up to 130 m and apparently clast-supported and unstratified. Yang et al. (2007b) measured the imbrication direction in this gravel layer, and proposed that the Beigang River brought the gravel from the north and deposited it as an alluvial fan sediment. The gravel layers in the Uni (Figure 4-6) and SC (Figure 4-7) tablelands also have the same texture; however, it was formed by the Nangang River and the Taomi River from the south (Tomita, 1951; Yang et al., 2007b). The Taomi River is accordingly thought to have been much longer at that time than it is at present, so that it was able to transport such coarse gravels (e.g., cobbles and boulders).

Figure 4-6: Alluvial gravel with interbedded silty sediment. The silty sediment exists as an intercalated layer (between the two dashed lines) in the western part of the Uni tableland (650 m a.s.l.). The sediments have undergone strong weathering, so they appear reddish in color.

Figure 4-7: Cover sediment and gravel of the SC tableland. The fine-grained sediment at the top and the underlying gravel layer in the SC tablelands (550 m a.s.l.) have also been weathered and hence appear reddish in color owing to the warm and humid climate conditions. The phenomena of strong weathering are commonly observed within the sediments near the surfaces of other tablelands in the Puli Basin.

B.-C. Chen (2003) and M.-M. Chen (2003) found an exposure of lacustrine sediments with a thickness of at least 8 m (about 540 m a.s.l.) in the northern part of the DP tableland and interpreted them as mud and peat (Figure 4-8). This layer is exposed at a depth of about 100 m below the surface and is overlain by the coarse-grained gravel layer. Within the lacustrine sediments, they also found normal-sense displacement which does not penetrate the gravel layer (Figure 4-8). Similar sediments in the same altitude were also reported by B.-C. Chen (2003) in the eastern part of the DP tableland. However, no similar lacustrine sediments were found or reported at other sites of the DP tableland or in the Uni tableland in the southern part of the basin. In addition, the exposure of the 8 m thick lacustrine sediments cannot be observed nowadays owing to a retaining wall; thus, it is not possible to examine its composition.

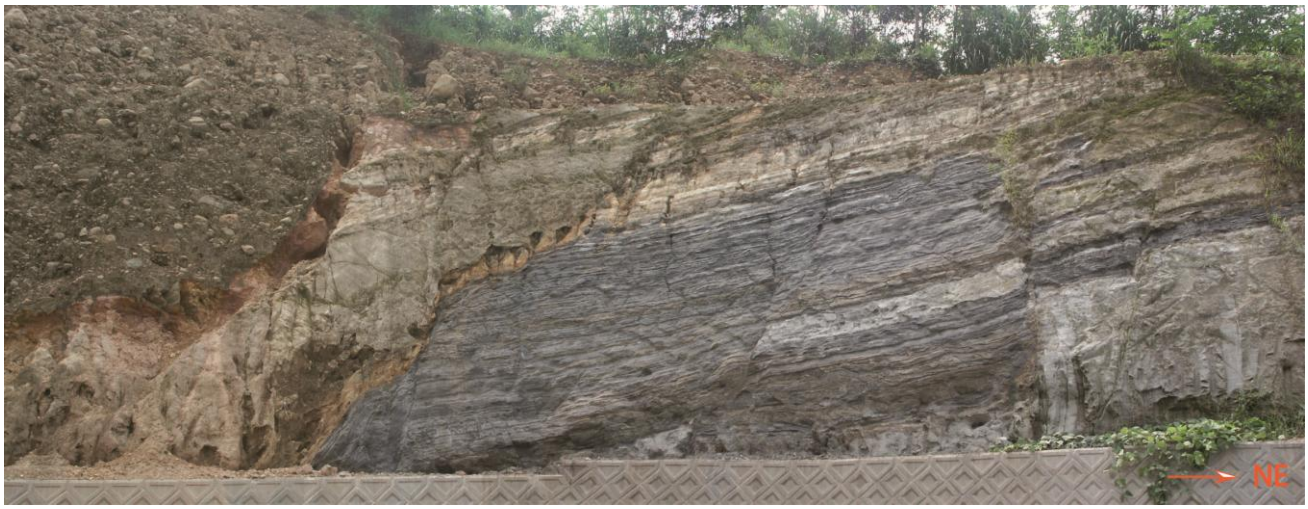

Figure 4-8: Lacustrine sediments in the DP tableland. This exposure (540 m a.s.l.) is not visible nowadays as it is covered by the retaining wall. Accordingly, the composition of the lacustrine sediments cannot be assessed from the photo alone, although M.-M. Chen (2003) interpreted them as peat (photo taken by M.-M. Chen in 2003). Note the normal-sense displacement in the middle and right parts of the blackish sediments.

On the top of the tablelands, a layer of reddish fine-grained sediment is commonly observed (Figures 4-6 and 4-7), with depths from 0.8 to 3 m (Huang, 1978). Differences in the reddish color tones of the cover sediment were observed by Tomita (1951), possibly indicating different levels of laterization. The uppermost gravel below the cover sediment has also been weathered and thus appears fragile and reddish in color (Figures 4-6 and 4-7). A silty sediment of irregular thickness is also observed as an interbedded layer within the gravel (650 m a.s.l., Figure 4-6). It has been laterized due to its shallow depth under the surface but cannot be traced laterally because of dense vegetation.

4.2.1.3 Alluvial deposits

The Mei River and the Nangang River deposited alluvium as alluvial fans and plains in the basin center, which were then dissected to become fluvial terraces in some areas (Figure 4-1). Lin (1957) suggested that clay, sand, and gravel formed the alluvial plain. Huang et al. (2000) proposed that the deposits in the basin center include gravel, sand, mud, and peat. A report made by an office for infrastructure construction (mentioned by M.-M. Chen, 2003) depicts a gravel layer at least 50 m thick along the Mei River and the Nangang River channels, representing the younger material (Huang et al., 2000).

There had been no detailed descriptions of the sediments in the lowest part of the basin until a 350 m deep borehole accompanied by well logging was constructed by the CGS (Central Geological

Survey of Taiwan) in 2003 (LC, Figure 4-1). This is because sediment exposures in this area are rare, and almost all the ground surface is covered by artificial objects and plantations, leading to limited observations and assumptions about the sediments. M.-M. Chen (2003) interpreted this to mean that the sediments are composed of poorly sorted gravel (4−256 mm) as a main component with several thin layers of silt and sand (Figure 4-9). According to the results of natural gamma logging (M.-M. Chen, 2003), the material between 200 m and 350 m in depth is characterized by a higher proportion of clay and sand. M.-M. Chen (2003) assumed these sediments to be debris flow deposits brought by the Mei River because of the texture of the sub-angular to sub-rounded mixture of coarse sand, pebbles and cobbles. Chen's interpretations indicate that the clasts consist of argillite, slate and fine to medium grain-sized metamorphic sandstone, which possibly derive from the Central Range to the east. The matrix of the material is dominated by mud (equivalent to clay in grain size). In addition, compact sandstone gravel was also found in the material; in Chen's opinion, it probably came from the adjacent terraces formed by gravel originating from the Paileng Formation.

➔ *See the next page for the figure.*

Figure 4-9: Columnar section of the alluvium in the basin center derived from the borehole data together with well logging. According to the natural gamma logging, the proportion of fine-grained sediment (silt and sand) increases below the depth of 200 m, probably showing the change in dominant sedimentary environment, differing from the above part (200−0 m) (modified after M.-M. Chen, 2003).

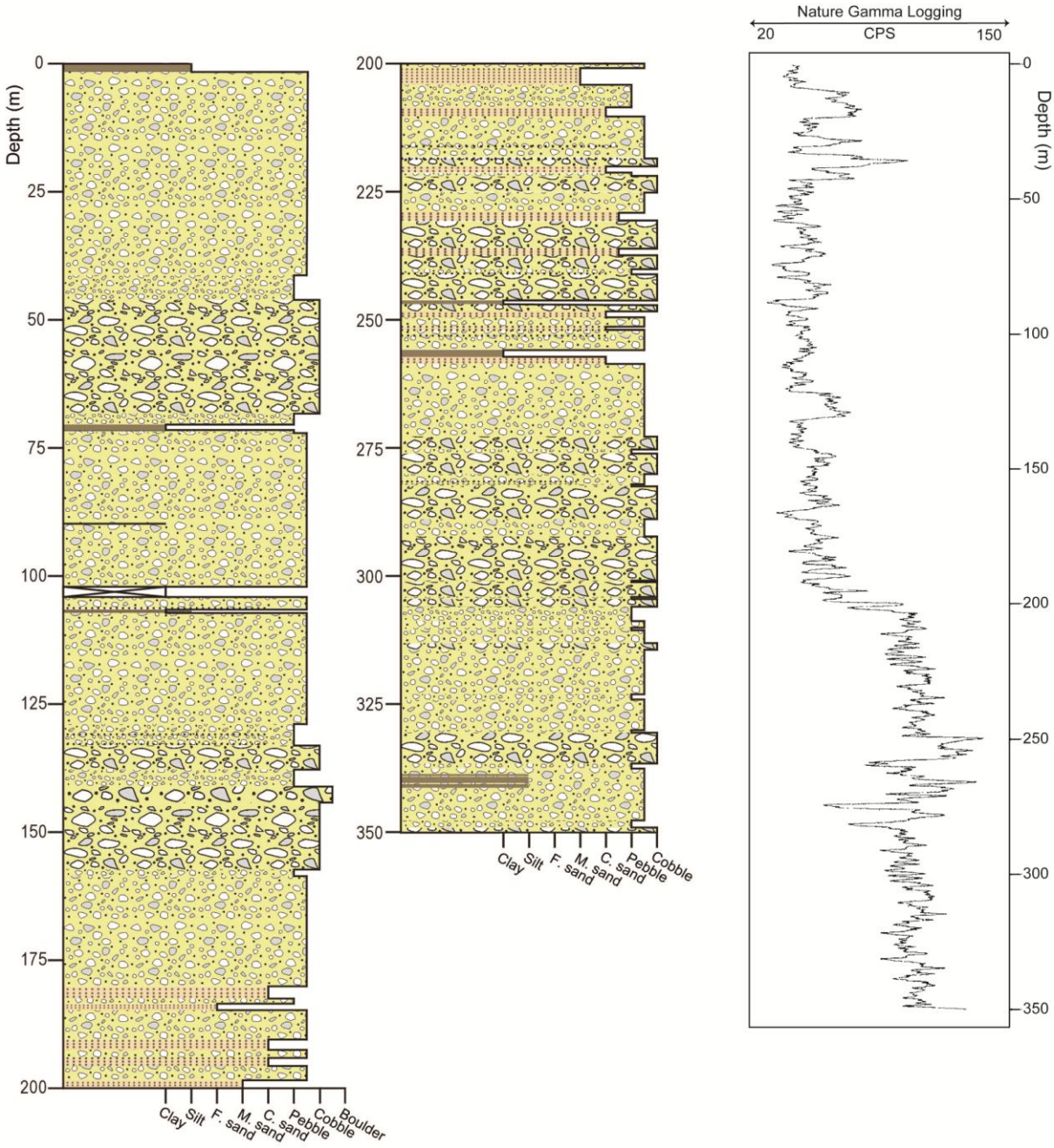

4.2.2 Sedimentary sequence of the DP tableland

Applying seismic reflection, Huang (2008) and Ke (2009) concluded that there are three main sediment units above the bedrock in the Puli Basin (Figure 4-3). Gravel with mud and sand as intercalations constitute the lowest (below the gray boundary) and the middle (between the gray and orange/red boundaries) layers with a total thickness ranging from 300 m on the northern edge to 500 m in the basin center (Figure 4-3). This alluvium was then dissected and became the DP and CK tablelands. The uppermost layer in the basin center is mainly composed of gravel with a thickness of about 200 m, unconformably overlying the middle layer.

The data and results of the previous studies are integrated into a columnar section for the DP tableland deposits shown in Figure 4-10. The thickness on the northern edge of the DP tableland is about 280 m. The lower gravel layer (*lower unit*) keeps its thickness in the whole basin area, whereas the upper gravel layer (*upper unit*) becomes thicker toward the basin center. Therefore, the total thickness could be as much as 500 m in the basin center (Ke, 2009). Planes of unconformity in the columnar section represent possible erosion events (i.e., between the bedrock and the *lower unit*) or change in sedimentary environments (i.e., between the *lower unit* and the *upper unit*).

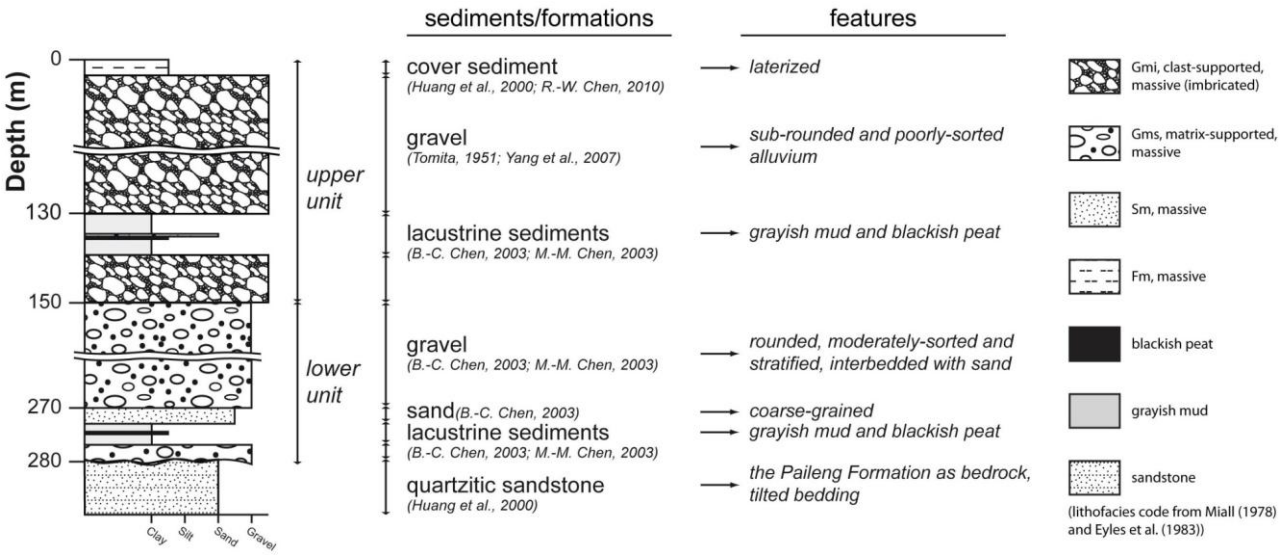

Figure 4-10: Columnar section of the DP tableland. The thickness of the sediment sequence above the bedrock is about 280 m in the outer part and increases toward the basin center. Two main sediment units are distinguished by means of field surveys and seismic reflection analyses.

4.2.3 Relative dating of sediments by morphologic and pedogenic analyses

Dating of sediments is an important element helping researchers to reconstruct the sedimentary sequence of a geomorphic unit and to infer a reliable geomorphic evolution in an area. However, an insufficient number of absolute ages for the sediments give rise to discussions about the formation order of the landforms. Therefore, only a relative timing of the sediments can be acquired by comparing spatial relationships, morphologic features, and the weathering degree of the sediments among the geomorphic units in the Puli Basin.

According to the altitudes of the Puli Basin's geomorphic units, Lin (1957) proposed possible formation periods by correlating the units to known stratigraphic ones in other areas in Taiwan. These are: LT (i.e., tablelands in Figure 4-1) in the Late Pleistocene, FT (Fluvial Terrace) in the early Holocene, and FP (Alluvial Plain) in the late Holocene. In the geologic map made by Huang et al. (2000), the Fluvial Terrace and Alluvial Plain are defined as the same material of Pleistocene age. In

accordance with altitude, continuity, existence of absence of laterized soil cover, and displacement conditions, Yang et al. (2007b) classified the landforms into three groups: LT (Lateritic Terrace with a higher altitude), FT (Fluvial Terrace with a lower altitude) and FP (Flood Plain with the lowest altitude). The LT group is further divided into three sub groups: the highest LT1 (the DP, Uni, and SC tablelands), LT2 (the CK, SW, and WG tablelands) and the lowest LT3 (the AL and NS tablelands). They accordingly inferred that the LT1 was formed first, the LT3 was the last (Table 4-1), and the FT and FP are the youngest modern alluvium.

and SC tablelands have the highest development degree, and the AL tableland has the lowest among the tablelands. In addition, the sample of the tableland SW has a noticeably lower degree than that of CK. From his results, Chen also reconstructed a model of geomorphic evolution controlled by tectonic activities and fluvial processes which, is similar to that proposed by Yang et al. (2007b) (Table 4-1).

Table 4-1: Pedogenic degree of the cover sediment of the tablelands and formation order

Tableland	Weighted mean profile-development index (WPDI)[a, b]	Soil order[a, c]	Formation order proposed by Chen (2010) (sample ID[a])	Formation order proposed by Yang et al. (2007b) (landform groups[d])
DP	0.70	Oxisols	1 (PL-1a)	1 (LT1)
Uni	0.65–0.67	Oxisols	1 (PL-s1b)	
	0.72–0.74	Oxisols	1 (PL-s1c)	
SC	0.68–0.7	Oxisols	1 (PL-s1a)	
CK	0.62	Ultisols	2 (PL-2b)	2 (LT2)
SW	0.54	Ultisols	3 (PL-2a)	
AL and NS	0.51	Inceptisols	4 (PL-3a)	3 (LT3)

[a]Data from Chen (2010)
[b]WPDI proposed by Birkeland (1999)
[c]Soil order according to Soil Survey Staff (2006)
[d]Landform groups proposed by Yang et al. (2007b)

It has been demonstrated that the pedogenic degree of soils can be applied to compare relative ages of different geomorphic units (e.g., fluvial terraces in Salamanca, Spain, by Alonso et al., 1994 and lateritic river terraces in the Western Foothills west of the Puli Basin by Tsai et al., 2007). Chen (2010) sampled the laterized sediments covering the tablelands in the Puli Basin and analyzed the development of the sediment profile. His results from WPDI (weighted mean profile development index revised by Birkeland, 1999) for the samples show that the laterized sediments on the DP, Uni, and SC tablelands have the highest development degree, and the AL tableland has the lowest among the tablelands. In addition, the sample of the SW tableland has a noticeably lower degree

than that of the CK tableland. From his results, Chen (2010) also reconstructed a model of geomorphic evolution controlled by tectonic activities and fluvial processes which is similar to that proposed by Yang et al. (2007b) (Table 4-1).

An exposure of the WG tableland on the eastern bank of the Taomi River is investigated (Figure 4-11), and opposite imbrication directions of the gravel layers are found. The lower gravel layer shows a flow direction toward downstream (i.e., northward) of the Taomi River (Figure 4-11a), whereas the overlying one reveals that the gravel was brought from the northeast and deposited by the Nangang River (Figure 4-11b). This phenomenon could support the model proposed by Yang et al. (2007b) that the WG tableland was formed later than the SC and Uni tablelands.

Figure 4-11: Opposite directions of imbrication. This outcrop is found in the gravel layer shown in the WG tableland on the eastern bank of the Taomi River. The imbrication of the lower gravel layer (a) is oriented from south to north (downstream), whereas that in the gravel layer 1 m above (b) appears to have an opposite direction. The yellow arrows indicate the opposite imbrication directions of the gravel layers.

Tseng et al. (2013) proposed three OSL (optically stimulated luminescence) ages of a section in the fluvial terrace on the slope of the Uni tableland in the Taomi River catchment in the south of the Puli Basin. These ages are 12.3 ± 1.7 ka and 12.0 ± 2.1 ka (both at a depth of about 3.7 m under the surface) of a silty deposit and 8.7 ± 1.4 ka of a sandy lens in the overlying gravel layer. One radiocarbon age of 14.5 ± 0.4 ka cal B.P. of the same silty deposit cross-checked the OSL ages. To explain and confirm the spatial relationship between the fluvial terrace section and the Uni tableland, further studies are necessary. Another OSL age of 42.1 ± 4.3 ka of a sandy lens in gravel (PK003) deposited by the Beigang River at the northern fringe of the basin was presented by Yanites et al. (2010), and is much older than their samples (from 1.4 ± 0.6 to 13.8 ± 1.1 ka) of other fluvial terraces along the river channel. They think that this age may represent a different sedimentary environment under dissimilar climatic conditions. The gravel layer from which the sample was collected is likely part of the DP tableland according to its location shown on the map in their study. If the relationship between the gravel and the DP tableland can be confirmed, this OSL age can be an important timing constraint for the deposition of the lower gravel unit in the Puli Basin.

On the basis of pollen analyses, the sediments in other intramontane basins, such as the Yuchih Basin (Liew, 1982), the Sun Moon Lake (Tsukada, 1967) and the Toushe Basin (S.-Y. Huang, 1975; Liew et al., 2006), are thought to have been deposited later than 200 ka. Although there are no palynological studies and other numeric dating results for the sediments in the Puli Basin so far, it is still assumed that the sediments in the Puli Basin have the same deposition timing as those in the southern basins (B.-C. Chen, 2003; Figure 2-7).

4.3 Landform development of the Puli Basin

Models of the landform development of the Puli Basin have been proposed (Tomita, 1951; Yang et al., 2007b; Chen, 2010), based on imbrications of gravel, relationships between geomorphic surfaces and active structures (e.g., deformed surfaces of tablelands), and the pedogenic degree of cover sediments of the tablelands. Owing to the lack of numerical ages (i.e., chronological point in time) of the sediments, these models provide only the formation order of each geomorphic unit. Although a few deposition ages of sediment samples from different sedimentary facies in the Puli Basin have been reported (Tseng et al., 2013), the geomorphologic context is not yet well understood.

4.4 Discussions

In this section, the genetic mechanisms and the question whether a lake filled the whole Puli Basin in the past will be discussed first. Then, a landform development model of the basin will be

proposed, based on these discussions.

4.4.1 Genetic mechanisms

For the model of faulting leading to a depression, normal faults and strike-slip faults are essential structures within the region, and repeated activation of these faults will make an area within which crusts will sink to form a graben. According to the field survey, dislocation of the old river channels of the Shihgang River (Figure 4-1) owing to a strike-slip fault is not evident, but could result from fluvial processes (Yang et al., 2007b). In addition, seismic reflection data (Ke, 2009) do not detect any faults within the sediments except the Meiyuan Fault and the Tili Fault within the bedrock. Although normal-sense displacement was observed in the lacustrine sediments (Figure 4-8), it could have been caused by later tectonic activities after the deposition of the lacustrine sediments, but not by faulting forming a graben. Therefore, the graben genesis is not very likely.

With an assumption of a shortening value of about 45 mm/a of the WFH and the restoration of the slip of the Chelungpu and Shaungdong Faults that connect the detachment, Wilcox et al. (2011) estimated the formation timing (during 700−500 ka) of the intramontane basins. In addition, sediment ages of at least 200 ka were derived from the pollen analyses in the Yuchih Basin. In view of these two results, it is not possible to exclude the piggyback basin model related to detachment movements as the genetic mechanism for the Puli Basin. Because of the lack of ages for the oldest sediments in the Puli Basin (the *lower unit* in Figure 4-10), however, the development of the landform and sedimentary conditions from 700−500 ka to 200 ka is still an open question and needs to be further studied. AAA The seismic reflection profiles reveal a disk-like shape of the unconsolidated sediments (i.e., *the Lower unit* and *upper unit*) together with the bedrock (Figure 4-3). In addition, from observations on the topography of the Uni and SC tablelands, the western slope of the SC tableland is not as steep as the eastern slope on the Uni tableland (Figure 4-12). This phenomenon can be explained that lateral erosion of the Taomi River increased after the river bed had been tilted by downwarping, including more mass wasting on the slope. Most of the resultant colluvium still stayed at the slope toe, for the power stream was possibly not strong enough to entrain the colluvium of gravel material. The surface of the DP tableland in the northwestern part also appears southeastward tilting (Figure 4-13). Based on the observations, downwarping as a genesis mechanism of the Puli Basin is plausible. Nevertheless, the directions of the compressional stress leading to downward curving of the sedimentary strata still need to be further studied in relation to other geologic observations (e.g., related folding or faulting patterns in the adjacent areas) in the context of the ongoing NW-SE oriented orogenic stress (Figure 2-1).

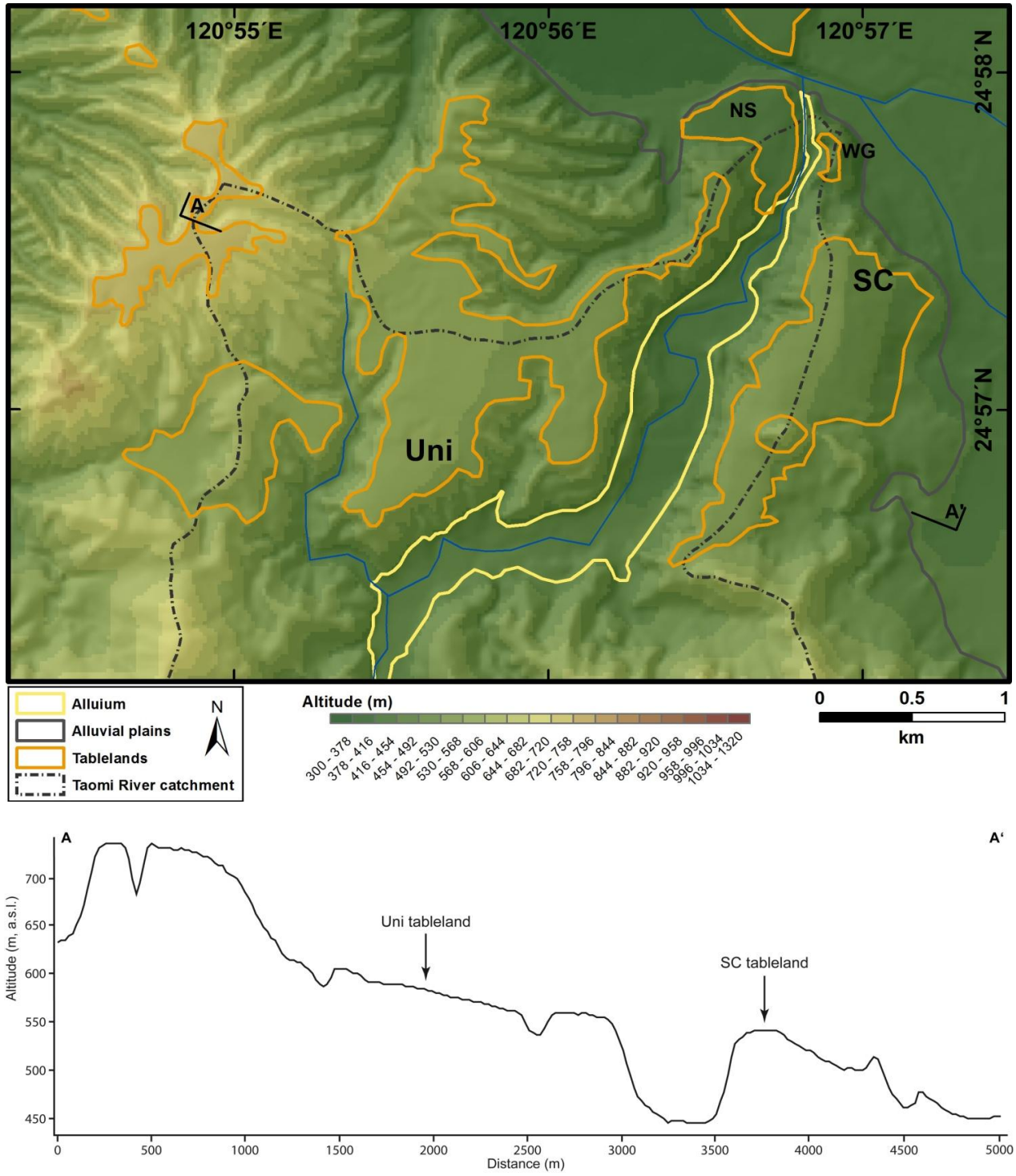

Figure 4-12: Deformed surfaces and cross-section profile of the Uni and SC tablelands. The topography reveals that the tablelands surfaces descend eastward and that the western slope the SC tableland is smoother than the eastern slope of the Uni tableland. This phenomenon can be interpreted that the eastward inclination of the river bed due to downwarping induced lateral erosion of the Taomi River stronger on the western slope of the SC tableland.

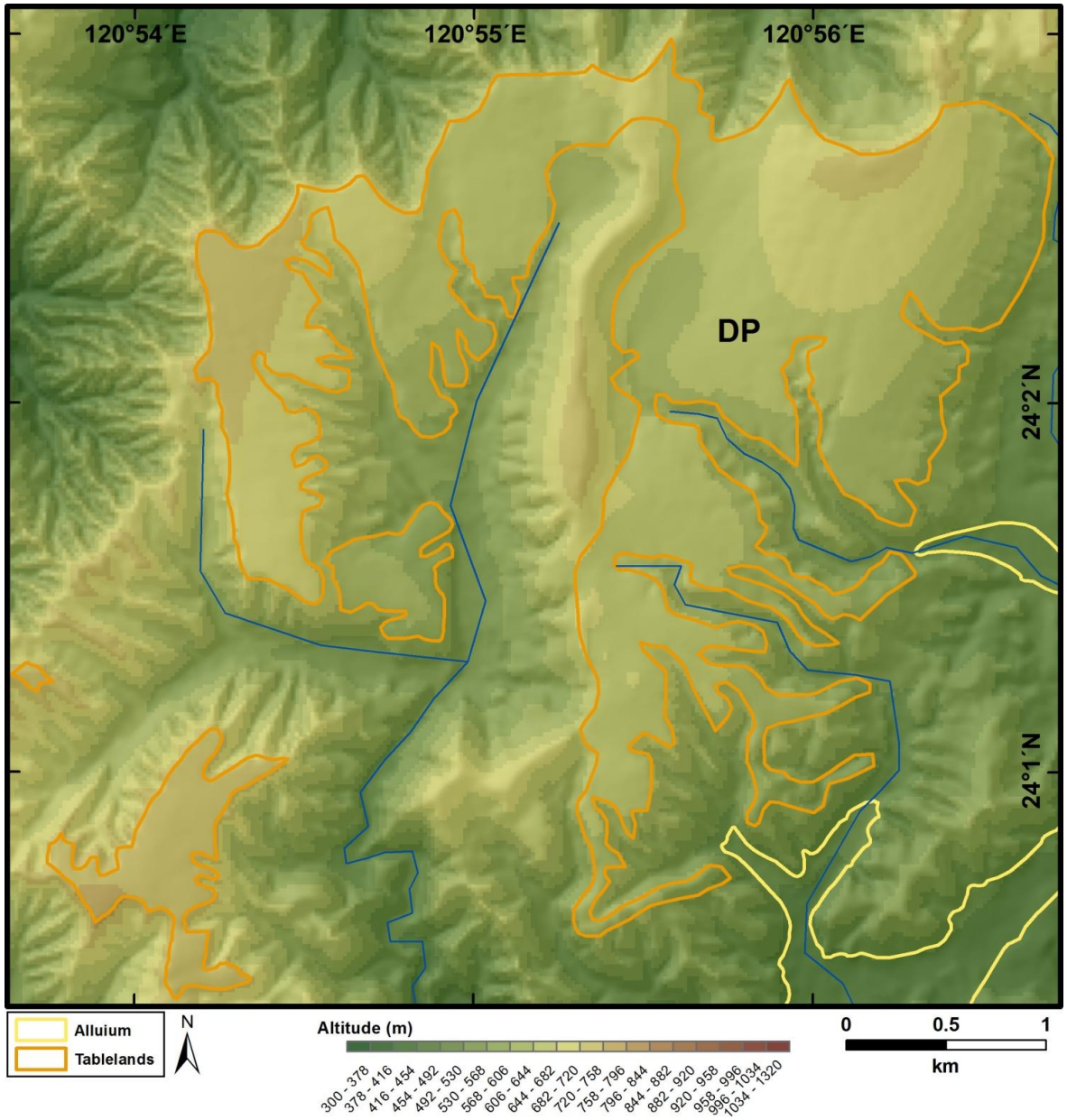

Figure 4-13: Tilted and deformed surfaces of the DP tableland. Downwarping in the Puli Basin is plausible to tilt and deform the geomorphic unit.

Therefore, to conclude, the detachment movements accompanied by downwarping in the context of compressional stress as the genetic mechanisms for the Puli Basin and other southern basins may have begun during the Middle Pleistocene.

4.4.2 Lacustrine environment in the basin

It has been supposed that a lake filled the Puli Basin twice in the past because lacustrine sediments were observed in two outcrops at different altitudes in the DP tableland (B.-C. Chen, 2003; M.-M. Chen, 2003). However, this assumption only based on the observations of two lacustrine sediments is questionable. First, no other similar lacustrine sediments exposures have been reported at other sites in the DP tableland and in the Uni tableland in the southern part of the basin. Second, during the period of deposition of the alluvial gravel of the tablelands, the sediment composition revealed by the borehole data (the material below the depth of 200 m) does not show an evident alternation of alluvial gravel and lacustrine deposits. Third, Yang et al. (2007b) did not describe the sediments as peat or mud when investigating this exposure. Therefore, it is inferred that small depressions, e.g., ponds or even oxbow lakes, within which the lacustrine sediments had accumulated were only very local during the period of deposition of the alluvial gravel constituting the tablelands. These arguments can also be applied to the hypothesis that the Puli Basin contained lakes right after the basin was formed. Moreover, the exposure of the lacustrine sediments is not visible as it is covered by a retaining wall, so the material cannot be examined from the photo alone (Figure 4-8).

4.4.3 Landform development model

On the basis of the previous studies, a model is proposed for the landform development of the Puli Basin according to the sedimentary facies and geomorphic features (Figure 4-14). The model is presented in one N-S and one NW-SE cross-section which include all the geomorphic units and underground structures to show possible spatial relationships. Six development stages in the model represent the formation of the geomorphic units as well as a detailed description of each stage:

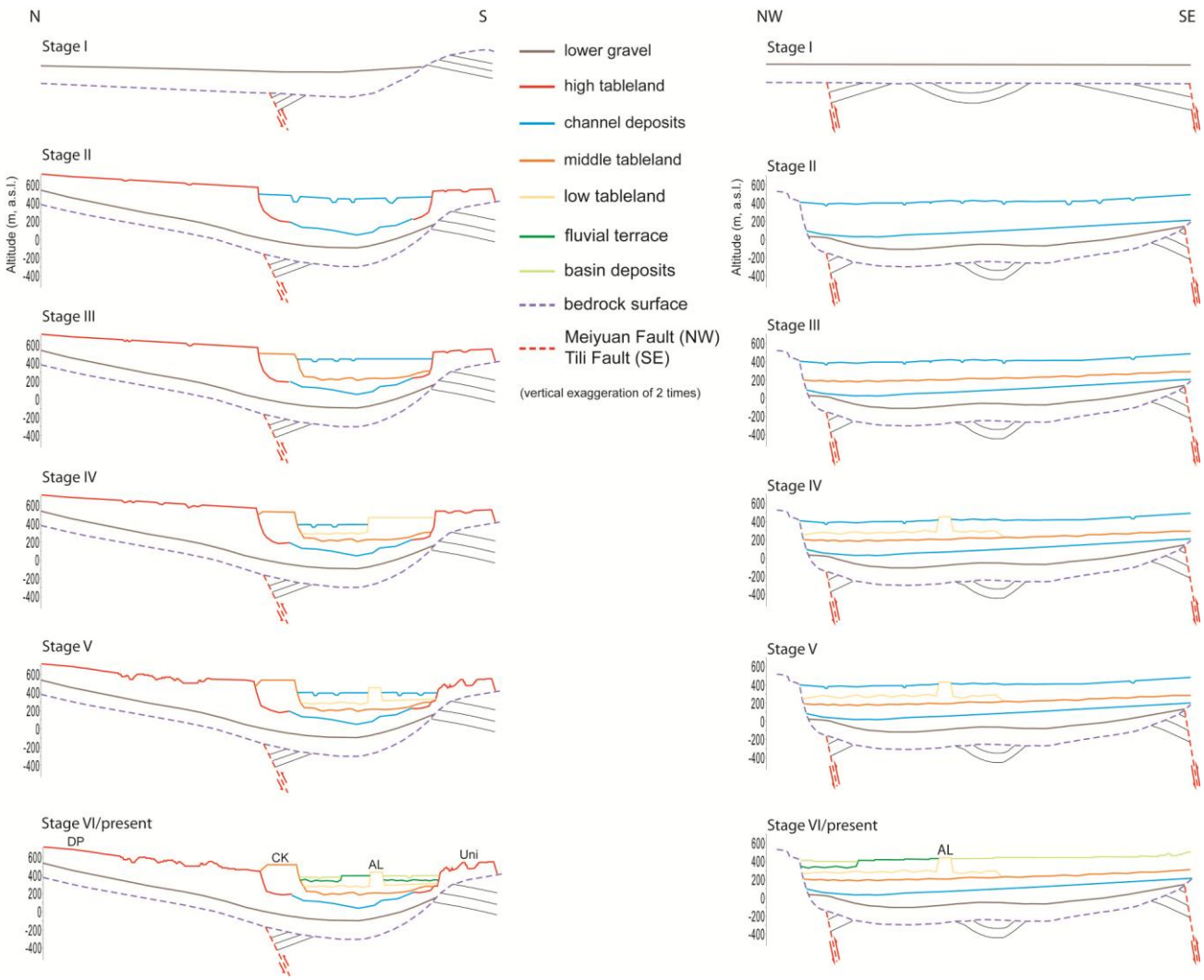

Figure 4-14: Geomorphic evolution model profiles for the Puli Basin. This model reveals two directions of N-S (a) and E-W (b). Positions of these two profiles are shown in white straight lines NS and EW in Figure 4-1.

Stage I: During the Middle Pleistocene (700–500 ka, Wilcox et al., 2011), the detachment movements and downwarping caused by compressional stress led to the formation of a shallow basin, which resulted in the deposition of the "lower gravel" (i.e., *lower unit* in Figure 4-10). The alternation of the fluvial gravel and fine-grained material layers reflects changes in sedimentary conditions. The relative weakness of stream power during this period may result from a temperate climate or low relief around the basin according to Tomita (1951). Lacustrine sediments were deposited probably in small depressions along river channels.

Stage II: Downwarping resulting from compressional stress bent both the sediments (the "lower gravel") and the bedrock (shown by the "bedrock surface") to form a disk-like shape. The higher relief accordingly resulted in stronger stream power, so alluvial gravel brought by

rivers from the north (the Beigang) and south (the Taomi and the Nangang) was deposited over the “lower gravel” layer to form broad alluvium (the “high tableland” deposits, i.e., *upper unit* in Figure 4-10; Yang et al., 2007b). In the early period of the alluvial facies, lacustrine sediments were possibly formed and deposited in some small depressions. Confluent rivers flowed westward and settled the “channel deposits” between the two alluvium masses. Downwarping led to a steeper slope of the outer part of the basin, and then these rivers incised to form the “high tableland” (i.e., DP, Uni, and SC tablelands, Figure 4-1). The Beigang River was forced to change its flow direction to the west owing to continuing crustal uplift in the marginal part of the tableland DP, thus flowing around the Puli Basin in the north.

Stage III: Dissection of the tablelands by the rivers (i.e., confluence of the Mei, Taomi and Nangan Rivers) took place again, and fluvial terraces were formed on the northern bank of the rivers in the basin and on the northern bank of the Beigang River outside the basin. In this stage, the climate turned humid and warm, so the sediments on the top of the tablelands began to be weathered (Lin, 1957).

Stage IV: River incision again formed the “middle tableland” (i.e., CK/SW and WG tablelands, Figure 4-1) and a fluvial terrace (the “low tableland”) on the southern riverbank. Compressional stress deformed the tablelands (Figure 4-1) after their formation (Yang et al., 2007b).

Stage V: The “low tableland” was eroded and dissected by the Nangang River, and two small remnants were preserved (i.e., the AL and NS tablelands, Figure 4-1). Hereafter, the Holocene fluvial material accumulated in the river channels. Tectonic activities have not yet visibly influenced the youngest geomorphic units (Yang et al., 2007b).

Stage VI/present: Incision of the Nangang River and Mei River led to the formation of the “fluvial terrace”. Yang et al. (2007b) proposed that the incision resulted from dissection of the western outlet of the basin. During the Holocene, the Nangang River and the Mei River, and their tributaries (e.g., the Dongpu River and the Shihgang River) deposited modern fluvial sediments in channels and alluvium as the “basin deposits” to form the basin bottom after the “fluvial terrace” was formed.

In plan view, some small remnants with weathered cover sediments exist west of the main tableland bodies. This phenomenon may indicate that the ancient basin bottom was bounded by ridges west of the tablelands (triangular marks in Figure 4-1 representing summits of the ridges). In other words, old tableland surfaces possibly extended further westward as far as these ridges during the period when accumulation of the alluvial gravel reached the maximum amount. After the tablelands

formed, surface runoff started to carve and erode the tableland sediments into gullies and valleys. These topographic features resulting from the erosional processes are presented by the slope of the DP and Uni tablelands (Figures 4-12 and 4-13).

In Figure 4-15a, the gullies with steep slopes develop intensively to the north and west of the remnants, where are the outer parts of the alluvium. This phenomenon reflects relatively higher erodibility of the loose alluvium and a long period of erosion. In the area to the south, where the alluvium accumulated against the bedrock, gullying could hardly occur on the alluvial deposits. Accumulation of modern basin deposits took place to the east and north of the Uni and SC tablelands, so old gullies in these areas could have been buried. Furthermore, the ground subsidence in the eastern area to the tablelands revealed by the eastward inclination of the tableland surfaces (Figure 4-15b) facilitated the deposition. In the area where the DP tableland is located, the phenomenon similar to that of the Uni and SC tablelands is observed as well (Figure 4-16). Subsequently, sub river catchments began to develop within the tablelands. Therefore, the present situation is the result of denudation and erosion since the tablelands were formed.

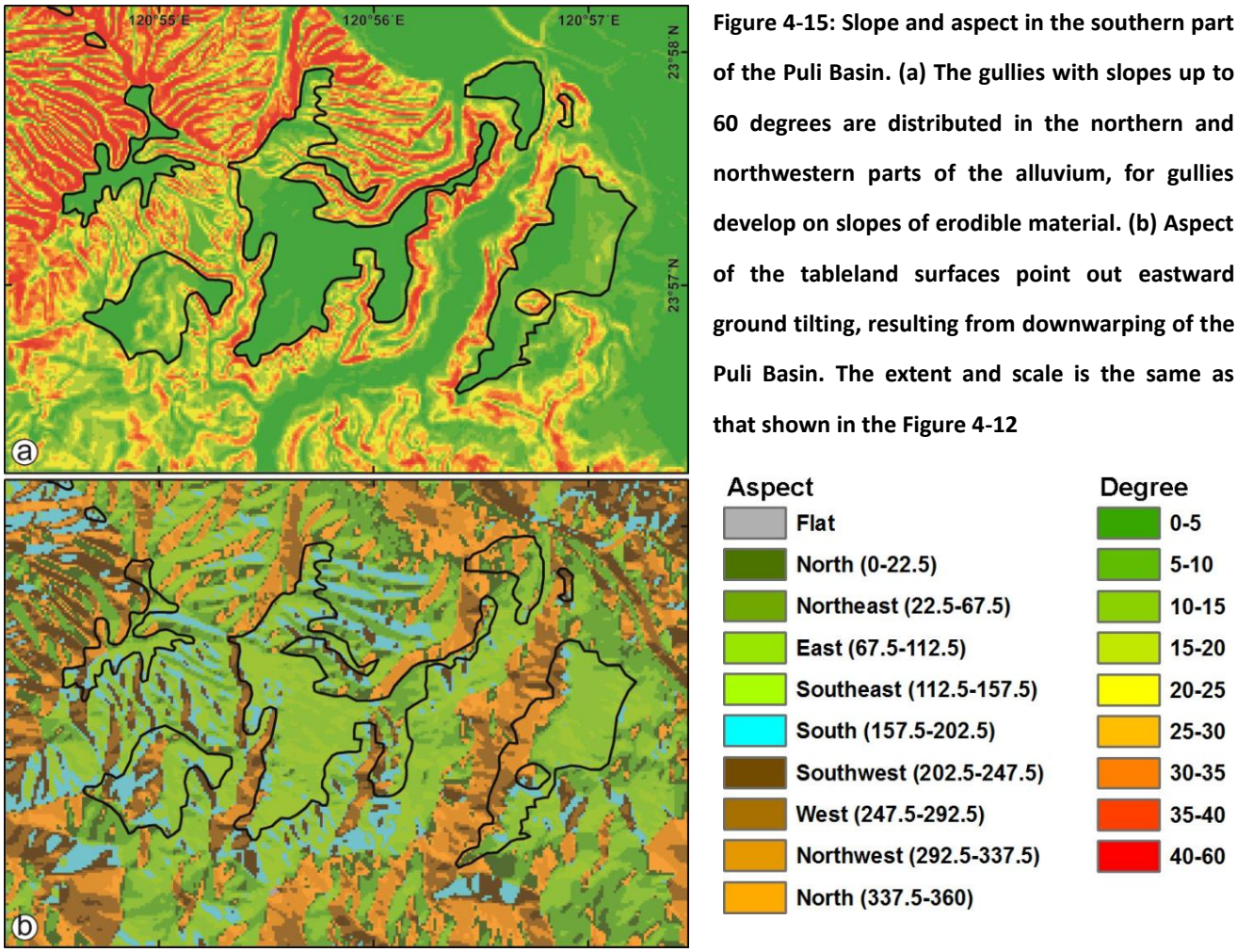

Figure 4-15: Slope and aspect in the southern part of the Puli Basin. (a) The gullies with slopes up to 60 degrees are distributed in the northern and northwestern parts of the alluvium, for gullies develop on slopes of erodible material. (b) Aspect of the tableland surfaces point out eastward ground tilting, resulting from downwarping of the Puli Basin. The extent and scale is the same as that shown in the Figure 4-12

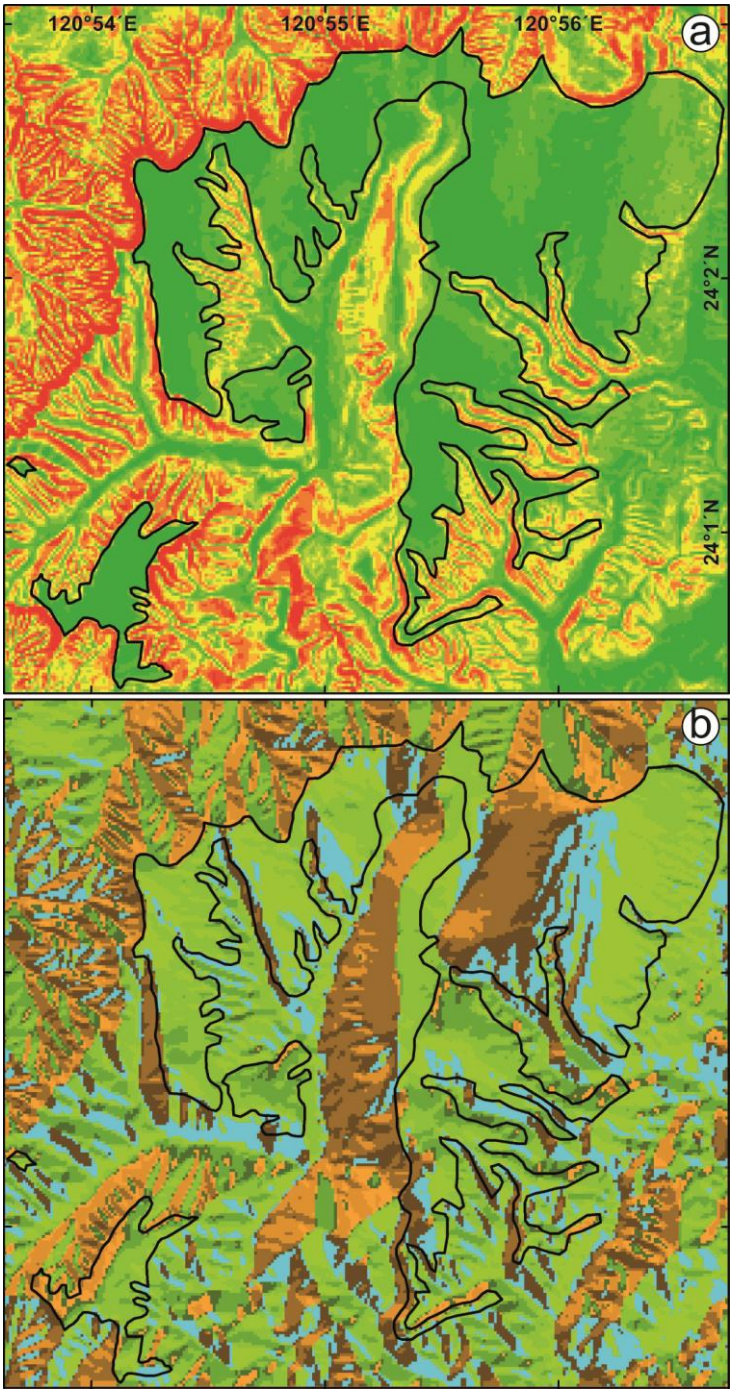

Figure 4-16: Slope and aspect in the northwestern part of the Puli Basin. (a) The gullies also develop to the north and west of the remnants of the DP tableland. Similar slopes of these gullies to those of the Uni tableland reflect similarity of the alluvial material. (b) Downwarping in the basin also tilted the tableland surface southeastward.

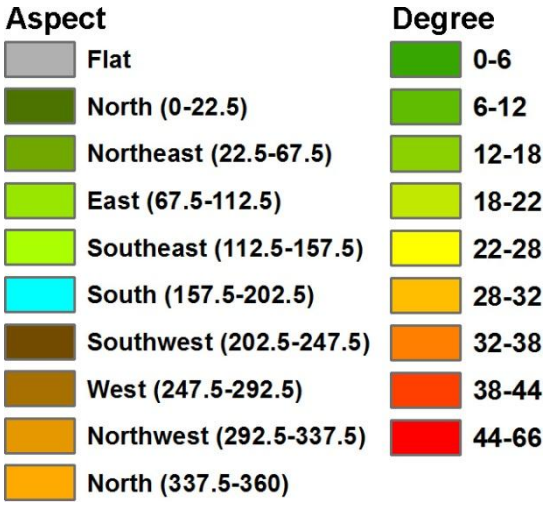

4.5 Conclusions

Research has been carried out to investigate genetic mechanisms, sedimentary facies, and landform development of the Puli Basin since the 1930s. Because different methodologies were applied and new findings were presented, some results and conclusions of former research dealing with these research topics need to be reexamined.

Geomorphic analyses and geophysical methods suggest that downwarping resulting from compressional stress may not be the only genetic mechanism involved. Underground detachment movements caused the intramontane basins as well. According to the Chelungpu and Shuangdong fault activity and palynological studies, basin formation started in the Middle Pleistocene.

Outcrop surveys, borehole data, and seismic reflection analyses have revealed sedimentary sequences in the Puli Basin. In the tableland deposits, lacustrine sediments interbedded in the gravel layers can be distinguished. These lacustrine deposits were formed at different depths in the sequence. However, their discontinuity and the borehole data do not support the idea of an ancient lake that filled the whole basin in the past, but point to only local small depressions. Besides, the composition previously interpreted as peat and mud requires further examination.

A geochronological frame of the sediments in the basin cannot be established yet, owing to the insufficient number of their absolute ages. Nevertheless, a chronosequence of the geomorphic units can be built, based on analyses of geomorphology and pedogenic degree of the sediments. Accordingly, a six-stage model of the landform development of the Puli Basin is constructed, which can point out variations in sedimentary environments and tectonic activities.

CHAPTER 5

Sedimentary features and ages of fluvial terraces and their implications for geomorphic evolution of the Taomi River catchment: A case study in the Puli Basin, central Taiwan

Within the following section, the study results of the outcrop TM01 by applying the methods, including radiocarbon dating, OSL dating, grain size analyses, and mineral components determination, described in Chapter 3 are presented. This chapter has been previously published in *Journal of Asian Earth Sciences*.

Paper information:

Title:	Sedimentary features and ages of fluvial terraces and their implications for geomorphic evolution of the Taomi River catchment: A case study in the Puli Basin, central Taiwan
Journal:	Journal of Asian Earth Sciences
Volume, Issue, pages:	62, 759-768
First author:	Chia-Han Tseng
Co-author(s):	Dirk Wenske, Margot Böse, Tony Reimann, Christopher Lüthgens, Manfred Frechen
Date of acceptance:	12 November 2012
Date of online publication:	22 November 2012
Link:	www.sciencedirect.com/science/article/pii/S1367912012005147
DOI:	10.1016/j.jseaes.2012-11.028

CHAPTER 6
Geochronology and sedimentary sequences in tablelands and their implications for landform development and paleoclimatic conditions

In this chapter, the focus is on the tablelands in the southern part of the Puli Basin. By means of field investigations and grain size analyses in laboratory, sedimentological characteristics of the tableland deposits in newly found outcrops in the tableland are examined. In addition, their burial ages are estimate d by applying the luminescence dating method. Furthermore, on the basis of topographical features and comparison with terraces and tablelands in other areas in Taiwan, a landform development and its related processes are proposed.

6.1 Outcrop features and sampling

6.1.1 Descriptions of the outcrops

In the southwestern part of the basin, where the outcrops are located, a height difference is estimated about 100 m between the surface of the Uni tableland and the modern riverbed of the Taomi River. The bedrock (Paileng Formation) exposes not only to the south of tableland, but also on the SC tableland as a hill with a height of 40–50 m. The SC tableland surface is obviously deformed and tilts toward southeast, so an anticline is proposed to exist in the tableland (Yang et al., 2007b). For luminescence dating and grain size analysis, five samples of different sediments were taken in the Uni tableland (Figure 2-3). Three outcrops of TM02 are located at three different sites in a gully (Figure 6-1), whereas the one of TM03 is on a slope along a road. The samples of TM02 belong to three different types of material: sub- to rounded and moderately sorted alluvial gravel (clasts mainly of quartzitic sandstone) with sand-silt matrix (TM02-A), homogeneous fine-grained sediment (TM02-B), and fluvial sand (TM02-E and TM02-F, Figures 6-2 and 6-3).

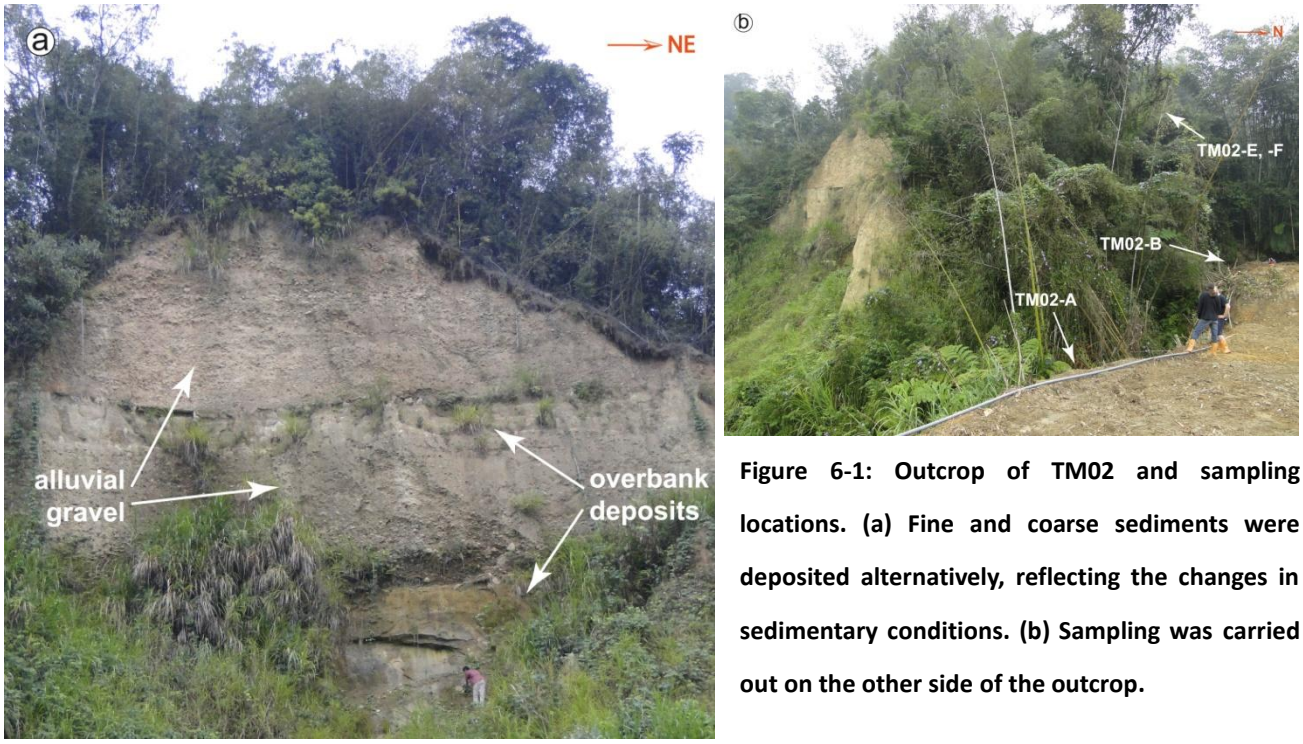

Figure 6-1: Outcrop of TM02 and sampling locations. (a) Fine and coarse sediments were deposited alternatively, reflecting the changes in sedimentary conditions. (b) Sampling was carried out on the other side of the outcrop.

The sample of TM03-A was taken from an alluvial gravel layer (sub- to rounded and moderately sorted gravel and sandy matrix) at a position near the boundary between the gravel and an overlying fine-grained sediment (Figure 6-2). The samples of TM02-A and TM03-A were taken near the upper boundary of the layers where they are located, for their ages can represent the last stage of the aggradation periods. The samples of TM02-E and TM02-F belong to two stratified sand layers, between which two thin (70 cm thick in total) gravel layers exist with different grain sizes (max. 30 cm and max. 5 cm, respectively).

➔ *See the next page for the figures.*

Figure 6-2: Sample positions in each outcrop of TM02. (a) TM02-A. Sub-rounded and moderately sorted alluvial gravel indicates a sedimentary environment with relatively higher stream power. (b) TM02-B. The silty sediment (Munsell color 2-5 Y 5/4) appears a homogeneous nature. (c) TM02-E and TM02-F. Pure sand and round gravel with a laminar sedimentary structure reflect a fluvial environment. (d) TM03-A. Alluvial gravel with features of sub-rounded, moderately-sorted, and slight imbrication is covered by the weathered fine-grained sediment.

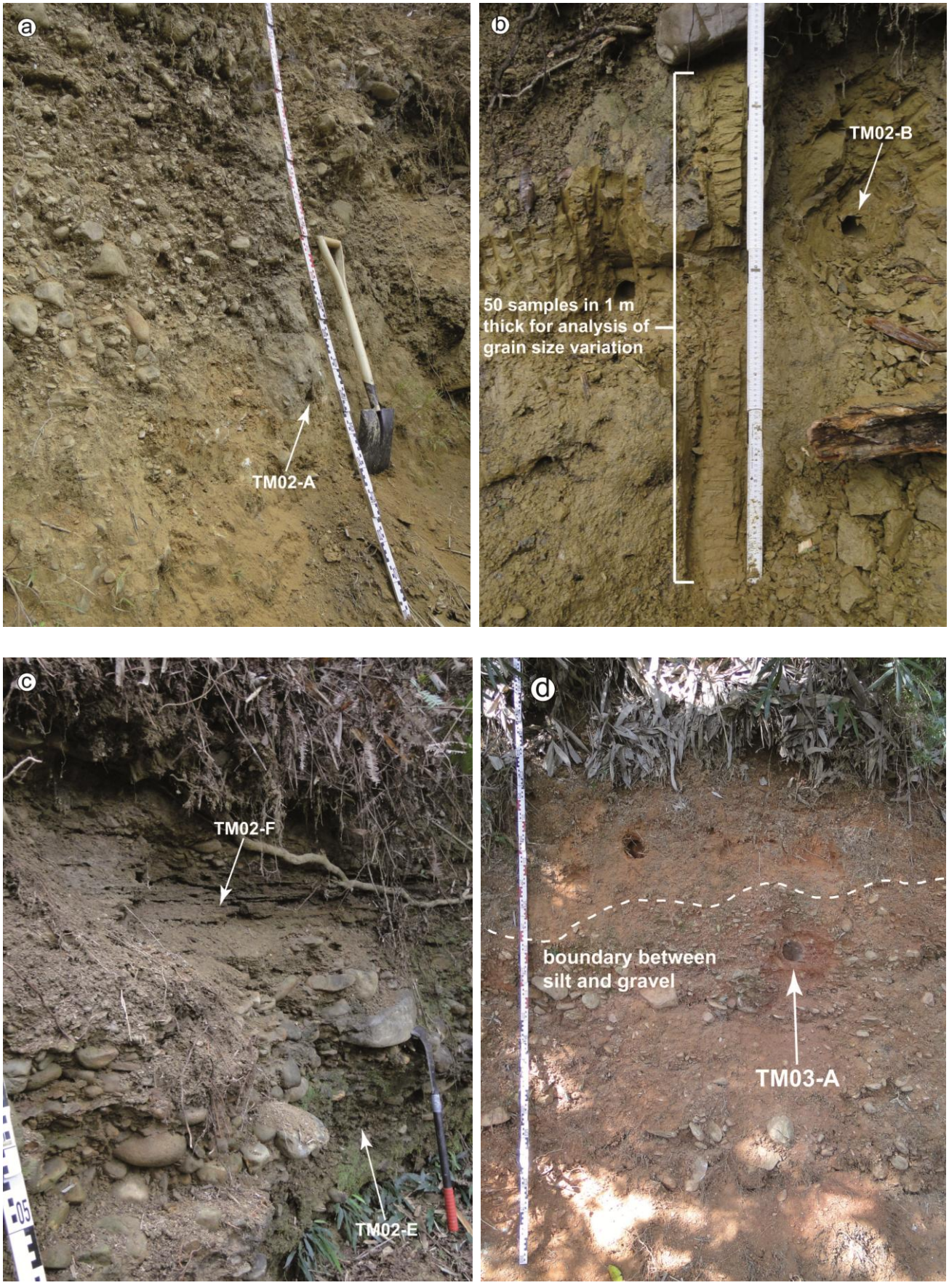
a
TM02-A
b
TM02-B
50 samples in 1 m
thick for analysis of
grain size variation
c
TM02-F
TM02-E
d
boundary between
silt and gravel
TM03-A

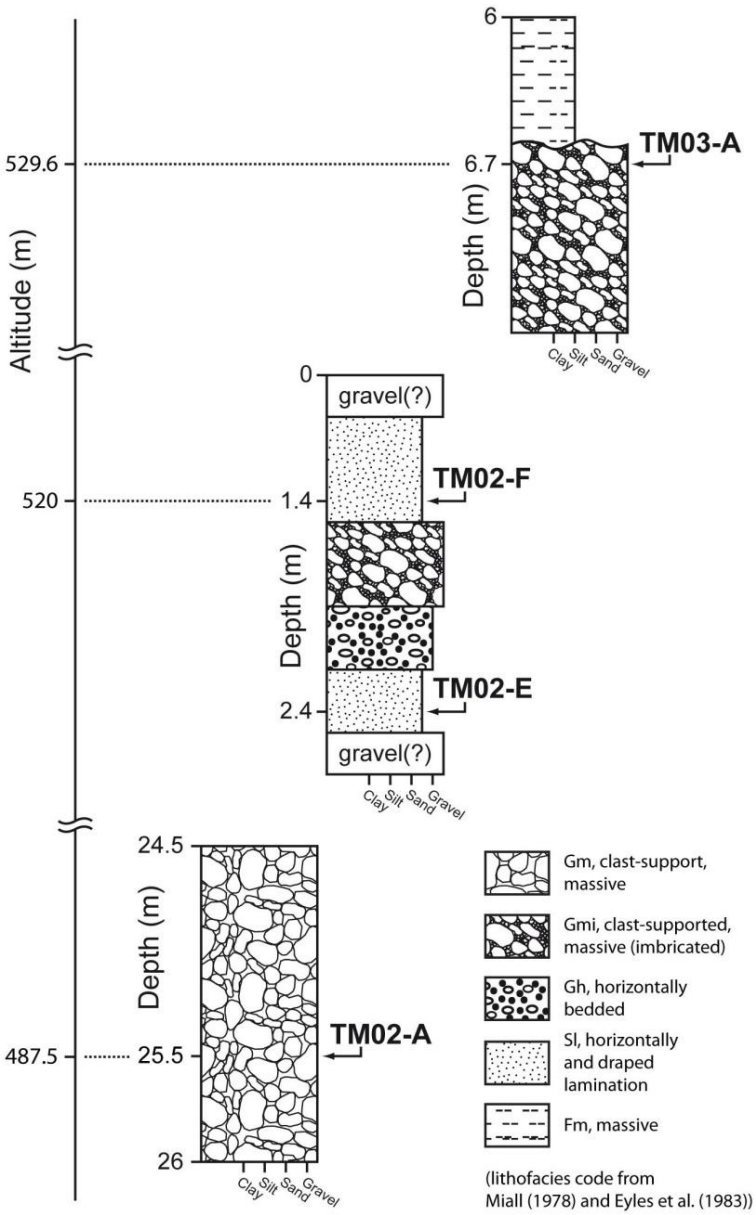

Figure 6-3: Stratigraphic columns for individual sub-outcrops of TM02. Each stratigraphic column is drawn on the same scale to compare the thickness of each sediment layer. The altitude of each sampling position marked by the arrows is also indicated on the left to show the spatial relationships between the sub-outcrops. The descriptions and lithofacies codes of the sediments follow the criteria for describing sediments proposed by Miall (1978) and Eyles et al. (1983).

6.2 Applied methods

6.2.1 Optically stimulated luminescence (OSL) dating

To calculate the dose rate, conversion factors according to Adamiec and Aitken (1998) and beta attenuation factors according to Mejdahl (1979) were used. For calculation of the cosmic dose rate, latitude, altitude, depth below the surface, as well as density of the overlying material of the samples were taken into account following Prescott and Stephan (1982) and Prescott and Hutton (1994). For the samples of the profile TM02, whose overlying material has a changed thickness over time by denudation, an error of ± 30% for the cosmic dose rate is adopted in this study.

Water content of the sediment to be dated also affects the attenuation of naturally occurring radiation, so it is necessary to use a correction for water content to determine an appropriate dose

rate. The *in situ* water content of each sample was first measured in the laboratory, and the correction factors developed by Aitken (1985) were applied in this study. All the parameters obtained for determining the dose rate are listed in Table 6-1.

The sample preparation for the luminescence measurements in this study follows the procedures presented in Aitken (1985) and Alappat et al. (2010). The grain size fraction of 100–150 µm for TM02-B, and 150–250 µm for TM02-A, TM02-E, TM02-F and TM03-A was first separated using wet sieving. After drying, the samples were treated with hydrochloric acid (HCl, removing carbonates), sodium oxalate ($Na_2C_2O_4$, resolving aggregations) and hydrogen peroxide (H_2O_2, removing organics). Afterward, the samples were rinsed with deionized water and dried again. Sodium polytungstate (density: $2.62 < \rho < 2.70$) was then used to separate the quartz-rich fraction of the samples. To obtain ideally pure quartz minerals, concentrated hydrofluoric acid (HF) was applied to remove feldspar impurities and to etch away the alpha-irradiated surface of the quartz. After the etching procedure, the quartz minerals were sieved again to obtain the grain size fraction of 100–150 µm and 150–250 µm, respectively for pure quartz.

Sub-samples (aliquots) were prepared by mounting quartz grains on stainless-steel discs with a diameter of 9.8 mm. Small-sized aliquots (2.5 mm) were used for determination of the equivalent dose, while medium-sized (6 mm) aliquots were used for tests of preheat temperature and dose recovery in this study. The luminescence measurements were executed on a Risø TL/OSL-DA-15 reader equipped with a 90Sr/90Y beta source (Bøtter-Jensen et al., 2000). A UV filter (270−380 nm, HOYA U-340) was mounted to detect the luminescence signals of quartz.

A single-aliquot regenerative-dose (SAR) protocol (Murray and Wintle, 2000; Murray and Wintle, 2003) was applied for both, quality testing and equivalent dose determination. To deal effectively with feldspar contamination in the samples, the SAR protocol used in this study was modified following Roberts (2007), using an IR shine before the stimulation in blue (post IR OSL) to minimize signal contribution from feldspar. Relatively dim OSL signals for quartz samples observed in this study were also revealed in previous research on other Taiwanese samples (Dörschner et al., 2012; Tseng et al., 2013).

6.2.2 Grain size analysis

To understand variation in grain size fraction of the homogeneous fine-grained sediment (TM02-B, 2-5 Y 5/4 according to Munsell color chart (Munsell Color, 1992)) with depth, 50 samples were taken with an interval of 2 cm in the profile. In addition, samples of TM02-A (matrix part), TM02-E, TM02-F, and TM03-A (matrix part) were also collected for the grain size analyses to examine their possible processes of sedimentation. A Beckman and Coulter ISO 13320 (Aqueous Liquid Module

2824) laser diffraction particle size analyzer at the LIAG was used. The analysis procedure repeated the measurements five times for each sample and then sorted the results into 116 fractions. According to FAO (2006), a standardized grain-size classification was made, converted from the fractions obtained.

6.3 Results

6.3.1 OSL dating

The results of dose rate and OSL measurements for the five samples are listed in Table 6-1 and Table 6-2, respectively. For each sample, its equivalent dose (D_e) had to be derived from the D_e distribution of individual aliquots by applying a statistical model. For fluvial sediment samples, there is a high chance that their luminescence signals are not totally reset during transport, so that the resulting D_e distributions appear broad and scattered. Consequently, a pattern of right skewed distributions (i.e., toward high D_e values) is often observed for samples from fluvial sediments. In the cases of aeolian or coastal samples (e.g., Reimann et al., 2011), the D_e distributions exhibit relatively narrow and symmetrical distributions owing to sufficient bleaching. A statistical model called minimum age model (MAM, Galbraith et al., 1999) is widely used in luminescence dating method for deriving D_e values of incompletely bleached samples. It is assumed that the low D_e values in a distribution represent the grain population most probably being sufficiently zeroed before deposition, so the final D_e is calculated from a minimum D_e portion. For these calculations, a threshold for the *sigmab* parameter (termed overdispersion) as a measure for the naturally occurring scatter has to be defined. This is ideally derived from a well bleached sample within a sediment sequence to be dated. Unfortunately, none of the samples of this study shown good bleaching characteristics.

Accordingly, a bootstrap version of the MAM proposed by Cunningham and Wallinga (2012) based on the original MAM was adopted in this study by assigning an overdispersion value of 0.2 ± 0.1 to obtain reliable D_e values. Two main advantages arising by using the method are indicated by Cunningham and Wallinga (2012): (1) better estimation of uncertainty in OSL ages in the context of partial bleaching and (2) potentiality of combining data of partially bleached OSL samples with chronological models by means of Bayes' theorem. However, with the bootstrap version of the MAM, overall uncertainties of the ages obtained will be higher compared to standard MAM calculations.

Table 6-1: Results of dose rates derived from gamma spectrometry

Sample ID	Depth [m]	Laboratory ID	^{238}U [ppm]	^{232}Th [ppm]	^{40}K [%]	Water content [%]	Sediment dose rate [Gy/ka][a]	Cosmic dose rate [Gy/ka][b]
TM02-A	25.5	LUM 2669	3.72 ± 0.21	18.6 ± 1.0	2-36 ± 0.14	10 ± 5	3.92 ± 0.15	0.022 ± 0.002
TM02-B	12.0	LUM 2670	3.36 ± 0.20	17.9 ± 1.0	2-44 ± 0.14	20 ± 5	3.58 ± 0.13	0.06 ± 0.01
TM02-E	2.4	LUM 2671	3.28 ± 0.19	20.3 ± 1.1	2-55 ± 0.15	10 ± 5	4-11 ± 0.15	0.17 ± 0.02
TM02-F	1.4	LUM 2672	3.42 ± 0.20	20.8 ± 1.1	2-60 ± 0.15	10 ± 5	4-21 ± 0.15	0.19 ± 0.02
TM03-A	6.7	LUM 2673	3.49 ± 0.20	19.6 ± 1.0	2-64 ± 0.15	10 ± 5	4-18 ± 0.15	0.10 ± 0.01

[a]Sediment dose rate was calculated using the dose rate conversation factors of Guerin et al. (2011). For details see also Aitken (1985).

[b]Cosmic dose rate was calculated according to Prescott and Hutton (1994).

Table 6-2: Results of OSL ages

Sample ID	Depth [m]	Laboratory ID	Mineral type	Grain size [µm]	n [aliquots][b]	Total dose rate [Gy/ka][a]	D_e [Gy][c]	Age [ka][d]
TM02-A	25.5	LUM 2669	Qz-OSL	150–250	57	3.94 ± 0.15	13.1 ± 1.4	3.3 ± 0.4
TM02-B	12.0	LUM 2670	Qz-OSL	100–150	15	3.64 ± 0.13	19.0 ± 21.4	5.2 ± 5.9
TM02-E	2.4	LUM 2671	Qz-OSL	150–250	42	4.28 ± 0.15	46.7 ± 10.6	10.9 ± 2.5
TM02-F	1.4	LUM 2672	Qz-OSL	150–250	58	4.31 ± 0.15	59.0 ± 11.4	13.7 ± 2.7
TM03-A	6.7	LUM 2673	Qz-OSL	150–250	32	4.18 ± 0.15	45.6 ± 11.9	10.9 ± 2.9

[a]Total dose rate is the sum of sediment dose rate and cosmic dose rate. Both are listed in Table 1.

[b]Accepted aliquots (i.e., aliquots that met the rejection criteria as follows: Recycling ratio ± 10%, recuperation 10% of the natural signal, maximum 15% error on the test dose, except for LUM 2671 and LUM 2672 30% error on the test dose were accepted.

[c]D_e estimate was calculated using the bootstrap version of the minimum age model (Cunningham and Wallinga, 2012) assuming a sigma_b of 0.2 ± 0.1.

[d]OSL ages represent depositional ages and are expressed relative to the date of sampling. TM02 was sampled in 2012, while TM03 in 2011.

6.3.2 Grain size distributions

For the fine-grained sediment of TM02-B, more than 50% of the material in the studied outcrop (1 meter thick) is silty in grain size (Figure 6-4). The silty component above the depth of 12.4 m increases upward, showing a pattern of normal grading. Sandy material remains the proportion of 30–40% at depths between 12.4 m and 12.8 m. The sediment fines downward again deeper than 12.8 m, whereas the amount of clay-sized component is relatively constant in proportion (8–15%) through the studied section. This homogeneous fine-grained sediment is composed almost of rounded quartz grains (based on the observation with a 40 × binocular microscope), within which very few small pieces of charcoal are seen. This phenomenon can probably indicate that a flood event occurred and deposited the homogeneous silty sediment as an overbank deposit along the Taomi River.

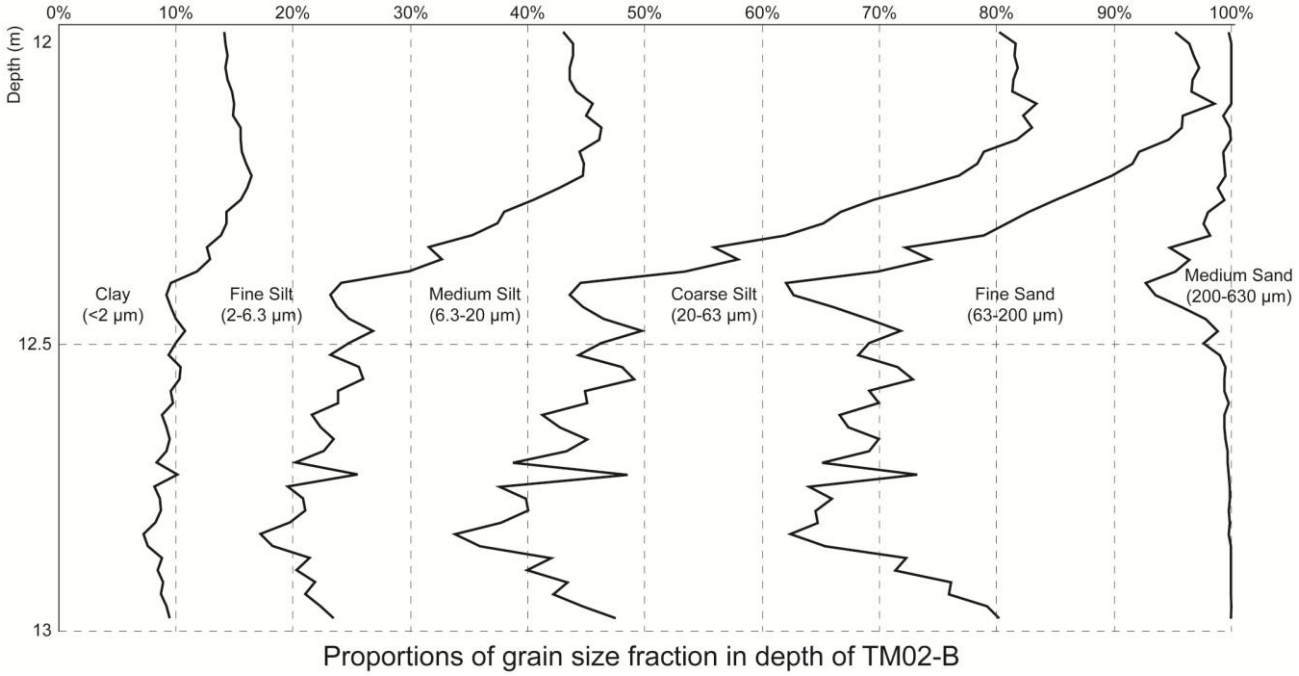

Figure 6-4: Distribution of grain size fraction in depth of TM02-B. The changes in proportions of different-sized sediments probably show more than one sedimentation event.

Grain size distributions of the samples of TM02-A, TM02-E, TM02-F, and TM03-A are shown in Figure 6-5. For TM02-E and TM02-F, their curve patterns are very similar to each other and consistent with those of typical fluvial sediments (Middleton, 1976; Ashley, 1978; Sun et al., 2002). The curve of TM03-A also shows a pattern resembling that under a fluvial process, with an increasing proportion of silty component and decreasing sand amount .This change indicates that suspended load has increased in the Taomi River. Moderately sorting characterizes the curve

pattern of TM02-A, and it can reflect a turbid flow condition that transported mixed material of gravel, sand, and silt.

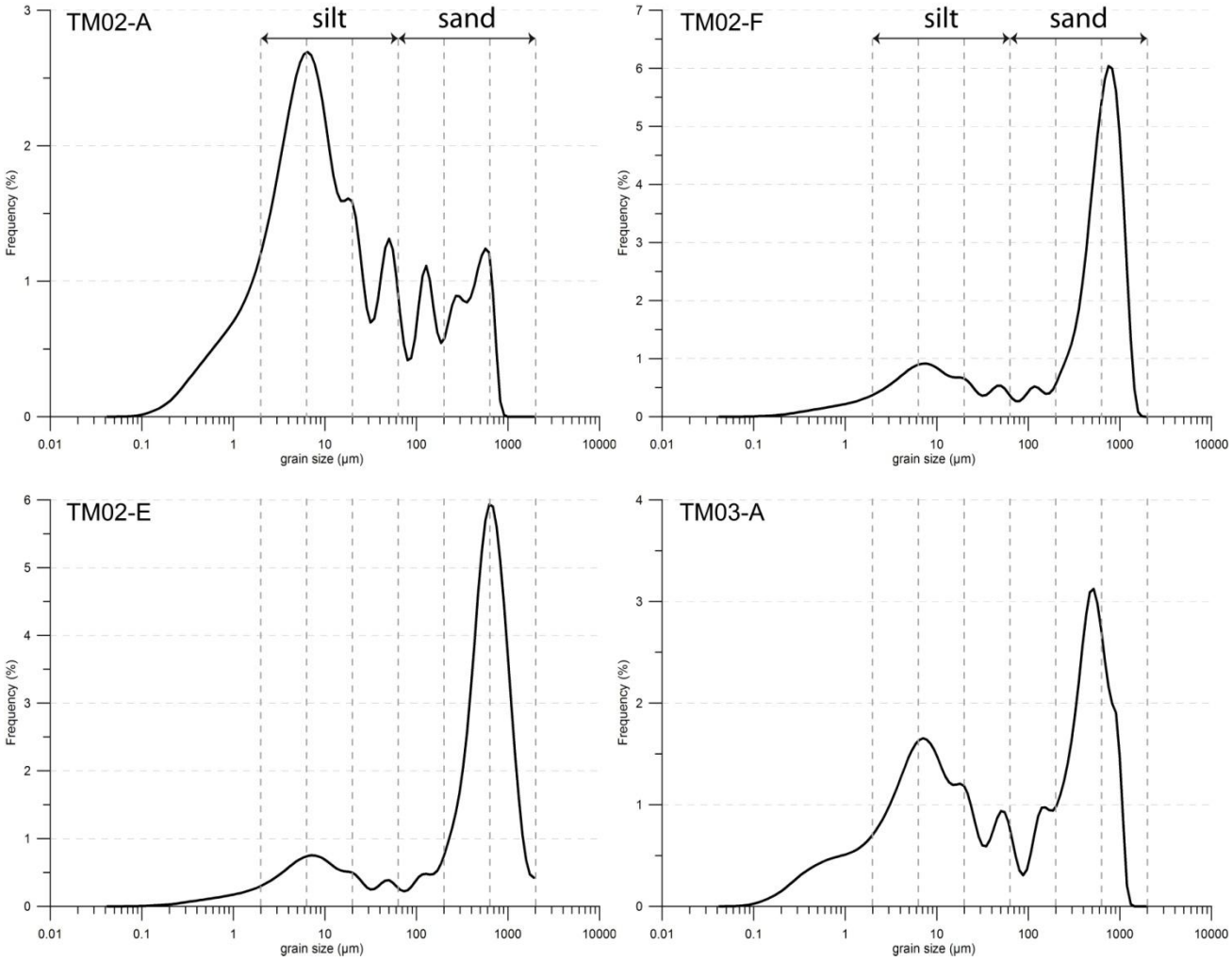

Figure 6-5: Grain size distribution curves (< 2 mm) of the studied samples. The curve of TM02-A shows a moderately sorting feature, probably indicating a condition of turbid flow. A fluvial process is obvious for TM02-E and TM02-F from the curves. For TM03-A, its curve is similar to those of TM02-E and TM02-F, but the silt has more proportion and the sand has less.

6.4 Discussions

6.4.1 OSL ages

In Table 6-2, the chronology of the studied deposits derived from the four OSL age estimates seem reasonable and robust. However, the relatively high uncertainties in the D_e values, which exceed a normal level between 5% and 10% (Murray and Olley, 2002) need to be discussed.

The main reason for the relatively high uncertainties is the broad and right-skewed character of the

D_e distributions for all samples. As already summarized above, this phenomenon can be explained by mixing processes of some moderately bleached mineral grains with well-bleached ones in the sediments (Olley et al., 1998 and Olley et al., 1999; Wallinga, 2002). During fluvial transport, it is common that some mineral grains are not sufficiently exposed to the sunlight, so that their luminescence signals cannot be completely reset (Wallinga, 2002). These moderately bleached grains accordingly have higher D_e values. On the other hand, the features of the sediments in the outcrops, e.g., the sub-rounded gravel of TM02-A and TM03-A and the laminar texture of the sandy material of TM02-E and TM02-F, reflect the depositional conditions of the fluvial environment in which the studied sediments were deposited. Therefore, the sedimentary characteristics mentioned above support the assumption that the samples may have suffered from incomplete bleaching. However, a small aliquot approach in combination with the application of the bootstrap MAM yielded consistent ages within on sigma uncertainty. Because incomplete bleaching is a random process, it is therefore assumed that the chronology is robust. However, the error of TM02-B is larger than 100%. This can mainly be attributed to the samples intrinsic luminescence properties (i.e., dimness of the quartz OSL signal) which decreased the number of acceptable or aliquots. In addition, the sample only contained a very small amount of coarse grain quartz at all, so that only few aliquots could be measured. Because of its high uncertainty, the age of sample TM02-B is excluded from all further stratigraphic and geomorphological discussions. Unfortunately, the luminescence characteristics of the quartz from the studied sediments do not allow the application of a single grain approach, the ultimate method (Wallinga, 2002), for single mineral grains are the smallest units during sediment transport.

6.4.2 Relationships between the tableland and the studied sediments

By investigating the distribution and height of the gravel mass within which the TM02-A is located, it was assumed that this gravel mass continues laterally and becomes the gravel layer underlying the overbank deposits in the outcrop shown in Figure 6-1b. The TM02-A profile (Figure 6-2a) was accordingly thought to have been covered by 25 m thick sediments including the alluvial gravel and the overbank deposits. However, a new outcrop TM-N (Figure 6-6) which appeared recently caused by slope failures could give another viewpoint. The sedimentary sequence of the outcrop TM-N not only resembles that shown in Figure 6-1a, but also has a reddish sediment at the top. Although the reddish sediment does not exist in the sequence of the outcrop shown in Figure 6-1a, the irregular surface of the outcrop reflects an outcome of erosional processes which commonly exert on the tablelands in the Puli Basin (Chen, 2003; cf. Chapter 4). In addition, the sample TM02-A is remarkably younger than the others (Table 6-2), so two possibilities are to account for its formation

mechanism. First, the gravel mass comprising TM02-A was former colluvium accumulated in the gullies of the tableland and then washed down by rainfall. Finally, these gravel deposits were brought into the Taomi River and part of them settled to become the huge gravel mass. The second possibility is that the Taomi River transported a mixture of gravel, sand and silt coming from upstream and deposited these sediments in this reach. Hereafter, another downcutting event of the Taomi River took place and created a terrace-like feature on the studied site.

The burial ages and positions of TM02-E, TM02-F, and TM03-A reflect that these sediments are consistent with the stratigraphic sequence, so they are assumed to be deposited successively and became parts of the tableland itself. A maximum age of 14.5 ± 0.4 ka cal BP (before present) derived from radiocarbon dating of a fine-grained sediment (TM01) with a lower altitude about 470 m a.s.l. was reported (Tseng et al., 2013). Tseng et al. (2013) interpreted that this fine material was deposited after the tableland had been formed. However, with the data from the studied exposures in the Uni tableland, new knowledge of the relationship between the fine material (TM01) and the tableland is given in this chapter. By integrating the positions and ages of TM01 (except TM01-S), TM02 (except TM02-A), and TM03, it is proposed that these sediments were deposited in 5–6 thousand years successively, settling unconformably on the quartzitic sandstone as the bedrock exposing upstream at an altitude of about 480 m a.s.l. (Figure 6-7). The three intercalated layers of silty sediments together with the fluvial sand and alluvial gravel represent the entire alluvium mass with an estimated thickness over 100 m. The cover sediment at the top of the tableland has been weathered with a thickness of about 7 m, and accordingly appears reddish and silty.

Figure 6-6: Outcrop of TM-N. This outcrop newly appearing has the same sedimentary sequence as TM02. This outcrop exposes by slope erosion owing to heavy precipitation. Reddish color of the outcrop is caused by the weathered material falling from the top layer. (Photo taken by M. Böse in 2013)

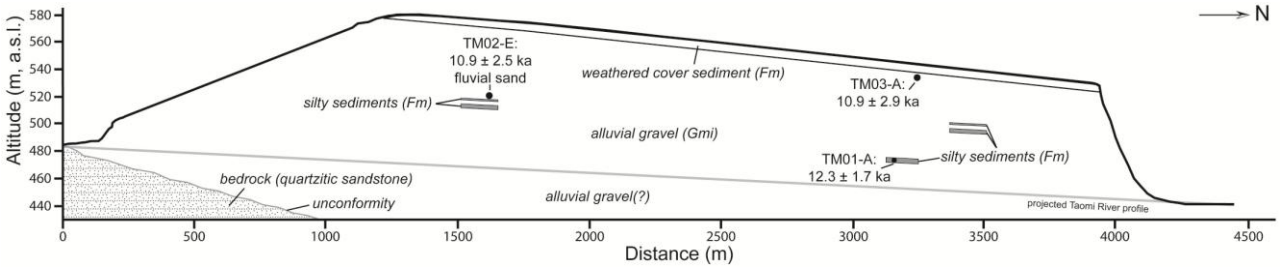

Figure 6-7: Profile with the burial ages of the studied sediments of the Uni tableland. The alluvial gravel with intercalated fluvial sand and gravel, and silty overbank sediments are composed of the Uni tableland. The bedrock exposes in the river channel upstream, being separated by an unconformity from the overlying gravel layer. The seismic reflection data (Ke, 2009) reveal that the bedrock surface (Paileng Formation) descends northward.

6.4.3 Distribution of the alluvium and its source

Tomita (1951) and Yang et al. (2007b) proposed that the alluvium forming the Uni tableland was an alluvial fan created by the Taomi River. Imbrication directions of the alluvial gravel can support the viewpoint. Directions of northwest in the western part of the Uni tableland (Yang et al., 2007b) and of north in the northern end of the SC tableland (Figure 4-11) are consistent with a radial pattern of deposition for the alluvial fan with a trunk river coming from the south. In addition, the sedimentological characteristics of the studied outcrops, such as clast-support, maximal gravel size (< 20 cm), poor to moderate sorting, and locally stratified fluvial gravels, are also accordant with a type of alluvial fan concluded by Wells and Harvey in 1987 (i.e., transitional-flow deposits (T1)). The distribution of the alluvial gravel (Figures 2-3 and 6-8) proposed by M.-M. Chen (2003) could accordingly mark the probable extent of the alluvial fan. The potential alluvial fan area is much larger than the Uni and SC tablelands, indicating that it has undergone constant erosional processes since being formed.

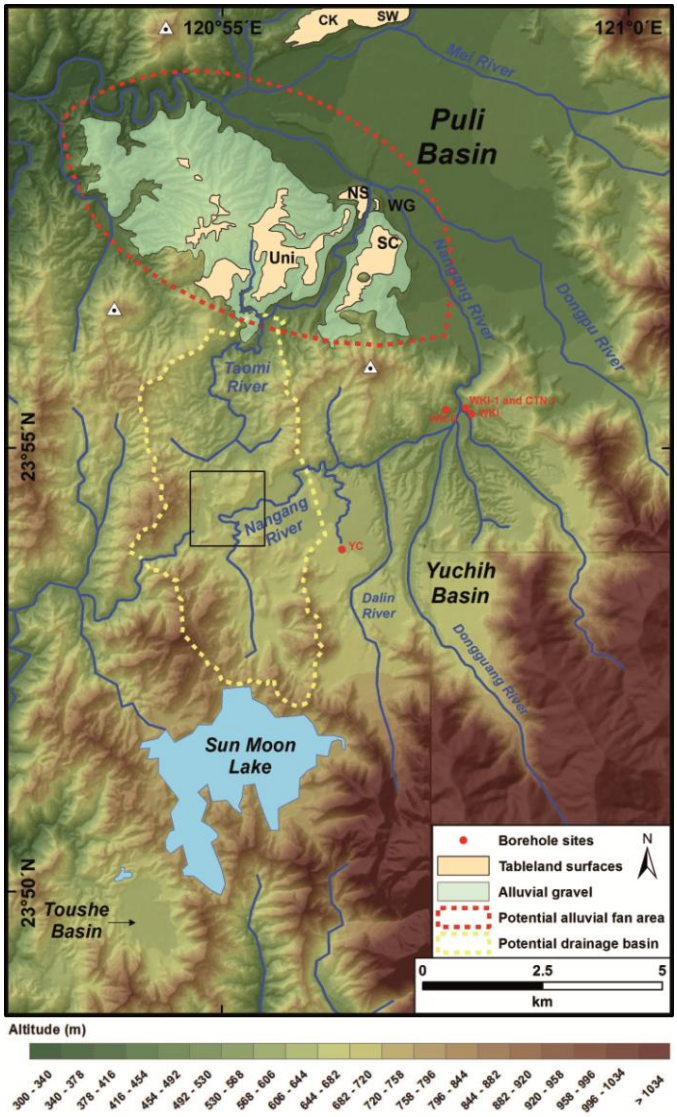

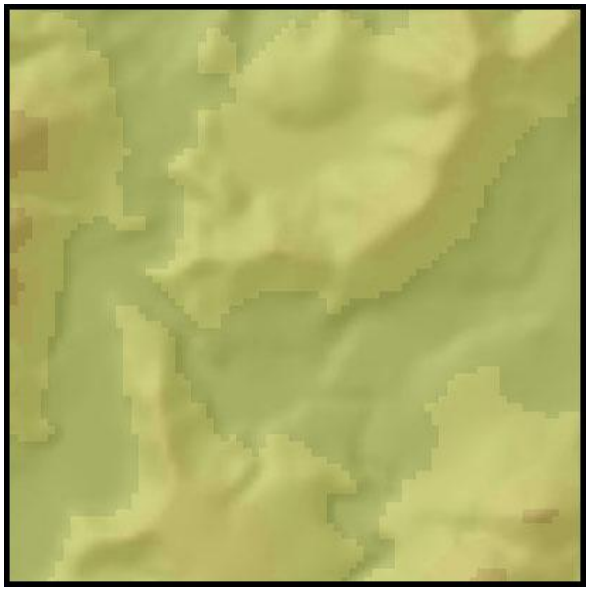

Figure 6-8: Potential alluvial fan area with its drainage basin west of the Yuchih Basin. The enlarged area on the right marked by the black square reveals that the topography likely appears the remnants of river channels of the old Taomi River, which could be captured by the headward erosion of the Nangang River after the Yuchih Basin had been drained. The boreholes studies were derived from B.-C. Chen (2003).

To provide big amounts of alluvium, the Taomi River should have been longer than it is nowadays. The sharp turn of river course of the Nangang River in the western part of the Yuchih Basin shows that it had possibly flowed northwestward and been the upstream reach of the Taomi River before it was diverted (Figure 6-8). B.-C. Chen (2003) studied the stratigraphic sequences in the Yuchih Basin derived from five boreholes and three sediment exposures and obtained ages of organic material in lacustrine sediments by applying radiocarbon dating method. According to the results, B.-C. Chen (2003) interpreted that a lake existed only in the eastern part of the Yuchih Basin, whereas alternations of massive gravel and sand layers characterize the stratigraphic sequence in the western part. The old Taomi River transported coarse-grained sediments in the drainage basin (area bounded by the yellow dashed line) and deposited as an alluvial fan at the valley mouth in the Puli Basin. At 6 ka, the lake had been drained through a gorge in the northern edge of the basin, and then the modern Nangang River was formed (B.-C. Chen, 2003).

On the basis of the topography and borehole data (B.-C. Chen, 2003) in the Yuchih Basin, a development of the Taomi River could be: the Taomi River originated to the west of the Yuchih Basin, and its head was located to the north of the Sun Moon Lake. After the old lake in the Yuchih Basin had been drained, the Nangang River started to develop in the Yuchih Basin and also elongated itself by headward erosion. Afterwards, the old and longer Taomi River was diverted into the Yuchih Basin when the headward erosion of the Nangang River reached the old Taomi River valley. The modern Taomi River developed again in a smaller catchment with a shorter and narrower river channel.

6.4.4 Paleoenivronmental implications

To find out a link between the deposition of the studied alluvium and paleoclimatic conditions, their burial ages with a complete climate record in the late Quaternary of Taiwan were compared (Figure 6-9), derived from pollen and vegetation data in the Toushe Basin (Liew et al., 2006) about 13 km southwest of the Puli Basin (Figure 6-8). From the comparison, the alluvial deposition took place at the end of the Late Pleistocene and stopped in the early Holocene. The climatic conditions at that time during the transition of the two epoches turned from dry and cool into wet and warm. The same climatic trend is also reflected by the end of glacier advance in the Nanhutashan in central northern Taiwan (above 3000 m a.s.l., Hebenstreit et al., 2011). It is identified that phases of morphological instability and hence erosion is consistent with climatic transitions (Vandenberghe, 2002). The deposition of the alluvium, i.e., TM01, TM02 (except TM02-A), and TM03, are thus likely related to the erosion (e.g., channel scour and slope failure) in the upstream area of the old Taomi River. During the early Holocene, catastrophic mass-wasting events also happened on the eastern

coast of Taiwan and produced alluvial fans and fan-deltas at beaches (11.3–8.3 ka derived from radiocarbon dates, Hsieh at al., 2011). In central southern Taiwan, Hsieh and Chyi (2010) also observed mass-wasting events leading to formation of large fan terraces (debris flow/fluvial gravel, 100–200 m thick) in two river catchments (550–800 m a.s.l.) with radiocarbon dates of 9.5–8.9 ka. These cases may attribute to severe rainfall events during the early Holocene characterized by wet and relatively warm climate. In the same catchment, Chao (2003) also dated a selected alluvial fan and obtained a similar age of 12100 years before present. These cases mentioned above can probably reflect that the erosional processes resulting from climatic change may be widespread in Taiwan during the climatic transitions.

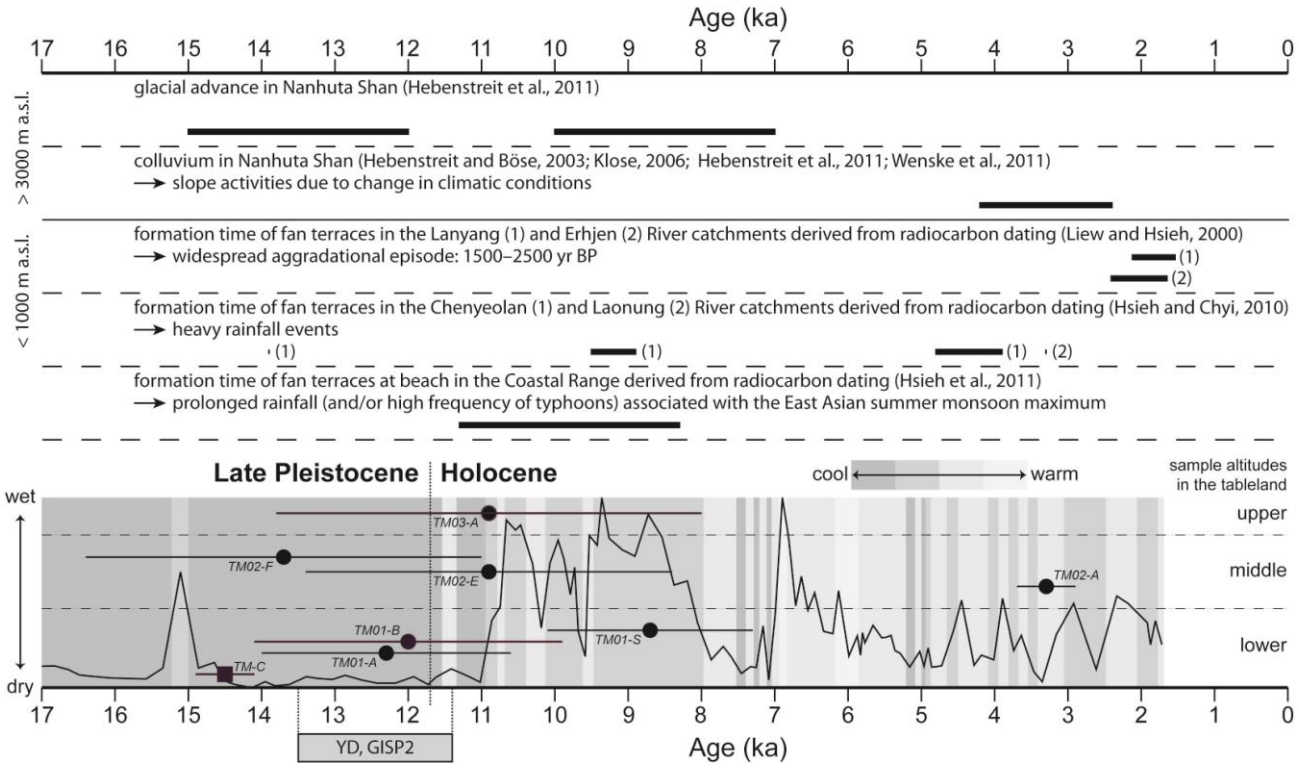

Figure 6-9: Comparison among ages of alluvial fans, fluvial terraces, and colluvium in different areas. The burial ages of this work (black solid circles with uncertainties) are plotted directly on the paleoclimatic record in the Toushe Basin studied by Liew et al. (2006). The dry/wet curve is derived from the percentage of sum of pollen and spores, whereas variations in temperature are represented by different types of forest. Ages of other geomorphic features are presented as black bars with uncertainties, and the altitudes at which they are located are also indicated on the left.

The young sediment of TM02-A (3.3 ± 0.4 ka) was deposited also within the alternations of climatic conditions. The age is well in agreement with those of slope sediments (OSL ages of 3.3 ± 0.9 ka and 3.1 ± 0.3 ka by Klose, 2006; OSL ages of 3.3 ± 0.7 ka and 3.1 ± 0.3 ka by Hebenstreit et al., 2006; OSL

age of 3.7 ± 0.6 ka by Wenske et al., 2011) in high mountain areas (above 3000 m a.s.l.) in central northern Taiwan, which are interpreted as slope activities caused by climate change. Some events happening at around 3 ka are also reported in other places in Taiwan. Along the Beigang River to the north of the Puli Basin, Yanites et al. (2010) dated a series of fluvial terraces by means of OSL dating and obtained their burial ages between 3.9 ka and 2 ka. Fan terraces studied by Hsieh and Chyi (2010) were also formed at about 3.3 ka in the two river catchments mentioned above. In central eastern Taiwan, fluvial terraces dated 3.4–3.2 ka are also observed to develop in a bedrock channel of the Liwu River (Chyi, 1995).

River terraces dated 2120–1540 years before present exist in a river catchment in northeastern and 2410–1650 years before present in another one in southwestern Taiwan, respectively (Liew and Hsieh, 2000). Liew and Hsieh (2000) assume that the depositional ages of the terraces derived from radiocarbon dating show an island-wide aggradational processes following an incisional behavior before 2500 years before present (Hsieh et al., 1997). They further interpreted that this change in environments was caused by increased frequency of typhoons or precipitation, which had triggered slope failures and thus produced more sediment yield. As a result, river aggradation and/or lateral erosion prevailed during this period. By integrating the events at around 3 ka mentioned above, the aggradation period may extend back to around 4 ka.

6.4.5 Implications for landform development

The accumulation of the studied alluvium mass and the subsequent evolution of the tableland are probably subject to both meteorological and tectonic events. With the timing constraints of the sediments, a model of the landform development for the tableland in the southern part of the Puli Basin is to be reconstructed. The model is proposed in four stages in a chronological order (Figure 6-10):

State I: Alluvial deposits may have been transferred by the old Taomi River from the areas west of the Yuchih Basin before 12.3 ± 1.7 ka to settle at the mouth of the river valley. Gravel together with mixture of fine-grained sand and silt as the matrix was transported downstream probably resulting from severe rainfall in the area. Later flood events could be in a small scale, so they were confined in the river channel. Silty and finer deposits brought by the events were taken out of the channel and deposited as overbank sediments by overflow of the flood (e.g., TM01, Tseng et al., 2013) in the adjoining areas along the river. Weakening of the river flow then led to the formation of the thin fluvial sand and gravel layers (TM02-E and TM02-F) at 10.9 ± 2.5 ka. Afterwards, the accumulation of the alluvial gravel (TM03) occurred again and ended at 10.9 ± 2.9 ka. A total thickness of the alluvium

mass then was estimated to be over 100 m.

Stage II: The Taomi River started to incise the alluvium mass, a process lasting for 5–6 thousand years. This inference for the incision amount and duration is according to the observation of an unconformity existing between the fine-grained sediment (TM01-A) and the overlying fluvial gravel and sand lens (Tseng et al., 2013). The unconformity represents an erosion event leading to the hiatus. As a result, the vertical height difference caused by the incision is estimated to be 80 m from the top of the alluvium mass to the position of TM01, and the terrace was formed consequently. The cause of the Taomi River incision may be associated with crustal uplift which is assumed to be the main mechanism of forming the oldest tablelands in the Puli Basin (Yang et al., 2007b). Since this stage, the uppermost sediment has been weathered.

Stage III: The erosional process of the Taomi River stopped owing to the cease of the crustal uplift in this stage. The climatic condition characterized by humidity may cause more precipitation leading to the introduction of clasts deriving from the erosion in the drainage basin into the river. Increase in the discharge let the river transport the sediments downstream and deposit them in the Taomi River catchment in the Puli Basin at 8.7 ± 1.4 ka (Tseng et al., 2013). These sediments include sub-rounded fluvial gravel as the main part and minor sand-sized material such as sand lenses in the gravel (e.g., TM01-S, Tseng et al., 2013) growing along the river banks.

Stage IV: The incision occurred again probably resulting from another crustal uplift event. The erosional processes resulted in the formation of the small-scale fluvial terrace (i.e., TM01, Tseng et al., 2013). The Taomi River subsequently deposited younger alluvium, which is interpreted to consist of gravel, sand, and mud (Huang et al., 2000). The tableland (i.e., the SC tableland) to the east of the Taomi River was then bent obviously, whereas the surface to the west was tilted slightly eastwards. The stress deforming the tableland surface was assumed to be a compressional stress in the orientation of SE-NW (Figure 4-12; Yang et al., 2007b).

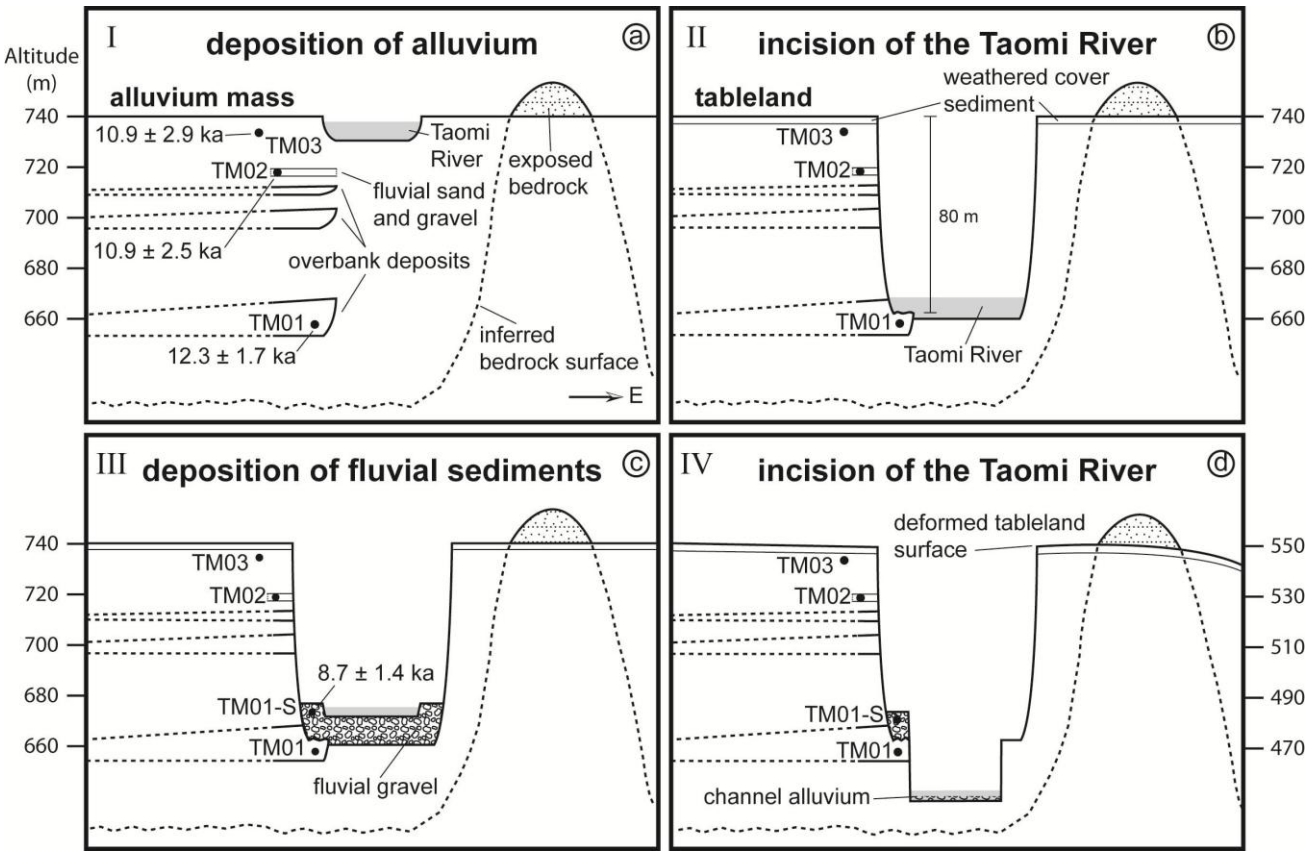

Figure 6-10: Geomorphic evolution model of the studied tableland. See detailed descriptions of each stage in the text.

During the period of the first stage, the causes of the alluvial fan are assumed to be climatic change and tectonic activities. The former introduced immense amounts of sediment into the old Taomi River, and the latter had created a depression in the central to let the sediments be deposited (Tomita, 1951; Yang et al., 2007b). These events also result in other alluvial fans formed by the Mei River in the eastern and by the Beigang River in northwestern parts in the Puli Basin (Yang et al., 2007b). Ke (2009) further interprets the tectonic mechanism as downwarping on the basis of seismic reflection data which reveal the underground structure in the Puli Basin that the unconsolidated deposits and the unconformably underlying bedrock (i.e., Paileng Formation) deform in a disk-like shape. The field surveys exhibit that the bedrock exposes on the SC tableland as a hill (Figures 4-2 and 6-10), probably indicating a high relief in this area at that time. This high-relief topography may retrain the development of the alluvial fan during the early period of this stage. The fine-grained sediments including the overbank deposits and fluvial sand and gravel are only observed in the Uni tableland on the western side of the Taomi River, for the slope of the SC tableland is covered by dense vegetation.

The incision of the Taomi River created a river valley with height difference of about 80 m in the

stage II. In terms of geomorphology, the alluvial fan is located in the downstream reach of the river, so stream power in the reach should not be strong enough to incise the alluvium. Thus, crustal uplift in marginal areas of the basin is considered to be the main cause, which also led to the change in flow direction of the Beigang River (Yang et al., 2007b). This could be explained by distribution of fluvial terraces with different burial ages within the Beigang River valley. Yanites et al. (2010) dated the fluvial terraces developing in the Beigang River valley by applying the luminescence dating method. The results show that the terraces with burial ages of younger than 6.6 ± 0.8 ka exist only downstream of the boundary between the Paileng Formation and the Shuichangliu Formation (Figure 2-3). The phenomenon can possibly support that the crustal uplift at the basin margins started after the formation of the alluvial fan. The crustal uplift not only caused the incision of the Taomi River, but also diverted the Beigang River, which then deposited young sediments in the modern channel of the Beigang River.

According to the burial age of the fluvial gravel in the Taomi River in the third stage of the model, the incision rate could be at least 15 mm/a. The study of Lee et al. (2006) reveals an exhumation rate of 4–10 mm/a within the time period of < 1 ma by means of fission track study in the Central Range of Taiwan (cf. Section 2.1). This difference between the two values can probably be explained by that the magnitude of the tectonic activities in the Puli area is bigger than in other places in the Central Range.

The intermittent tectonic activities resulting from compressional stress led to crustal uplift in the marginal areas of the Puli Basin. After the fluvial gravel had been deposited at 8.7 ± 1.4 ka (i.e., TM01-S, Tseng et al., 2013), the crustal uplift reactivated to result in another incision event of the river in the fourth stage. The compressional stress deformed and tilted the Uni, SC, and DP tableland surfaces towards east or southeast. The tectonic tilting can also probably be revealed by the asymmetric slope pattern of the tablelands on the both sides of the Taomi River. After the tilting, the Taomi River eroded laterally its eastern bank, causing more slope failure due to the undercutting of the slope base. Accordingly, the gentler feature on the eastern facing slope by the Taomi River is observed (Fig 4-12). It is also possible that the crustal uplift led to not only the formation of the terrace (TM01, Tseng et al., 2013), but also other terraces in the basin (e.g., CK, SW, and WG tablelands). Yang et al. (2007b) also proposed that CK, SW, and WG tablelands (i.e., LT2 in the study of Yang et al. (2007b)) were formed after Uni, SC, and DP tablelands (i.e., LT1).

A second scenario could also be made. The fluvial gravel and sand (TM01-S) could be deposited in the first stage in which the alluvial fan was formed, for the burial age of 8.7 ± 1.4 ka and those of other studied material overlap. In this case, a period of river erosion could follow the flood event (i.e., deposition of the overbank sediment TM01), and the fluvial process turned into aggradation

again. Afterwards, an erosional terrace was then formed by the two intermittent incision events. However, the incision rate of the Taomi River cannot be estimated because of the lack of a time constraint from sediments being deposited later in the valley. To confirm the relationship between the TM01-S and the Uni tableland, a more precise burial age of the fluvial gravel or its exposures in other positions are needed.

6.5 Conclusions

The studies on the tablelands in the southern part of the Puli Basin first give a geochronological framework of its sediments by applying luminescence dating methods. Investigations of the sediments also reveal that changes in sedimentary environments may be due to occasional severe rainfall related to alternations of climatic conditions within the period when the alluvium was deposited. Local lithology and tectonic activities also played a critical role in shaping the landform in the studied area.

A new statistic model developed for calculating equivalent doses derived from the OSL dating method makes plausible the burial ages of the studied sediments of 3.3 ± 0.4 ka, 10.9 ± 2.5 ka, 13.7 ± 2.7 ka, and 10.9 ± 2.9 ka. By integrating the burial age of TM01 (i.e., 12.3 ± 1.7 ka, Tseng et al., 2013), the studied alluvium could be deposited as an alluvial fan in 5–6 thousand years. To provide huge amounts of sediment (at least 100 m thick), the Taomi River should be longer than it is today. Topographical and sedimentological features give implications that the former Taomi River may originate in the western part of the Yuchih Basin and three flood events owing to overflow either of the Yuchih Basin or the Sun Moon Lake also took place during the deposition of the alluvium. During the transition from the Late Pleistocene to the Holocene, the climatic change led to intense rainfall to bring much material from slopes to the river by erosional processes. In addition, aggradational processes around 3 ka could be in an island-wide scale and had started from 4 ka. A landform development model for the studied area is then reconstructed. An estimated incision rate of at least 15 mm/a of the Taomi River reflects local tectonic activities with a higher magnitude than other areas in the Central Range in Taiwan.

Factors that controlled the fluvial processes are climate change, lithology and topography in the Taomi River catchment. Accompanied by the local tectonic activities, various geomorphic units in the Puli Basin, such as tablelands, river terraces, alluvial fans, and alluvial plain, have been formed.

CHAPTER 7
Overall conclusions

The objectives of this work are to find answers to the main research questions, which are:

1. Does the tableland formation in the Puli Basin link to climate changes in the past?
2. Is the tectonic framework a factor that influences the tableland formation?
3. Is the Puli Basin a sole situation in Taiwan?

The analysis results of this work, i.e., the sedimentary sequences of the tablelands associated with fluvial processes and the landform development influenced by paleoclimatic conditions and tectonic activities, have been described in previous chapters. On the basis of the results, arguments and evidence for the overall conclusions will be stated in this chapter to answer the questions.

7.1 Does the tableland formation in Puli Basin link to climate changes in the past?

The sedimentological characteristics in the alluvial deposits forming the Uni tableland, i.e., clast-support, maximal gravel size (< 20 cm), poor to moderate sorting, and locally stratified fluvial gravels (cf. Section 6.4), are accordant with a type of alluvial fan concluded by Wells and Harvey in 1987 (i.e., transitional-flow deposits (T1)). In addition, the imbrication directions (Figure 4-11 and Yang et al., 2007b) and distribution of the alluvial gravel (M.-M. Chen, 2003) also point out an alluvial fan origin for the alluvium in the southern part of the Puli Basin.

Alluvial fans were also formed by the Beigang River and the Mei River in the northern and eastern parts of the Puli Basin, respectively (Tomita, 1951; Yang et al., 2007b). The stratigraphic sequence of the DP tableland, i.e., the former alluvial fan formed by the Beigang River, displays two main types of sedimentary facies (Tomita, 1951). Small-sized gravel (< 10 cm) intercalated with sand layers reflects a braided river environment in the earlier period (B.-C. Chen, 2003), whereas coarser gravel (> 15 cm) layers reveal a process similar to that of the Uni and SC tablelands in the later one. Although peat layers were found within the DP tableland, borehole data in the basin show no lacustrine sediments (Figure 4-8; M.-M. Chen, 2003). It is more likely that small lakes or swamps existed locally during the formation of the DP tableland. Furthermore, lacustrine sediments are not observed within the Uni and SC tablelands, so the Puli Basin was not filled with water during the formation of the alluvial fans.

By comparing the OSL and radiocarbon dating results of the studied sediments with the paleoclimatic records derived from palynological analyses in the Toushe Basin (Figure 6-9; Liew et al.,

2006), the alluvial fans were formed during the transition from the Late Pleistocene to the Holocene. According to the records, humidity and temperature increased greatly during this period, resulting in much more precipitation and thus erosional processes than before. In the climatic background, immense amounts of sediment from mass wasting in the drainage basin were accordingly produced and stored in adjacent areas (e.g., the Yuchih Basin). Increased discharge of rivers delivered these sediments in the river valley downstream, and dropped off them to form alluvial fans at the valley mouths. This accumulation of the alluvium had lasted for 5 to 6 thousand years.

On the basis of the arguments and evidence mentioned above, therefore, the answer to the question in this section is positive. That is, formation of tablelands being composed of alluvial fan deposits in the Puli Basin indeed links to climate changes in the past.

7.2 Is the tectonic framework a factor that influences the tableland formation?

The Puli Basin, together with other intramontane basins, was formed probably as a piggyback basin related to underground detachment sliding at about 700 ka (Wilcox et al., 2011). Stress triggering the detachment sliding resulted from the movement of the Philippine Sea Plate, so the arrangement of these basins is perpendicular to the stress direction or parallel to the geological terrains in Taiwan. Folding and faulting within the bedrock took place by the stress as well (Huang et al., 2000; Ke, 2009), possibly after the basins had been formed (Yang et al., 2007b).

Erosional processes by rivers carved the bedrock and caused a rugged surface, which became an unconformity separating the bedrock and overlying sediments when the erosion turned into aggradation (Figure 4-3). Fluvial gravel as the main component of sediments was transported by rivers coming from the north, east, and south, and braided river systems thus developed in the Puli Basin during the period of the aggradation (Figure 4-3; B.-C. Chen, 2003; Ke, 2009).

The alluvial fans were then formed at the river valleys in the margin areas owing to the climate changes. During the deposition of the alluvial fan in the southern part of the basin, different layers of homogeneous fine-grained sediments as intercalations in the gravel material were formed. These fine-grained sediments are interpreted as overbank deposits of flood events derived from binocular observation and grain size analyses (Figure 6-4; Tseng et al., 2013). The increase in discharge of the Taomi River which led to the flood events may be attributed to overflow of an old lake in the Yuchih Basin (Figure 6-8). As on the Uni and SC tablelands, the silty cover sediments of the DP tableland have been weathered and thus appear reddish or brownish in color. The weathered cover sediments are also observed on the top of other tablelands with lower altitudes in the basin.

Incision of the Taomi River then occurred, and dissected the alluvial fan up to 80 m deep at a rate of at least 15 mm/a to create the fluvial terraces first (i.e., later Uni and SC tablelands; Figure 6-10).

The incision event may result from the crustal uplift at marginal areas of the Puli Basin, and also led to diverting the Beigang River (Yang et al., 2007b). Erosional processes started to shape the alluvial fans at the same time, so remnants of the alluvial fans became smaller with time. Gullies or even streams began to develop on their slopes as well (Figures 4-12, 4-13, 4-15, and 4-16).

Incision of rivers stopped at around 9 ka, and rivers began to deposit fluvial sediments in channels. Braided rivers developed again, within which sand lens as point bars were formed on insides of river bends in Taomi River valley (Tseng et al., 2013). Rivers cut downward the sediments again due to following crustal uplift, and fluvial terraces were then formed (i.e., TM01 as well as CK and WG tablelands). Younger tablelands (i.e., AL and NS tablelands) were formed later because of alternations in aggradation and incision of the rivers related to the tectonic activities. The compressional stress deformed these tablelands after they had been formed (Figure 6-10).

Fluvial terraces in the western part of the basin were formed owing to the incision of the Nangang River and the Mei River resulting from the dissection of the Nangang River at the western outlet of the basin (Yang et al., 2007b). Afterwards, aggradation of rivers resulted in formation of modern alluvial plain, floodplains alluvial fans within the basin. These geomorphic units are not covered by the reddish silty sediments, giving evidence that the tablelands had been formed prior to the fluvial terraces and the alluvial plain, and are thus regarded as the old geomorphic surfaces of the Puli Basin.

The incision of the Taomi River caused a deep dissection into the alluvial fan in a short time period. Since the river is not strong to incise the alluvium in the downstream reach, an external factor is taken into account. Data of seismic reflection and borehole reveal that a 200 m thick coarse-grained sediment layer in the basin center overlies unconformably a coarse-grained gravel layer being correlated to the upper gravel unit in DP tableland (M.-M. Chen, 2003; Ke, 2009). In addition, deformed surfaces are also observed in the Uni, SC, and DP tablelands (Figures 4-12 and 4-13). Therefore, local tectonic activities did influence the landform and accordingly resulted in the incision of river, so tablelands and later fluvial terraces were formed (Yang et al., 2007b; Tseng et al., 2013). These tectonic activities are proposed as downwarping (Tomita, 1951; Ke, 2009), a process of curving inward and downward of the ground.

7.3 Is the Puli Basin a sole situation in Taiwan?

7.3.1 From 14 ka to 7 ka

7.3.1.1 14–9 ka

The results of this study are strongly supported by evidence from other areas in Taiwan. For

instance, palynological analyses in the Toushe Basin (Liew et al., 2006) give evidence of paleoclimate changes which coincide with the time period of the formation of the tablelands in the Puli Basin. Increased sediment load in rivers resulting from slope failures or mass wasting was caused by frequent high-level precipitation in the Taomi River valley to west of the Yuchih Basin. These sediments were then transported downstream and deposited as an alluvial fan, which became the Uni and SC tablelands in the Puli Basin owing to tectonic activities. The frequent rainfall to high level also induced overflow of an old lake in the Yuchih Basin, resulting in flood events of the Taomi River. The alluvial fan becoming the later DP tableland in the northern part of the basin was also formed in the climatic condition within this period.

During this period, large fan terraces (12 ka by Chao (2003); 13 ka and 9.5–8.9 ka by Hsieh and Chyi (2010)) being composed of debris flow material or fluvial gravel with thickness of 100–200 m were also formed in two river catchments (i.e., the Chenyeolan River and the Laonung River, 550–800 m a.s.l.) to the south of the Toushe Basin. Mass wasting events triggered by heavy rainfall within these two catchments are proposed by the authors. Responses of geomorphic processes to the change in climate during the transition are observed also in low-altitude areas in Taiwan. Hsieh at al. (2011) dated alluvial fans and fan-deltas resulting from catastrophic mass wasting events near the eastern coast of Taiwan and obtained ages of 11.3–8.3 ka. The global climate entered a relatively stable period from 9 ka compared to the transition of climatic conditions (Knox, 1995). However, the data of pollen analyses (Liew et al., 2006) reveal that fluctuations in humidity and temperature in central Taiwan were at a high frequency during this period.

7.3.1.2 9–7 ka

Between 9 ka and 7 ka, humidity decreased from a high level. Nevertheless, alluvial fans developed in the Chenyeolan River catchment (8.1–7.1 ka, Chao, 2003) and on the eastern coast (11.3–8.3 ka, Hsieh at al., 2011). These phenomena can imply that duration of erosional processes on landforms could extend till 7 ka. This can then be explained that sediments eroded in upstream area of the Taomi River were deposited downstream to form the channel deposits (8.7 ± 1.4 ka, Tseng et al., 2013).

To sum up, erosional processes on the landforms, e.g., fluvial incision and mass wasting, caused by increased precipitation during the climatic transition between 14 ka and 7 ka can prevail over Taiwan.

7.3.2 From 4 ka to 1.5 ka

Hsieh et al. (1997) and Liew and Hsieh (2000) proposed that a period of aggradation between 2.5 ka and 1.5 ka following a long-term incisional behavior over Taiwan. This change in geomorphic processes is interpreted that frequency of precipitation or typhoon increased and thus triggered slope failures and produced more sediment yield (Liew and Hsieh, 2000). This interpretation may support the slope failures in the Taomi River (3.3 ± 0.4 ka). Along the Beigang River to the north of the Puli Basin, a series of fluvial terraces are also dated 3.9–2 ka (Yanites et al., 2010). In addition, alluvial fans formed from mass wasting owing to heavy rainfall in the Cheyeolan River and the Laonung River (3.3 ka, Hsieh and Chyi, 2010) can also be attributed to the geomorphic processes during this period. The processes could also influence areas in high mountain areas (above 3000 m a.s.l.). In central northern Taiwan, sediments dated between 3.7 ka and 3.1 ka (Klose, 2006; Hebenstreit et al., 2006; Wenske et al., 2011) are assumed to result from slope movements caused by climate change. However, reports on geomorphic units or events during 7 ka to 4 ka are rare, so the geomorphic processes in the period are still an open question.

7.3.3 Factors controlling landform development of the Puli Basin

Factors dominating development of terraces and tablelands in Taiwan are concluded (Tsai, 2004): fall in sea level (e.g., fluvial terraces formed at 30 ka), local tectonic activities (e.g., the Pakua Tableland and Hsinshe Terraces), and changes in adjacent base level (e.g., fan terraces in the Lanyang River catchment (2.5–1.5 ka, Liew and Hsieh, 2000)). Based on the results of this study, an additional conclusion can also be drawn. That is, the climate change during the transition from the Late Pleistocene to the Holocene produced huge amounts of sediment by increased erosional processes on the terrains in Taiwan. These sediments create a favorable condition for later landform development which can be influenced by various factors, e.g., tectonics, lithology, base level change, and/or climate.

It is the background that the landform in the Puli Basin developed in. The old longer Taomi River originating west of the Yuchih Basin collected sediments created by erosional processes in the drainage basin. Increasing river discharge owing to heavy precipitation then transported the sediment loads downstream. These sediments were then laid down as an alluvial fan at the valley mouth in the Puli Basin, which were formed by tectonic processes. Later local and intermittent tectonic activities led to incision of the Taomi River and other rivers, and then created several levels of tablelands and fluvial terraces in Puli Basin.

Appendix

A1 List of overall references

Adamiec, G. and M. Aitken, 1998. Dose-rate conversion factors: update. *Ancient TL* **16**, pp. 37–50.

Aitken, M.J., 1985. Thermoluminescence Dating. Academic Press, London, p. 359.

Aitken, M.J., 1998. An Introduction to Optical Dating. The Dating of Quaternary Sediments by the Use of Photon-stimulated Luminescence. Oxford University Press, Oxford, p. 267.

Alappat, L., A. Vink, S. Tsukamoto and M. Frechen, 2010. Establishing the Late Pleistocene-Holocene sedimentation boundary in the southern North Sea using OSL dating of shallow continental shelf sediments. *Proceedings of the Geologists' Association* **121(1)**, pp. 43–54.

Alonso, P., C. Sierra, E. Ortega and C. Dorronsoro, 1994. Soil development indices of soils developed on fluvial terraces (Peñaranda de Bracamonte, Salamanca, Spain). *Catena* **23**, pp. 295–308.

Anstey, R.L. and T.L. Chase, 1974. Environments through time: A laboratory manual in the interpretation of ancient sediments and organisms. Burgass publishing company, Minneapolis, Minnesota, USA, p. 136.

Ashley, G.M., 1978. Interpretation of polymodal sediments. *Journal of Geology* **86**, pp. 411–421.

Biq, C.-C., 1989. The Yushan-Hsuehshan Megashear zone in Taiwan. *Proceedings of the Geological Society of China* **20**, pp. 61–70.

Birkeland, P. W., 1999. Soils and Geomorphology (3rd ed). Oxford Univ. Press, New York.

Bradley, R.S., 2000. Past global changes and their significance for the future. *Quaternary Science Reviews* **19(1–5)**, pp. 391–402.

Bøtter-Jensen, L., E. Bulur, G.A.T. Duller and A.S. Murray, 2000. Advances in luminescence instrument systems. *Radiation Measurements* **32**, pp. 523–528.

Byrne, T., Y.-C. Chan, R.-J. Rau, C.-Y. Lu, Y.-H. Lee and Y.-J. Wang, 2011. The Arc-Continent Collision in Taiwan. Arc-Continent Collision, Frontiers in Earth Sciences. Springer-Verlag, Berlin Heidelberg, doi: 10,1007/978-3-540-88558-0_8. 213-245.

Charlton, R., 2010. Fundamentals of Fluvial geomorphology. Routledge, Abingdon, Oxon, p. 234.

Chang, J.-C. and K.-S. Yang, 2004. Deformation and occurrence of the Che-lung-pu Fault from geomorphic evidence. *Quaternary International* **115–116**, pp. 177–188.

Chao, C.-Y., 2003. The River Terraces and Landscape Evolution of the Chenyulan Drainage Basin in Central Taiwan (in Chinese). Master Thesis, Department of Geography, National Kaohsiung Normal University, Kaohsiung, Taiwan, p. 145.

Chen, B.-C., 2003. Sedimentology and Neotectonics of the Puli and Yuchi Basins, Central Taiwan (in Chinese). Master Thesis. Institute of Geosciences, National Taiwan University, Taipei, Taiwan, p. 97.

Chen, C.-H., 1998. Metamorphic rock of Taiwan (in Chinese). *Geological Series of Taiwan* **11**. ISBN: 9570227214.

Chen, M.-M., 2003. Quaternary geology in the Puli Basin and surrounding terraces (self-translation, in Chinese). Annual Report of Central Geological Survey, pp. 53–56.

Chen, P.-H., 1984. A Geoelectric Resistivity Survey in Puli Basin. *Bulletin of Geophysics, National Central University* **26**, pp. 107–124.

Chen, R.-W., 2010. The terrace correlation based on pedogenics degree of the lateritic soils on the tablelands in the Puli Basin (in Chinese). Master Thesis. Department of Geography, National Changhua University of Education, Changhua, Taiwan, p. 80.

Chen, W.-S., B.-S. Huang, Y.-G. Chen, Y.-H. Lee, C.-N. Yang, C.-H. Lo, H.-C. Chang, Q.-C. Sung, N.-W. Huang, C.-C. Lin, S.-H. Sung and K.-J. Lee, 2001. 1999 Chi-Chi Earthquake: A Case Study on the Role of Thrust-Ramp Structures for Generating Earthquakes. *Bulletin of the Seismological Society of America* **91(5)**, pp. 986–994.

Chen, W.-S., K.-J. Lee, L.-S. Lee, D.J. Pontib, C. Prenticeb, Y.-G. Chen, H.-C. Chang and Y.-H. Lee, 2004. Paleoseismology of the Chelungpu Fault during the past 1900 years. *Quaternary International* **115–116**, pp. 167–176.

Chen, W.-S., Y.-G. Chen, R.-C. Shih, T.-K. Liu, N.-W. Huang, C.-C. Lin, S.-H. Sung and K.-J. Lee, 2003b. Trust-related river terrace development in relation to the 1999 Chi-Chi earthquake rupture, Western Foothills, central Taiwan. *Journal of Asian Earth Sciences* **21**, pp. 473–480.

Chen, Y.-G. and T.-K. Liu, 1991. Radiocarbon dates of river terraces along the lower Tahanchi, northern Taiwan: their tectonic and geomorphic implications. *Proceedings of the Geological Society of China* **34(4)**, pp. 337–347.

Chen, Y.-G., J.Bruce H. Shyu, Y. Ota, W.-S. Chen, J.-C. Hu, B.-W. Tsai and Y. Wang, 2004. Active structures as deduced from geomorphic features: a case in Hsinchu Area, northwestern Taiwan. *Quaternary International* **115–116**, pp. 189–199.

Chen, Y.-G., J.-H. Hung, K.-Y. Lai, Y.-N. N. Lin, T. Wilcox and K. Mueller, 2007. River terrace development in response to folding above active wedge thrusts in Houli, Central Taiwan. *Journal of Asian Earth Sciences* **31(3)**, pp. 240–250.

Chen, Y.-G., Y.-W. Chen, W.-S. Chen, J.-F. Zhang, H. Zhao, L.-P. Zhou and S.-H. Li, 2003a. Preliminary results of long-term slip rates of 1999 earthquake fault by luminescence and radiocarbon dating. *Quaternary Science Reviews* **22**, pp. 1213–1221.

Chen, Y.-W., Y.-G. Chen, A.S. Murray, T. Watanuki, W.-S. Chen, C.-C. B. Yang, T.-K. Liu and C.-W. Lin, 2009. Long-term crustal movement caused by the Chiuchiungkeng Fault in southwestern Taiwan: Constraints from luminescence dating. *Quaternary International* **199(1–2)**, pp. 15–24.

Ching, K.-E., M.-L. Hsieh, K.M. Johnson, K.-H. Chen, R.-J. Rau and M. Yang, 2011. Modern vertical deformation rates and mountain building in Taiwan from precise leveling and continuous GPS observations, 2000–2008. *Journal of Geophysical Research* **116**, B08406, p. 16.

Chiu, H.-T., 1971. Folds in the Northern Half of Western Taiwan. *Petroleum Geology Taiwan* **8**, pp. 7–19.

Chou, S.-A., 1981. Investigation on clay deposit in Yu-Chih-Wai-Chia-Tao Area, Nantou, Central Taiwan (in Chinese). *Mining Technology* **19(2)**, pp. 146–158.

Chu, C.-R., 1991. Discussions on the genesis of the Puli Basin (in Chinese, self-translation). Bachelor Thesis. Department of Geosciences, National Taiwan University, Taipei, Taiwan, p. 24.

Chyi, S.-J., 1995. Landscape evolution of Liwn-hsi drainage basin (in Chinese). Doctoral Dissertation. Institute of Geography, National Taiwan University, Taipei, Taiwan, p. 187.

Cunningham, A.C. and J. Walling, 2012. Realizing the potential of fluvial archives using robust OSL chronologies. *Quaternary Geochronology* **12**, pp. 98–106.

Dadson, S.J., N. Hovius, H. Chen, W.B. Dade, M.-L. Hsieh, S.D. Willett, J.-C. Hu, M.-J. Horng, M.-C. Chen, C.P. Stark, D. Lague and J.-C. Lin, 2003. Links between erosion, runoff variability and seismicity in the Taiwan orogen. *Nature* **426**, pp. 648–651.

de Jong, A. F. M., 1981. Natural ^{14}C variations. PhD dissertation, University of Groningen.

Delcaillau, B., 2001. Geomorphic response to growing fault-related folds: example from the foothills of central Taiwan. *Geodinamica Acta* **14**, pp. 265–287.

Delcaillau, B., B. Deffontaines, L. Floissac, J. Angelier, J. Deramond, P. Souquet, H.-T. Chu and J.-F. Lee, 1998. Morphotectoic evidence from lateral propagation of and active frontal fold: Pakuashan anticline, foothills of Taiwan. Geomorphology 24, pp. 263–290.

DIN EN 13346, 2001. Characterization of sludges – determination of trace elements and phosphorus – aqua extraction methods (in German).

Dong, J., Y.J. Wang, H. Cheng, B. Hardt, R.L. Edwards, X.G. Kong, J.Y. Wu, S.T. Chen, D.B. Liu, X.Y. Jiang and K. Zhao, 2010. A high-resolution stalagmite record of the Holocene East Asia monsoon from Mt. Shennongjia, central China. *The Holocene* **20**, pp. 257–264.

Dörschner, N., T. Reimann, D. Wenske, C. Lüthgens, S. Tsukamoto, M. Frechen and M. Böse, 2012. Reconstruction of the Holocene coastal development at Fulong Beach in north-eastern Taiwan using optically stimulated luminescence (OSL) dating. *Quaternary International* **263**, pp. 3–13.

Duller, G.A.T., 2008. Luminescence Dating guidelines on using luminescence dating in archaeology. Swindon: English Heritage. Institute of Geography and Earth Sciences, Aberystwyth University, UK, p. 44.

Dury, G.Y., 1959. The face of the earth. Penguin Books, p. 220.

Eyles, N., C.H. Eyles, and A.D. Miall, 1983. Lithofacies types and vertical profile models: an alternative approach to the description and environment interpretation of glacial diamict and diamictite sequences. *Sedimentology* **30**, pp. 393–410.

FAO, 2006. Guidelines for Soil Description. Fourth edition. FAO, Rome, p. 97.

Forman, S.L., M.E. Jackson, J. McCalpin and P. Maat, 1988. The potential of using thermoluminescence to date buried soil developed on colluvial and fluvial sediments from Utah and Colorado, U.S.A.: preliminary results. *Quaternary Science Reviews* **7**, pp. 287–293.

Frechen, M., E. Horváth and G. Gábris, 1997. Geochronology of Middle and Upper Pleistocene loess sections in Hungary. *Quaternary Research* **48**, pp. 291–312.

Galbraith, R.F., R.G. Roberts, G.M. Laslett, H. Yoshida and J.M. Olley, 1999. Optical dating of single and multiple grains of quartz from Jinmium rock shelter, northern Australia: Part I, experimental design and statistical models. *Archaeometry* **41(2)**, pp. 339–364.

Guérin, G., N. Mercier and G. Adamiec, 2011, Dose-rate conversion factors: update. *Ancient TL*. **29**, pp. 5–8.

Hayasaka, I, 1930. Observations in the Intramontane Basins Region of Central Taiwan, A Preliminary Note (in Japanese). *Taiwan Tigaku Kizi* **1**.

Hebenstreit, R., M. Böse and A. Murray, 2006. Late Pleistocene and early Holocene glaciations in Taiwanese mountains. *Quaternary International* **147(1)**, pp. 76–88.

Hebenstreit, R., S. Ivy-Ochs, P.W. Kubik, C. Schlüchter and M. Böse, 2011. Lateglacial and early Holocene surface exposure ages of glacial boulders in the Taiwanese high mountain range. *Quaternary Science Reviews* **30**, pp. 298–311.

Heermance, R.V. and J.P. Evans, 2006. Geometric evolution of the Chelungpu fault, Taiwan: the mechanics of shallow frontal ramps and fault imbrications. *Journal of Structural Geology* **28**, pp. 929–938.

Ho, C.-S., 1988. An introduction to the geology of Taiwan, Explanatory text of the geologic map of Taiwan, Sec. Ed. Central Geological Survey, MOEA, Taiwan, p. 192.

Hou, C.-S., J.-C. Hu, K.-E. Ching, Y.-G. Chen, C.-L. Chen, L.-W. Cheng, C.-L. Tang, S.-H. Huang and C.-H. Lo, 2009. The crustal deformation of the Ilan Plain acted as a westernmost extension of the Okinawa Trough. *Tectonophysics* **466(3-4)**, pp. 344–355.

Hsieh, M.-L, S.-J. Chyi, B.-L. Chen and P.-M. Liew, 1997. Holocene river terraces in the Lanyang and Erhjen Rivers and their climatic implications. In: Program and expanded abstracts of Conf. Geomorphology and Environmental Education across the Taiwan Strait, Taipei, pp. 65–70.

Hsieh, M.-L. and R.-J. Rau, 2009. Late Holocene coseismic uplift on the Hua-tung coast, eastern Taiwan: Evidence from mass mortality of intertidal organisms. *Tectonophysics* **474**, pp. 595–609.

Hsieh, M.-L. and S.-J. Chyi, 2010. Late Quaternary mass-wasting records and formation of fan terraces in the Chen-yeo-lan and Lao-nung catchments, central-southern Taiwan. *Quaternary Science Reviews* **29**, pp. 1399–1418.

Hsieh, M.-L., P.-M. Liew and H.-W. Chen, 2011. Early Holocene catastrophic mass-wasting event and fan-delta development of the Hua-tung coast, eastern Taiwan. *Geomorphology* **134**, pp. 378–393.

Hsieh, M.-L., P.-M. Liew and M.-Y. Hsu, 2004. Holocene tectonic uplift on the Hua-tung coast, eastern Taiwan. *Quaternary International* **115–116**, pp. 47–70.

Hsieh, M.-L., T.-H. Lai and P.-M. Liew, 1994. Holocene climatic river terraces in an active tectonic-uplifting area, middle part of the Coastal Range, Eastern Taiwan. *Journal of Geological Society China* **37(1)**, pp. 97–114.

Hsu, T.-H., 2013. Tectonic activity in the Puli Basin of Central Taiwan: Observation from space and field. Master Thesis. Department of Earth Sciences, National Central University, Jhongli, Taiwan, p. 125.

Hu, C.Y., G.M. Henderson, J.H. Huang, S.C. Xie, Y. Sun and K.R. Johnson, 2008. Quantification of Holocene Asian monsoon rainfall from spatially separated cave records. *Earth and Planetary Science Letters* **266**, pp. 221–232.

Huang, C.-C. 2008. Shallow seismic reflection study in the Puli Basin (in Chinese). Master Thesis, Institute of Geophysics, National Central University, Jhongli, Taiwan, p. 48.

Huang, C.-E., 1978. A Geomorphologic Quantitative Study on the Slope Element of Tapingting Area in Puli Basin. *Journal of Geographical Research* **4(7)**, pp. 173–212.

Huang, C.-S., K.-S Shea and M.-M. Chen, 2000. Explanatory text of the geologic map of Taiwan (in Chinese). Central Geological Survey of Taiwan, PULI, **SHEET 32**, p. 75.

Huang, S.-Y., 1975. Pollen analyses in the Toushe Basin (self-translation, in Chinese). Master Thesis. Institute of Botany, National Taiwan University, Taipei, Taiwan, p. 28.

Huang, T.-C., 1975. Paleoecological Study of Taiwan Waichiataoken Profile. *Taiwania* **20(1)**, pp. 1–22.

Ichimura, T., 1937. On Gravel Beds and Associated Lateritic Soils of the Hori Table-land (in Japanese). *Taityu Pref., Taiwan Tigakukizi* **8(3)**, pp. 17–23.

IPCC, 2007. Climate Change 2007: Synthesis Report. Contribution of Working Groups I, II and III to the Fourth Assessment Report of the Intergovernmental Panel on Climate Change, Intergovernmental Panel on Climate Change, Geneva, Switzerland, p. 104.

Kao, C.-Y., E. Hong, H.-S. Yu and S. Wong, 2013. Stratigraphic Architecture and Lithofacies Analysis: Evidence for Development of the Pliocene-Holocene Taichung Foreland Basin, Central Taiwan. *Terrestrial, Atmospheric and Oceanic Sciences* **24**, pp. 41–58.

Ke, R.-S., 2009. Reflection Seismic Studies in the Puli Basin (in Chinese). Master Thesis. Institute of Geophysics, National Central University, Jhongli, Taiwan, p. 78.

Klose, C., 2006. Climate and geomorphology in the uppermost geomorphic belts ofthe Central Mountain Range, Taiwan. *Quaternary International* **147(1),** pp. 89–102.

Knox, J.C., 1995. Fluvial systems since 20,000 years BP. In: K.J. Gregory and L. Starkel (eds), *Global Continental Palaeohydrology*. John Wiley & Sons, Chichester, pp. 87–108.

Kuo, C.-M. and P.-M. Liew, 2000. Vegetational History and Climatic Fluctuations based on Pollen Analysis of the Toushe Peat Bog, Central Taiwan since the Last Glacial Maximum. *Journal of the Geological Society of China* **43(3)**, pp. 379–392.

Lai, H.-Y., 2010. Pollen record of the penultimate glacial sediments from the Yuchi Basin, Central Taiwan. Master Thesis. Institute of Geosciences, National Taiwan University, Taipei, Taiwan, p. 99.

Lai, K.-Y., 2002. Geomorphic Features and Active Structures: Cases of Hsinshe and Houli Area, Central Taiwan. Master These, Institute of Geosciences, National Taiwan University, Taipei, Taiwan, p. 79.

Lai, K.-Y., Y.-G. Chen, J.-H. Hung, J. Suppe, L.-F. Yue and Y.-W. Chen, 2006. Surface deformation related to kink-folding above an active fault: evidence from geomorphic features and co-seismic slips. *Quaternary International* **147**, pp. 44–54.

Lallemand, S., Y. Font, H. Bijwaard and H. Kao, 2001. New insights on 3-D plates interaction near Taiwan from tomography and tectonic implications. *Tectonophysics* **335(3–4)**, pp. 229–253.

Lancaster, N., 2008. Desert dune dynamics and development: Insights from luminescence dating. *Boreas* **37**, pp. 559–573.

Lee, J.-C., C. Rubin, K. Mueller, Y.-G. Chen, Y.-C. Chan, K. Sieh, H.-T. Chu and W.-S. Chen, 2004. Quantitative analysis of movement along an earthquake thrust scarp: a case study of a vertical exposure of the 1999 surface rupture of the Chelungpu fault at Wufeng, Western Taiwan. *Journal of Asian Earth Sciences* **23**, pp. 263–273.

Lee, Y.-H., C.-C. Chen, T.-K. Liu, H.-C. Ho, H.-Y. Lu and W. Lo, 2006. Mountain building mechanisms in the Southern Central Range of the Taiwan orogenic Belt—From accretionary wedge deformation to arc-continental collision. *Earth and Planetary Science Letters* **252(3–4)**, pp. 413–422.

Leica, 2006. Leica Photogrammetry Suite Automatic Terrain Extraction. Leica Geosystems Geospatial Imaging, LLC, p. 154.

Liew, P.-M., 1977. Pollen Analysis of Pleistocene Sediments at Waichiatokeng, Central Taiwan. *Acta Geologica Taiwanica* **19**, pp. 103–109.

Liew, P.-M., 1982. New Looks On The Pollen Data From The Yuchi Basin, Central Taiwan. *Ti-Chih* **4(1)**, pp. 53–58.

Liew, P.-M., 1988a. Quaternary stratigraphy of western Taiwan: palynological correlation. *Proceedings of the Geological Society of China* **31(1)**, pp. 169–180.

Liew P.-M., 1988b. Sedimentology and River-terrace Correlation of the Liwu River (in Chinese). National Taiwan University, Taipei, Taiwan.

Liew, P.-M. and M.-L. Hsieh, 2000. Late Holocene (2 ka) sea level, river discharge and climate interrelationship in the Taiwan region. *Journal of Asian Earth Sciences* **18**, pp. 499–505.

Liew, P.-M., B.-C. Chen, M.-L. Hsieh, S.-Y. Huang and C.-Y. Lee, 2013. Decreasing intensity of the last glacial stadials in low latitude terrestrial East Asia inferred by a new observation of pollen records. *Journal of Asian Earth Sciences* **69**, pp. 15–165.

Liew, P.-M., M.-L. Hsieh and B.H. Shyu, 2004. An overview of coastal development in a Young Mountain Belt-Taiwan. *Quaternary International* **115–116**, pp. 39–45.

Liew, P.-M., S.-Y. Huang and C.-M. Kuo, 2006. Pollen stratigraphy, vegetation and environment of the last glacial and Holocene—A record from Toushe Basin, central Taiwan. *Quaternary International* **147**, pp. 16–33.

Lin, C.-C., 1957. Topography of Taiwan (in Chinese). Publication of the Taiwan Provincial Documentary Committee, Taipei. pp. 317–322.

Lin, C.-C., 2005. The Density Structure Model of the Taichung and Puli basin of the Central Taiwan from the Gravity data (in Chinese). Master Thesis. Institute of Geophysics, National Central University, Jhongli, Taiwan, p. 62.

Lin, A.T., A.B. Watts and S.P. Hesselbo, 2003. Cenozoic stratigraphy and subsidence history of the South China Sea margin in the Taiwan region. *Basin Research* **15**, pp. 453–478.

Lin, J.-C., D. Petley, C.-H. Jen, A. Koh and M.-L. Hsu, 2006. Slope movements in a dynamic environment—A case study of Tachia River, Central Taiwan. *Quaternary International* **147**, pp. 103–112.

Liu, T.-K., S. Hsieh, Y.-G. Chen and W.-S. Chen, 2001. Thermo-kinematic evolution of the Taiwan oblique-collision mountain belt as revealed by zircon fission track dating. *Earth and Planetary Science Letters* **186(1)**, pp. 45–56.

Lu, C.-Y. and J. Malavieille, 1994. Oblique convergence, indentation and rotation tectonics in the Taiwan Mountain Belt: Insights from experimental modeling. *Earth and Planet Science Letters* **121**, pp. 477–494.

Lu, C.-Y., H.-T. Chu and J.-C. Lee, 1997. Structural evolution in the Hsuehshan Range, Taiwan. *Journal of the Geological Society of China* **40(1)**, pp. 261–279.

Lu, C.-Y., H.-T. Chu, J.-C. Lee, Y.-C. Chan, K.-J. Chang and F. Mouthereau, 2002. The 1999 Chi-Chi Taiwan earthquake and basement impact thrust kinematics. *West Pacific Earth Sciences* **2(2)**, pp. 181–190.

Lu, H.-C., 1959. Investigation report on the Puli coal field, Taiwan, China (in Chinese). MOEA, p. 22.

Malavieille, J., 2010. Impact of erosion, sedimentation and structural heritage on the structure and kinematics of orogenic wedges: analog models and case studies. *Geological Society of America, Account GSA Today*, **20(1)(2010)**, pp. 4–10.

Mejdahl, V., 1979. Thermoluminescence dating—beta-dose attenuation in quartz grains. *Archaeometry* **21(1)**, pp. 61–72.

Miall, A.D., 1978. Lithofacies types and vertical profile models in braided river deposits: A summary. In A.D. Miall (Ed.), Fluvial Sedimentology. *Canadian Society of Petroleum Geologists, Memoir* **5**, pp. 597–604.

Middleton, G.V., 1976. Hydraulic interpretation of sand size distributions. *Journal of Geology* **84**, pp. 405– 426.

Mouthereau, F., J. Angelier and J.-C. Lee, 2001. Le séisme du 21 setembre 1999: influence de l'héritage structural et implication du socle au front de la chaîne de Taiwan. *Earth and Planetary Sciences* **333**, pp. 93–103.

Munsell Color, 1992. Munsell Soil Color Charts. Munsell Color, Macbeth Division of Kollmorgen, Newburgh, NY, USA.

Murray, A.S. and A.G. Wintle, 2000. Luminescence dating of quartz using an improved single-aliquot regenerative-dose protocol. *Radiation Measurements* **32**, pp. 57–73.

Murray, A.S. and J.M. Olley, 2002. Precision and accuracy in the optically stimulated luminescence dating of sedimentary quartz: A status review. *Geochronometria* **21**, pp. 1–16.

Murray, A.S. and A.G. Wintle, 2003. The single aliquot regenerative dose protocol: potential for improvements in reliability. *Radiation Measurements* **37(4–5)**, pp. 377–381.

Olley, J.M., G.G. Caitcheon and A.S. Murray, 1998. The distribution of apparent dose as determined by optically stimulated luminescence in small aliquots of fluvial quartz: implications for dating young sediments. *Quaternary Science Review* **17**, pp. 1033–1040.

Olley, J.M., A.S. Murray and R.G. Roberts, 1996. The effects of disequilibria in the uranium and thorium decay chains on burial dose rates in fluvial sediments. *Quaternary Science Reviews* **15(7)**, pp. 751–760.

Olley, J.M., G.G. Caitcheon and A.S. Murray, 1999. The origin of dose distribution in fluvial sediments, and the prospect of dating single grains from fluvial deposits using optically stimulated luminescence. *Radiation Measurements* **30**, pp. 207–217.

Ori. G.G. and P.F. Friend, 1984. Sedimentary basins formed and carried piggyback on active thrust sheet. *Geology* **12**, pp. 475–478.

Plastino, W., L. Kaihola, P. Bartolomei and F. Bella, 2001. Comic background reduction in the radiocarbon measurements by liquid scintillation spectrometry at the underground laboratory of Gran Sasso. *Radiocarbon* **43**, pp. 157–161.

Powers, M.C., 1953. A new roundness scale for sedimentary particles. *Journal of Sedimentary Petrology* **23**, pp. 117–119.

Prescott, J.R. and J.T. Hutton, 1994. Cosmic ray distributions to dose rates for luminescence and ESR dating: large depths and long-term variations. *Radiation Measurements* **23**, pp. 497–500.

Prescott, J.R. and L.G. Stephan, 1982. The contribution of cosmic radiation to the environmental dose for thermoluminescent dating – latitude, altitude and depth dependences. *PACT* **6**, pp. 17–25.

Preusser, F., D. Degering, M. Fuchs, A. Hilgers, A. Kadereit, N. Klasen, M. Krbetschek, D. Richter and J.Q.G. Spencer, 2008. Luminescence dating: basics, methods and applications. *E&G Quaternary Science Journal* **57(1–2)**, pp. 95–149.

Rau, R.-J., K.-E. Ching, J.-C. Hu and J.-C. Lee, 2008. Crustal deformation and block kinematics in transition from collision to subduction: GPS measurements in northern Taiwan, 1995–2005. *Journal of Geophysics Research* **113**, B09404, p. 16.

Reimann, T., S. Tsukamoto, J. Harff, K. Osadczuk and M. Frechen, 2011. Reconstruction of Holocene coastal foredune progradation using luminescence dating – an example from the S´ wina barrier (southern Baltic Sea, NW Poland). *Geomorphology* **132(1–2)**, pp. 1–16.

Reimer, P.J., M.G.L. Baillie, E. Bard, A. Bayliss, J.W. Beck, P.G. Blackwell, C. Bronk Ramsey, C.E. Buck, G.S. Burr, R.L. Edwards, M. Friedrich, P.M. Grootes, T.P. Guilderson, I. Hajdas, T.J. Heaton, A.G. Hogg, K.A. Hughen, K.F. Kaiser, B. Kromer, F.G. McCormac, S.W. Manning, R.W. Reimer, D.A. Richards, J.R. Southon, S. Talamo, C.S.M. Turney, J. van der Plicht and C.E. Weyhenmeyer, 2009. IntCal09 and Marine09 radiocarbon age calibration curves, 0–50,000 years cal BP. *Radiocarbon* **51(4)**, pp. 1111–1150.

Ritter, D.F., R.C. Kochel and J.R. Miller, 2006. Process Geomorphology. Fourth Edition. Waveland Press, Inc, p. 560.

Rodnight, H., G.A.T. Duller, A.G. Wintle and S. Tooth, 2006. Assessing the reproducibility and accuracy of optical dating of fluvial deposits. *Quaternary Geochronology* **1**, pp. 109–120.

Schaller, M., N. Hovius, S.D. Willett, S. Ivy-Ochs, H.-A. Syna and M.-C. Chen, 2005. Fluvial bedrock incision in the active mountain belt of Taiwan from in situ-produced cosmogenic nuclides. *Earth Surface Processes and Landforms* **30**, pp. 955–971.

Seno, T., 1977. The instantaneous rotation vector of the Philippine sea plate relative to the Eurasian plate.

Tectonophysics **42(2–4)**, pp. 209–226.
Shih, T.-T., J.-C. Chang, K.-H. Teng and c.-A. Huang, 1996. Revised Geomorphology of Taiwan (in Chinese, self-translation). Geographical records of the Taiwan Province, pp. 678–679.
Siame, L.L., J. Angelier, R.-F. Chen, V. Godard, F. Derrieux, D.L. Bourlès, R. Braucher, K.-J. Chang, H.-T. Chu and J.-C. Lee, 2011. Erosion rates in an active orogen (NE-Taiwan): A confrontation of Cosmogenic measurements with river suspended loads. *Quaternary Geochronology* **6(2)**, pp. 246–260.
Siame, L.L., R.-F. Chen, F. Derrieux, J.-C. Lee, K.-J. Chang, D.L. Bourlès, R. Braucher, L. Léanni, C.-C. Kang and C.-P. Chang, 2012. Pleistocene alluvial deposits dating along frontal thrust of Changhua Fault in western Taiwan: the cosmic ray exposure point of view. *Journal of Asian Earth Sciences* **51**, pp. 1–20.
Simoes, M., J.P. Avouac, O. Beyssac, B. Goffé, K.A. Farley and Y.-G. Chen, 2007. Mountain building in Taiwan: a thermokinematic model. *Journal of Geophysical Research* **112**, p. B11405.
Soil Survey Staff, 2006. Keys to Soil Taxonomy. 10th ed., U. S. Pocahontas Press, Inc.
Stuiver, M. and H. Polach, 1977. Discussion; reporting of C-14 data. *Radiocarbon* **19**, pp. 355–363.
Sun, D.H., J. Bloemendal, D. K. Rea, J. Vandenberghe, F.C. Jiang, Z.S. An and R.X. Su, 2002. Grain-size distribution function of polymodal sediments in hydraulic and aeolian environments, and numerical partitioning of the sedimentary components. *Sedimentary Geology* **152**, pp. 263–277.
Suppe, J., 1981. Mechanics of mountain building in Taiwan. *Memoir of the Geological Society of China* **4**, pp. 67–89.
Suppe, J., 1984. Kinematics of arc-continent collision, flipping of subduction, and back-arc spreading near Taiwan. *Memoir Geological Society of China* **6**, pp. 21–33.
Suppe, J., 1986. Reactivated normal faults in the western Taiwan fold-thrust belt. *Memoir of the Geological Society of China* **7**, pp. 187–200.
Teng, L.S., 1990. Geotectonic evolution of late Cenozoic arc-continent collision in Taiwan. *Tectonophyiscs* **183**, pp. 67–76.
Teng, L.S., 1996. Extensional collapse of the northern Taiwan mountain belt. *Geology* **24(10)**, pp. 949–952.
Teng, L.S., 2007. Quaternary Tectonics of Taiwan (in Chinese). *Special Publication of the Central Geological Survey* **18**, p. 24.
Tomita, Y., 1937. On the correlation of the geomorphic surfaces of the Tanshui River terraces. *Taiwan Tigaku Kizi* **8(10–12)**, pp. 101–119.
Tomita, Y., 1951. Physiographic Development of the Hori (Puli) Basin Group of Central Taiwan (Formosa). *Annals of the Tohoku Geographical Association* **3**, pp. 1–7.
Tomita, Y., 1953. Physiographic development of the Hori (Puli) basin group of Central Taiwan (Formosa). *Bulletin of the Chinese Association for the Advancement of Science* **1(3)**, p. 19.
Tomita, Y. 1954. Surface Geology and Correlation of River Terraces. The science reports of the Tohoku University. 7th series, *Geography* **3(1)**, ISSN: 0375-7854, pp. 51–58.
Tsai, H. and Q.-C. Sung, 2003. Geomorphic evidence for an active pop-up zone associated with the Chelungpu fault in central Taiwan. *Geomorphology* **56**, pp. 31–47.
Tsai, H., 2004. Multiple Approaches to the Correlation of River Terraces in Taiwan (in Chinese). Doctoral Dissertation. Department of Earth Sciences, National Cheng Kung University, Tainan, Taiwan, p. 143.
Tsai, H., W.-S. Huang and Z.-Y. Hseu, 2007. Pedogenic correlation of lateritic river terraces in central Taiwan. *Geomorphology* **88**, pp. 201–213.
Tsai, H., Y. Maejima and Z.-Y. Hseu, 2008. Meteoric ^{10}Be dating of highly weathered soils from fluvial terraces in Taiwan. *Quaternary International* **188**, pp. 185–196.
Tsao, S.-H., 1996. The geological significance of illite crystallinity, zicon fission-track ages, and K-Ar ages of metasedimentary rocks of the Central Range of Taiwan. Doctoral Thesis, National Taiwan University, Taipei, Taiwan, p. 272.
Tseng, C.-H., D. Wenske, M. Böse, T. Reimann, C. Lüthgens and M. Frechen, 2013. Sedimentary features and ages of fluvial terraces and their implications for geomorphic evolution of the Taomi River catchment: A case study in the Puli Basin, central Taiwan. *Journal of Asian Earth Sciences* **62**, pp. 759–768.
Tsukada, M., 1967. Vegetation in subtropical Formosa during the Pleistocene Glaciation and the Holocene. *Paleogeography, Paleoclimatology, Paleoecology* **3**, pp. 49–64.
Vandenberghe, J., 2002. The relation between climate and river processes, landforms and deposits during the Quaternary. *Quaternary International* **91**, pp. 17–23.
Wallinga, J., 2002. Optically stimulated luminescence dating of fluvial deposits: a review. *Boreas* **31**, pp. 303–322.
Wang, C.-Y., C.-L. Li and H.-Y. Yen, 2002. Mapping the northern portion of the Chelungpu fault, Taiwan by shallow reflection seismics. *Geophysical Research Letters* **29(16)**, pp. 37-1–37-3.
Wang, Y.J., H. Cheng, R.L. Edwards, Y.Q. He, X.G. Kong, Z.S. An, J.Y. Wu, M.J. Kelly, C.A. Dykoski and X.D. Li, 2005. The

Holocene Asian monsoon: links to solar changes and North Atlantic climate. *Science* **308**, pp. 854–857.

Wells. S. and A. Harvey, 1987. Sedimentological and geomorphic variations in storm-generated alluvial fans, Howgill Fells, Northwest England. *Geological Society America Bulletin* **98**, pp. 182–198.

Wenske, D., M. Böse, M. Frechen and C. Lüthgens, 2011. Late Holocene mobilisation of loesslike sediments in Hohuan Shan, high mountains of Taiwan. *Quaternary International* **234(1–2)**, pp. 174–181.

Wenske, D., M. Frechen, M. Böse, T. Reimann, C.-H. Tseng and P. Hoelzmann, 2012. Late Quaternary river terraces in the Central Mountain Range of Taiwan: a study of cover sediments across a terrace section along the Tachia River. *Quaternary International* **263**, pp. 26–36.

Wilcox, T., K. Mueller, P. Upton, Y.-G. Chen, S.-T. Huang, B.J. Yanites and G. Tucker, 2011. Linking Taiwan's subcritical Hsuehshan Range topography and foreland basin architecture. *Tectonics* **30**, TC4011, doi:10.1029/2010TC002825.

Willett, S.D., D. Fisher, C. Fuller, E.-C. Yeh and C.-Y. Lu, 2003. Erosion rates and orogenic wedge kinematics in Taiwan inferred from apatite fission track thermochronometry. *Geology* **31**, pp. 945–948.

Yang, C.-C. B., W.-S. Chen, L.-C. Wu and C.-W. Lin, 2007a. Active deformation front delineated by drainage pattern analysis and vertical movement rates, southwestern Coastal Plain of Taiwan. *Journal of Asian Earth Sciences* **31**, pp. 251–264.

Yang, G.-S., J.-C. Chang, S.-M. Shen and T.-S. Shih, 2007b. Geomorphic Surfaces, Active Structures and Geomorphic Evolution of the Puli Basin (in Chinese). *Journal of Geographical Research* **46**, pp. 1–15.

Yanites, B.J., G.E. Tucker, K.J. Mueller, Y.-G. Chen, T. Wilcox, S.-Y. Huang and K.-W. Shi, 2010. Incision and channel morphology across active structures along the Peikang River, central Taiwan: Implications for the importance of channel width. *GSA Bulletin* **122(7/8)**, pp. 1192–1208.

Yen, H.-Y., Y.-H. Yeh, C.-H. Lin, K.-J. Chen and Y.-B. Tsai, 1995. Gravity survey of Taiwan, *Journal of Physics of the Earth* **43**, pp. 685–696.

Yu, S.-B., H.-Y. Chen and L.-C. Kuo, 1997. Velocity field of GPS stations in the Taiwan area. *Tectonophysics* **274**, pp. 41–59.

Yu, S.-B., L.-C. Kuo, R.S. Punongbayan and E.G. Ramos, 1999. GPS observation of crustal deformation in the Taiwan-Luzon region. *Geophysical Research Letters* **26**, pp. 923–926.

Yue, L.-F., J. Suppe and J.-H. Hung, 2005. Structural geology of a classic thrust belt earthquake: the 1999 Chi-Chi earthquake Taiwan (Mw=7.6). *Journal of Structural Geology* **27**, pp. 2058–2083.

Zonneveld, J.I.S., 1975. River terrace and Quaternary chronology in the Netherland. *Geologie en Mijnhouw* **19**, pp. 277–285.

A2 Terminology used in this work

Full name*	Taiwanese characters	Region in Taiwan	Description	Abbreviation
Ailan	愛蘭	Puli Basin	local name	AL
Ailan Anticline	愛蘭背斜	Puli Basin		
Beigang (Peikang) River	北港溪	central		
Changhua Fault	彰化斷層	central west	boundary of geological terrains	
Chaochou Fault	潮洲斷層	south	boundary of geological terrains	CF
Chelungpu Fault	車籠埔斷層	central	active reverse fault	
Chenyeolan River	陳有蘭溪	cnetral southern	boundary of geological terrains	
Chi-Chi Earthquake	集集地震	central	M_w = 7.6, occurred in 1999	
Chihkan	赤崁	Puli Basin	local name	CK
Chuchih Fault	屈尺斷層	central north	boundary of geological terrains	CHF
Chungkuei Basin	銃櫃盆地	central	0.7 km^2	
Coastal Plains	海岸平原	southwest	alluvial plain	CP
Central Range	中央山脈	from northeast to central south	schist and gneiss	CR
Coastal Range	海岸山脈	eastern	andesite agglomerate	CoR
Dalin (Talin) River	大林溪	Yuchih Basin		
Danan (Tanan) Anticline	大滴背斜	Puli Basin		
Dapingding (Tapingting)	大坪頂	Puli Basin	Local name	DP
Dongguang (Tungkuang) River	東光溪	Yuchih Basin		
Dongpu (Tungpu) River	東埔溪	Puli Basin		
Erren River	二仁溪	southwest		
Green Island	綠島	southeast offshore	volcanic island	
Hehuanshan (Hohuanshan)	合歡山	central	3417 m a.s.l.	
Hengchun Tableland	恆春台地	southern end	former marine terrace	
Houli Tableland	后里台地	west	former alluvial fan	
Hshinshe Tablelands	新社台地	west	former fluvial terrace	
Hsuehshan	雪山	central north	3886 m a.s.l., the second highest in Taiwan	
Hsuehshan Range	雪山山脈	central north to central	slate and metamorphic sandstone	HR

Ilan Plain	宜蘭平原	northeast	alluvial plain	IL
Jhuoshuei (Chuoshui) River	濁水溪	central	the longest in Taiwan	
Lancheng	籃城	Puli Basin	local name	LC
Lanyang River	蘭陽溪	northeast		
Laonung	荖濃溪	central southern		
Linkou Tableland	林口台地	northwest	former alluvial fan	
Lishan Fault	梨山斷層	central north to central south	boundary of geological terrains	LSF
Liwu River	立霧溪	eastern		
Longitudinal Valley Fault	花東縱谷斷層	eastern	boundary of geological terrains	LVF
Mei River	眉溪	Puli Basin		
Meiyuang Fault	眉原斷層	Puli Basin	reverse fault	
Nangang (Nankang) River	南港溪	Puli Basin and Yuchih Basin		
Nanhutashan	南湖大山	central east	3740 m a.s.l.	
Niousiangchu	牛相觸	Puli Basin	local name	NS
Orchid Island	蘭嶼	southeast offshore	volcanic island	
Paileng Formation	白冷層	central	Oligocene	
Pakua Tableland	八卦台地	west	former alluvial fan	
Puli Basin	埔里盆地	central	120 km^2 (including tableland surfaces); 60 km^2, without tableland surfaces	
Puli Syncline	埔里向斜	Puli Basin		
Shihpachunghsi Formation	十八重溪層	central	Eocene	
Shihgang (Shihkang) River	史港溪	Puli Basin		
Shueichangliou Fault	水長流斷層	central	reverse fault; also known as “Shueilikeng Fault“;	
Shueichangliou Formation	水長流層	central	late Oligocene	
Shueichiang	水墻	Puli Basin	local name	SC
Shueiwaku	水蛙窟	Puli Basin	local name	SW
Shuangdong (Shuantung) Fault	雙冬斷層	west	reverse fault	
Sun Moon Lake	日月潭	central	8 km^2, the second biggest in Taiwan	
Tachien Sandstone	達見砂岩	central	Eocene	

Tadu Tableland	大肚台地	west	fault propagation fold	
Taichung Basin	台中盆地	west	piggy basin; the biggest in Taiwan (380 km^2)	
Taipei Basin	台北盆地	north	half graben; the second biggest in Taiwan (243 km^2)	
Tamshui River	淡水河	north	the third longest in Taiwan	
Taomi River	桃米溪	Puli Basin		
Taoyuan Tableland	桃園台地	northwest	former alluvial fan	
Tatun Volcanoes	大屯火山群	northwest	last eruption 6000 years ago	
Tili Fault	地利斷層	Puli Basin	reverse fault	
Toukoshan Formation	頭嵙山層	West	Pleistocene; gravel	
Toushe Basin	頭社盆地	central	1.7 km^2	
University	(暨南)大學	Puli Basin		Uni
Western Foothills	西部麓山帶	west	fold and thrust belt	WF
Wugongku	蜈蚣窟	Puli Basin	local name	WG
Yuchih Basin (Yuchi Basin)	魚池盆地	central	21 km^2	
Yushan	玉山	central south	3952 m a.s.l., the highest in Taiwan	

*Terms in brackets are also used in other references.

A3 DTM extraction report

Date Created: 02/09/12

Time Created: 13:15:45

DTM PROJECT INFORMATION

Block File Used: puli2.blk

Block File Location: d:/dateien von taomi river einzugsgebiet/erdas lps/

DTM Correlation Time (seconds): 2488

Points Per Second: 1072-447

DTM Generation Time (seconds): 373

Total Processing Time (seconds): 2861

DTM Type: DEM

DTM Name: c:/users/chiahan/paper 1/dtm_puli_twd97_2m.img

Number of Columns: 2051

Number of Rows: 2150

Cell Width: 2.000 meters

Cell Height: 2.000 meters

Projection: Transverse Mercator

Spheroid: GRS 1980

Datum: GRS 1980

Horizontal Units: meters

Vertical Units: meters

Upper left DEM corner coordinates: (242432-1711, 2651138.3115)

Lower right DEM corner coordinates: (246532-1711, 2646840.3115)

Minimum Mass Point Elevation: 17.2103

Maximum Mass Point Elevation: 920.9842

Mean Mass Point Elevation: 541.8114

Adaptive ATE

Stop at pyramid: 0

Minimum correlation threshold: 0.3000

Strategy Parameter Settings:

Image Pair Name: 100719d_38~0061_hr4_100719d_38~0062_hr4

Region Description: Default Region

Name of Strategy Used: Default

List All of the Strategy Parameter Values Used:

Search Size: 21 x 3

Allow Adaptive Change: No

Correlation Size: 7 x 7

Allow Adaptive Change: No

Coefficient Limit: 0.8000

Allow Adaptive Change: No

Topographic Type: Rolling Hills

Object Type: Open Area

Use Image Band: 1

DTM Filtering: Low

Region elevation range: 432.0000 to 788.5630

Image Pair Name: 100719d_38~0062_hr4_100719d_38~0063_hr4

Region Description: Default Region

Name of Strategy Used: Default

List All of the Strategy Parameter Values Used:

Search Size: 21 x 3

Allow Adaptive Change: No

Correlation Size: 7 x 7

Allow Adaptive Change: No

Coefficient Limit: 0.8000

Allow Adaptive Change: No

Topographic Type: Rolling Hills

Object Type: Open Area

Use Image Band: 1

DTM Filtering: Low

Region elevation range: 409.0000 to 694.7935

Image Pair Name: 100719d_38~0063_hr4_100719d_38~0064_hr4

Region Description: Default Region

Name of Strategy Used: Default

List All of the Strategy Parameter Values Used:

Search Size: 21 x 3

Allow Adaptive Change: No

Correlation Size: 7 x 7

Allow Adaptive Change: No

Coefficient Limit: 0.8000

Allow Adaptive Change: No

Topographic Type: Rolling Hills

Object Type: Open Area

Use Image Band: 1

DTM Filtering: Low

Region elevation range: 432.0000 to 788.5630

Image Pair Name: 100719d_38~0064_hr4_100719d_38~0065_hr4

Region Description: Default Region

Name of Strategy Used: Default

List All of the Strategy Parameter Values Used:

Search Size: 21 x 3

Allow Adaptive Change: No

Correlation Size: 7 x 7

Allow Adaptive Change: No

Coefficient Limit: 0.8000

Allow Adaptive Change: No

Topographic Type: Rolling Hills

Object Type: Open Area

Use Image Band: 1

DTM Filtering: Low

Region elevation range: 409.0000 to 694.7935

Image Pair Name: 100719d_38~0065_hr4_100719d_38~0066_hr4

Region Description: Default Region

Name of Strategy Used: Default

List All of the Strategy Parameter Values Used:

Search Size: 21 x 3

Allow Adaptive Change: No

Correlation Size: 7 x 7

Allow Adaptive Change: No

Coefficient Limit: 0.8000

Allow Adaptive Change: No

Topographic Type: Rolling Hills

Object Type: Open Area

Use Image Band: 1

DTM Filtering: Low

Region elevation range: 432.0000 to 788.5630

Project elevation range: 409.0000 to 788.5630

ACCURACY INFORMATION

General Mass Point Quality:

Excellent % (1-0.85): 52-8130 %

Good % (0.85-0.70): 36.1404 %

Fair % (0.70-0.5): 11.0466 %

Isolated %: 0.0000 %

Suspicious %: 0.0000 %

Global Accuracy:

Vertical Accuracy:

Total # of 3D Reference Points Used: 146

Minimum, Maximum Error: -8.6242, 5.7219

Mean Error: -0.2392

Mean Absolute Error: 0.8664

Root Mean Square Error (RMSE): 1.5952

Absolute Linear Error 90 (LE90): 1.9845

NIMA Absolute Linear Error 90: +/- 2-5961

Planimetric (Horizontal) Accuracy:

Reference DEM Points Are Outside DTM or Inside Background Areas

Block Tie Point to DTM Vertical Accuracy

Total # of Tie Points Used: 146

Minimum, Maximum Error: -8.6242, 5.7219

Mean Error: -0.2392

Mean Absolute Error: 0.8664

Root Mean Square Error: 1.5952

Absolute Linear Error 90: 1.9845

NIMA Absolute Linear Error 90: +/- 2-204

Curriculum Vitae

For reasons of data protection, the curriculum vitae is not included in the online version.

Eidesstattliche Erklärung

Hiermit erkläre ich, dass ich die vorliegende Arbeit selbständig verfasst und keine anderen als die angegebenen Hilfsmittel benutzt habe. Die Beiträge der Co-Autoren der wissenschaftlichen Veröffentlichungen und technische Hilfe anderer Personen sind im Rahmen der Danksagung (Acknowledgements) dargelegt.
Ich erkläre, dass ich diese Dissertation erstmalig und nur am Fachbereich Geowissenschaften der Freien Universität Berlin eingereicht habe und damit in dieser oder anderer Form keinen entsprechenden Doktorgrad besitze. Der Inhalt der dem Verfahren zugrunde liegenden Promotionsordnung ist mir bekannt.

Berlin, den 28.03.2014

Chia-Han Tseng